

UC Berkeley

UC Berkeley Electronic Theses and Dissertations

Title

Radiological and Nuclear Threat Detection Using Small Unmanned Aerial Systems

Permalink

<https://escholarship.org/uc/item/7b241431>

Author

McManus, Keith David

Publication Date

2019

Peer reviewed|Thesis/dissertation

Radiological and Nuclear Threat Detection
Using Small Unmanned Aerial Systems

by

Keith David McManus

A dissertation submitted in partial satisfaction of the
requirements for the degree
Doctor of Philosophy

in

Nuclear Engineering

in the

Graduate Division

of the

University of California, Berkeley

Committee in charge:
Professor Kai Vetter, Chair
Professor Rhonda Righter
Professor Edward Morse

Summer 2019

**Radiological and Nuclear Threat Detection
Using Small Unmanned Aerial Systems**

Copyright 2019
by
Keith David McManus

Abstract

Radiological and Nuclear Threat Detection
Using Small Unmanned Aerial Systems

by

Keith David McManus

Doctor of Philosophy in Nuclear Engineering

University of California, Berkeley

Professor Kai Vetter, Chair

The aim of this research is to demonstrate the feasibility of remotely sensing nuclear and radiological threat materials by leveraging recent advances in radiation detectors, unmanned systems, and contextual sensors. The broad intent is to get detectors out of the hands of humans and onto semi-autonomous systems for a wide range of use cases. The search for special nuclear material is one specific mission area where radiation detectors employed on small unmanned aerial systems could provide significant operational value by exploiting the advantages that remote access enables: improved collection time, decreased source-to-detector distance, and reduced unintentional shielding. The goals of this study are fivefold: (1) assess current capabilities for directed search and substantiate the improvement that an unmanned approach would provide, (2) expand the understanding of the background radiation environment to include building rooftops, (3) establish system requirements and map out the parameter space of trade-offs (i.e., trade space) based on an analysis of current sensor and platform capabilities, (4) investigate and optimize search methods, and (5) identify and characterize additional mission areas for further investigation.

To achieve these five goals, we started by identifying boundary conditions for signal collection time, source-to-detector distance (i.e., standoff), and intervening material attenuation for three different search modes: vehicle-mounted standoff detection, rotary-wing aerial detection, and small unmanned aerial system-based remote detection. The objective of this analysis was to calculate the theoretical reduction in detector area required to achieve the same minimum detectable activity of a ^{137}Cs source for a given detector material. We found that measuring from the rooftop with just 50 cm^2 of detector area should detect smaller activity sources than $10,000\text{ cm}^2$ in a vehicle-borne approach or $5,000\text{ cm}^2$ in an aerial helicopter-borne approach.

Our next objective was to characterize the background radiation environment sensed from the rooftops of light industrial buildings. We conducted a measurement campaign across

fifteen buildings varying in geographic location, size, shape, height, wall construction, and roofing material. We discovered the variation in the background radiation ranged up to $\pm 50\%$ when analyzing contributions from seven prominent background peaks. Across a single building, this variation ranged 25–40% for contributions from potassium, uranium, and thorium. We also examined the attenuation of radiation by roofing materials both in simulation and experiment. We found that typical roof construction attenuates 1461 keV gamma-rays by approximately 50% when passing normal to the roof and continues to increase as the incident angle between the source and the detector increases. This observation directly influenced our approach to developing an optimal search scheme.

With knowledge of the background and consideration of threat signatures, we then initiated an effort to develop a system architecture and design a sensor suite capable of detecting relevant threats in the anticipated environment. We employed established requirements analysis techniques to frame the development of a system that will provide tangible operational value to the user. We examined the trade space for platforms and sensors in terms of size, weight, power, cost, and visibility profile. Although our survey of capabilities is a snapshot in time, it lays the foundation for future analysis of alternatives. We recommend a platform that can move both through the air and on the ground and suggest further exploration of tube-launched systems for several military mission areas employing radiation sensors. For detectors, we recommend room temperature semi-conductors: cadmium zinc telluride for gamma-ray spectroscopy and lithium-backfilled etched-silicon diodes for neutron detection. Technologies such as real-time kinematic positioning, solid-state light depth and ranging, and thermal infrared cameras warrant further study as auxiliary contextual sensors in the system.

Assuming an overmatched system is attainable, we then constructed a method to select advantageous measurement locations and developed techniques to optimize a search pattern. We devised a nonlinear programming routine and applied threshold cuts to reduce the time to converge to a near-optimal solution. We also explored several parameters that might be used as the objective quantity depending on the mission requirements and intelligence assessment.

Finally, with the intent of removing humans from the task of operating detectors in elevated radiation areas, we sought to expand our inquiry to seven additional military mission areas. We briefly examined a historical vignette where unmanned radiation detection assets would have provided considerable value, summarized the general operational conditions, assessed the impact that remote detection might have on the speed, accuracy, fidelity, safety, or feasibility of a given mission, and identified unique challenges that might arise in developing a materiel solution. These additional areas are ripe for exploration and contribution from the broader community of researchers.

Omnis cum in tenebris praesertim vita laboret—Titus Lucretius

Dedicated to Mr. Dumbjohn, the man in phat pants, and the hooligan crew.
We are all strugglers at some point in our lives. It is through those
struggles that we build character and grow in our faith.

*Ego sum lux mundi qui sequitur me non ambulabit
in tenebris sed habebit lucem vitae—John 8:12*

Contents

Contents	ii
List of Figures.....	iii
List of Tables	vi
List of Acronyms and Abbreviations	vii
Acknowledgments	ix
1 Introduction	1
1.1 Background.....	2
1.2 Mission Areas	3
1.3 Directed Search Vignette	7
1.4 Summary.....	9
2 Motivating Exemplar	11
2.1 Detection Schemes.....	11
2.2 Theoretical Performance for Notional Conditions	18
2.3 Summary.....	20
3 Radiological and Nuclear Threat Detection.....	21
3.1 Radioactive Signatures	21
3.2 Radiation Detection	32
3.3 Alternative Signatures, Indicators, and Other Sensors.....	45
3.4 Summary.....	48
4 Background Radiation and Source Measurements.....	50
4.1 Background Radiation	50
4.2 Source Detection.....	67
4.3 Summary.....	75
5 Sensor Suite Design	76
5.1 Requirements Analysis	76
5.2 Trade Space	84
5.3 Functional-level Components	89
5.4 Recommended Sensor Suite	97
6 Search Pattern Optimization.....	99
6.1 Measurement Location Selection.....	99
6.2 Collection Time Allocation	108
6.3 Future Considerations	115
7 Synopsis and Future Work.....	116
7.1 Summary of Contributions to the Field.....	116
7.2 Future Work.....	117
Bibliography	119
Appendix—Department of Defense Radiological and Nuclear Detection Missions	130

List of Figures

1.1:	11-year-old Ryan McManus pilots a DJI Phantom 3.....	2
2.1:	Representative detector platforms for comparison	11
2.2:	Height-Velocity diagram for Bell 412 multi-engine helicopter.....	15
2.3:	Effect of additional high-purity germanium detectors on the minimum detectable activity (MDA) of ^{137}Cs source in a vehicle-borne scenario	19
3.1:	Cosmic-ray exposure, elevation, and absorbed dose from terrestrial sources	22
3.2:	Simplified decay chain of naturally occurring uranium isotopes	25
3.3:	Representative high-purity germanium gamma-ray spectrum of 17 kg depleted uranium plates measured at 135 cm compared with nominal background	26
3.4:	Diagram of detection scheme for 4 kg of super-grade plutonium	29
3.5:	Photoelectric cross-section for various materials over a broad energy range.....	34
3.6:	Measured spectrum for 158 μCi ^{60}Co at 100 cm using ORTEC Detective-EX-100	35
3.7:	Diagram of Compton scattering with a target electron assumed at rest	36
3.8:	Differential scattering cross-section for 51, 511, 1022, & 2555 keV photons	36
3.9:	Schematic showing incident high-energy photon hitting a scintillating crystal	40
4.1	An inverted ORTEC DX-100 high-purity germanium (HPGe) detector on improvised stands and various prototype detectors used for background and source measurement... 51	51
4.2:	Illustration of single and repeated quincunx pattern.....	52
4.3	Representative light industrial buildings found at Richmond Field Station.....	53
4.4:	Noteworthy characteristics of light industrial buildings.....	54
4.5:	Attenuation (1/e) length for gamma-rays in air	56
4.6:	3-D model of building with a concrete slab, tilt-up concrete walls, steel roof decking, plywood decking, extruded polystyrene insulation, and waterproof membrane	57
4.7:	Comparison of measured background with typical long dwell background spectrum.....	58
4.8:	Regional contour map of the estimated surface concentration of potassium in the Los Alamos region of New Mexico and Richmond Field Station in California	59
4.9:	Probability distribution for seven naturally occurring background energy lines measured at twenty-eight positions on the rooftops of ten light industrial buildings.....	60

4.10:	Background probability distributions for four typical environments	60
4.11:	Average peak count rates for thirty-five measurements of terrestrial background.....	62
4.12:	Count rate charts and waterfall plots for background measurements on Bldgs. 128, 153, 158/158A, 472, and 486.....	63
4.13:	Variation of terrestrial background measured across a single building.....	64
4.14:	Attenuation of the background radiation by roof materials in Bldg. 486	66
4.15:	Zoomed in spectra from Figure 4.14 for representative background energies peaks	66
4.16:	Schematic of the varying path length for attenuation through roofing materials	68
4.17:	Graphical representation of the effect of lateral source-to-detector distance on the projected area of a cylindrical detector	69
4.18:	Effect of lateral source-to-detector distance on the detector count rate, illustrated by the ratio of projected detector area to the source-to-detector distance squared.....	69
4.19:	Semi-log plot illustrating the effect the doubling the source-to-detector distance has under varying background conditions with respect to source strength.....	70
4.20:	Time to detect 26 μCi of ^{137}Cs versus distance on the rooftop of Bldg. 128.....	71
4.21:	Zoomed in spectra from rooftop measurement with 26 μCi of ^{137}Cs present.....	72
4.22:	Sample spectra from three prototype detectors collected for 595 s from the rooftop of Bldg. 128 approximately 4 m above 25 μCi of ^{137}Cs	74
5.1:	Preliminary graphical depiction of a concept of operations concerning the use of unmanned systems for the directed search for radiological and nuclear material	77
5.2:	High-level block diagram illustrating the various functions, behaviors, tasks, components, and processes of the envisioned directed search system	79
5.3:	Simulated spectra of 1 kg-quantities of weapons-grade highly-enriched uranium and plutonium as measured from a rooftop	82
5.4:	Sub-system architecture depicting the location and role of sensors within the system	83
5.5:	DJI Matrice 600 Pro with prototype 3-D radiation mapping sensors	89
5.6:	AeroVironment's Vapor 55, an example of a battery-powered unmanned helicopter	90
5.7:	AeroVironment's Quantix, an example of a vertical takeoff and lift fixed-wing platform.....	90
5.8:	Pegasus III by Robotic Research driving, perched, and flying.....	91
5.9:	Examples of tube-launched projectiles and missiles	92
5.10:	GADRAS simulated spectra for six cadmium zinc telluride (CZT) detectors	94
5.11:	GADRAS simulated spectra for a high-purity germanium (HPGe) detector	94

6.1:	Extrapolated field-of-view for centerline and corner measurement locations.....	100
6.2:	Bldg. 128 characteristics.....	101
6.3:	DOE's Aerial Measuring System radiation survey method.....	101
6.4:	Derivation of optimal signal to noise for simple mobile search geometry	102
6.5:	Comparison of square versus triangular lattice with uniform counting time.....	103
6.6:	Example best-known packings of equal circles in a 1×0.5 rectangle	104
6.7:	Example hexagonal lattice tiling on a rectangle with an aspect ratio of 1:0.6 for different pitch values as a function of building height	105
6.8:	Modified Traveling Salesman Problem path optimizations.....	107
6.9:	Example search patterns which prioritize locations with the better fields-of-view while still attempting to minimize the total path length	108
6.10:	Cluster diagram of inputs to the information maximization model.....	109
6.11:	Schematic of variables required for information maximization routine.....	110
6.12:	Sample optimization based on various functions of the minimum detectable activity...	111
6.13:	Sample optimization based on maximizing the average probability of detection across all possible source locations.....	112
6.14:	Flowchart for the simple playbook method	113

List of Tables

2.1:	Estimated attributes for three possible detection schemes employed to interrogate a targeted light industrial building for the presence of radiological or nuclear material.....	17
2.2:	Calculated minimum detectable activity (MDA) of ^{137}Cs for thallium-doped sodium iodide NaI(Tl) scintillation gamma-ray detectors in search schemes	18
2.3:	Calculated minimum detectable activity (MDA) for ^{137}Cs based on fourteen high-purity germanium (HPGe) detectors in vehicle-borne scheme versus one cadmium zinc telluride (CZT) detector in a small unmanned aerial system-based scheme.....	20
3.1:	Nuclear reactions of interest in thermal neutron detection	43
4.1:	Estimated surface concentrations of potassium, uranium, and thorium, at locations where data were taken.....	55
4.2:	Comparison of % attenuation of background photons by various materials	56
4.3:	Attenuation of the 1461 keV background peak from ^{40}K by roof materials.....	57
4.4:	Background radiation peak regions of interest	59
4.5:	Summary statistics for the variation of terrestrial background on Bldg. 128	65
4.6:	Characteristics of sources used to test the efficacy of detection from the rooftop	67
4.7:	Performance of small prototype detectors on rooftop 4 m from 25 μCi of ^{137}Cs	73
5.1:	Proposed Key Performance Parameters for a small unmanned directed search system... ..	82
5.2:	Specifications for small unmanned aerial vehicles and tube-launched systems.....	85
5.3:	Sensor-level Size, Weight, Power, and Cost estimates.....	87
5.4:	Estimated time-to-detect (± 30 s) threshold and objective highly enriched uranium threats for several detector materials based on assumed parameters for the unmanned detection scheme using a 1-D model and the IsotopeID function in GADRAS.....	93
5.5:	Expected neutron detection distance for threshold and objective quantities of reactor- and weapons-grade plutonium evaluated for 60 seconds	95
6.1:	Comparison of measurement lattices for a 15 \times 25 m building as a function of pitch	105
6.2:	Properties of example traveling-salesman-problem path selection for gridded search ..	107

List of Acronyms and Abbreviations

AFP	amplifying fluorescent polymer
AGL	above ground level
AMS	aerial measurement system
AN/VDR-2	Army-Navy vehicle or dismounted radiac-meter
APD	avalanche photodiode
BDA	battle damage assessment
CBRN	chemical, biological, nuclear, and radiological
CLLBC(Ce)	cerium-doped cesium lanthanum lithium bromochloride
CLYC(Ce)	cerium-doped cesium lanthanum yttrium chloride
CONOPS	concept of operations
CsI(Tl)	thallium-doped cesium iodide
CZT	cadmium zinc telluride
DoD	Department of Defense
DTRA	Defense Threat Reduction Agency
EPDM	ethylene propylene diene monomer
FW	fixed-winged
FWHM	full width at half maximum
GADRAS	Gamma Detector Response and Analysis Software
GNSS	global navigation satellite system
HEU	highly enriched uranium (also identified as high-enriched uranium)
HPGe	high-purity germanium
IAEA	International Atomic Energy Agency
IMU	inertial measurement units
IND	improvised nuclear device
IR	infrared radiation
ISR	intelligence, surveillance, and reconnaissance
KPP	key performance parameter
KSA	key system attribute
KUT	potassium, thorium, and uranium

LaBr ₃ (Ce)	cerium-doped lanthanum bromide
LAMP	localization and mapping platform
LBNL	Lawrence Berkeley National Laboratory
LiDAR	light depth and ranging
NaI(Tl)	thallium-doped sodium iodide
NBCRV	nuclear, chemical, biological reconnaissance vehicle
NBCSPG	nuclear, biological, and chemical sensor processing group
NDT	nuclear disablement team
NIST	National Institute for Standards and Technology
NNSA	National Nuclear Security Administration
NRC	Nuclear Regulatory Commission
OMS/MP	operational mode summary and mission profile
PMT	photomultiplier tube
RadMAP	radiological multisensor analysis platform
RDD	radiological dispersal device
RED	radiological exposure device
RTK	Real-time kinematic
SiPM	silicon photomultiplier
SNM	special nuclear material
SQ	significant quantity
SrI ₂ (Eu)	europium-doped strontium iodide
sUAS	small unmanned aerial system
SUV	sport utility vehicle
SWaP	size, weight, and power
UAS	unmanned aerial system
UAV	unmanned aerial vehicle
UGV	unmanned ground vehicle
UUV	unmanned underwater vehicle
VTOL	vertical take-off and lift
WG	weapons-grade
ZnS(Ag)	silver-doped zinc sulfide

Acknowledgments

I would like to begin by acknowledging that without my faith in God and the continued blessings I receive through his hand, completing this work would not have been possible. When I was struggling and losing faith in myself, I would ask for his will to be done through prayer. I know that there were times on this journey that were difficult on my family. I believe the breaks I took to spend time with them were little gifts from God that allowed me to focus on what was truly important.

I want to recognize the hardship and additional parental load that I placed on my wife, Martina, by taking on this challenging program of study. She stood by me and supported me through my struggles and tried to provide an atmosphere to enable my success. I love her and cherish our time together, which should hopefully increase now that this milestone has been reached. I would also like to thank my three boys, Ryan, Callan, and Evan for enduring this chapter of our family story and being so resilient to all the challenges and adjustments that came with it. They tried not to mention the “D” word or ask too often if I was finally finished. I hope that my example of hard work and perseverance through adversity is something they take forward with them.

I am forever grateful to Bill Kastenberg for pushing for my acceptance to the nuclear engineering program at Berkeley and to Kai Vetter for agreeing to bring me into his research group. Kai has been very understanding of the non-traditional nature of my background as well as the topic that I was interested in researching. He took a risk on me, but I believe he also found value in some of the complementary knowledge, skills, and abilities I brought to the group from my experience in the Army. I would also like to thank Ed Morse for his candid counsel with regards to my research and the splendid class he developed from scratch. His insight into understanding the background radiation distribution jump-started my data collection effort. Likewise, I appreciate the time Rhonda Righter and Claire Tomlin took with me to discuss search pattern optimization ideas.

I would like to thank members of the Nuclear Detection Systems and Algorithms group at Lawrence Livermore National Laboratory for providing me a place to work and for making themselves and their tools available to me. I especially would like to thank Simon Labov for sitting on my oral exam committee and providing me with advice and guidance for my project. Brandon Seilhan and Karl Nelson provided me with sound advice and gave me a better understand some of the software tools that I was planning to use.

My first exposure to the Berkeley Applied Research on the Imaging of Neutrons and Gamma-rays (BeARING) group was quite surprising. The culture of students duking it out in front of the advisor was foreign to me. In the Army, peers generally do not dime each other out in front of the boss. However, as time went on, leading up to my preparation for my oral exam, I learned to appreciate the candid and assertive nature of the members in the group. I am proud to have been a part of such an accomplished group and know that I will cross paths with many of the former members of the group in the future.

Berkeley Lab's Applied Nuclear Physics group is phenomenal. I wish that I would have spent more time up the hill absorbing the knowledge and skills that emanate from 50C. I would be remiss if I didn't thank Andy Haefner, Tenzing Joshi, Ryan Pavlovsky, Brian Quiter, Ross Barnowski, Joey Curtis, Victor Negut, Ren Cooper, Mark Bandstra, Paul Barton, and Dan Hellfeld by name. I also would like to send a special thanks to Erika Suzuki for all of her help throughout my time working with Kai. I must also mention those involved with RadMAP—I am so glad you were not badly injured in the crash, and I am grateful for your willingness to support my research.

For the military students— Brian Champine, Tommy Halverson, John Davis, Drew Gillick, Blake Huff, and James Bevins—I am grateful that we had the opportunity to cooperate and graduate. I don't think I would have made it through some of the courses without your help. I also enjoyed the bond we shared outside of campus and was glad to be part of the family. For those in the Donuts office, thanks for helping guide us through those first few years—we certainly needed it.

I must express significant gratitude to the leadership of the Department of Physics and Nuclear Engineering at West Point for selecting me to come back to teach, giving me the opportunity to earn my Ph.D., and providing me extensive time to complete my dissertation. Thank you to Colonel's John Hartke and Ed Naessens. To the Army's Advanced Civil Schooling program, I give my thanks for your patience and understanding. I realize this is an incredible opportunity, and thank you for the support provided to me over these past five years.

While this research was not explicitly funded by any specific agency, I want to thank the Nuclear Science and Security Consortium for providing travel funding to me on several occasions. I would also like to thank members of the Defense Threat Reduction Agency for agreeing to fund related projects from Berkeley Lab and UC Berkeley. I know you got a significant return on your investment and hope you continue to see the value in efforts like this.

Finally, I would like to reach back and thank some of the people helped me along the way—without them, I would not be where I am today. My parents, Ken and Judy McManus; my siblings, grandparents, aunts and uncles, and my in-laws Greg and Ann Chateauvert. Tony Bartl, Mickey Roman, Maureen Toner, and Con Ryan from high school; Dan Mauro, Jason Meyer, Bruce Rohrbough, and Ryan Seagraves from my time as a cadet physics major; Jim Trimble, Rex Blair, Dave Palazzo, Jeff Spear, Chris Cross, and Jeff Musk as a junior faculty member; Brent Morris, Jason Blais, Jim Campbell, Bill Marshall, Pat Lofy, and many of the former operators from my time at DTRA. There are many more people who have helped develop, educate, and advise me throughout my twenty-one-year career in the Army and others before that—to those unnamed individuals I give my thanks as well.

1 Introduction

The means to remotely and autonomously sense the location and distribution of radiological and nuclear sources across a range of operational environments is a capability that could benefit nearly every field application of radiation detection. The applications for remote radiation detection are not new. For many years, instrumentation has often been accomplished remotely for activities in the nuclear field such as reactor control, weapons testing, spent fuel monitoring, and dosimetry. The aspect of remote radiation sensing that is novel and exciting is the vast improvement in the technology to access dangerous, harsh, denied, extensive, and otherwise complex environments. Unmanned systems, colloquially known as drones and robots, have rapidly matured in both capability and ubiquity over the past 20 years.

Most ionizing radiation detection methods, particularly for gamma and neutron sources, meet the basic definition for remote sensing, in that physical contact with the source is not required. However, the term remote sensing generally refers to the use of satellite- or aircraft-based sensor technologies at standoff distances. While large standoff distances are certainly desired, most operationally relevant scenarios involving radiation sources require source-to-detector distances of no greater than several to perhaps tens of meters. In this study, we use the term remote radiation detection to indicate one or more of the following conditions concerning a radiation source or distribution of sources with regards to the location of a sensor: (1) an operationally significant standoff distance between the source and sensor, (2) the presence of structures or other barriers between the source and sensor, or (3) a significant dissimilarity in the source environment and the environment at the location of the human operator or controller. Remote radiation detection generally assumes far-field application, with possible intervening material such as buildings, walls, or vehicles, and does not require an operator to be co-located with the system.

Unmanned systems are being developed at a rapid pace for military, commercial, industrial, and recreational uses. Improved radiation detection systems and associated imaging and mapping modalities are being mounted on unmanned aerial vehicles (UAVs), unmanned ground vehicles (UGVs), and even unmanned underwater vehicles (UUVs) to produce novel and innovative radiation detection capabilities. These unmanned systems are often equipped with auxiliary sensors that capture contextual information from a scene and measure the position, velocity, orientation, heading, and altitude to a high degree of precision many times per second. The advancement in these two fields presents a unique opportunity to provide significant improvement in source detection, localization, identification, and mapping, thereby delivering real operational value to the radiation detection community of users. While traditional incremental improvements to detector performance characteristics—better energy resolution, improved efficiency, faster timing—play a role in enhancing capability, it is access to the full range of contextual information and the ability to maneuver within a scene that truly advances the state of what is possible for remote radiation detection.

1.1 Background

One does not achieve operational capability by simply mounting a radiation detector to a commercially-available UAV, though that avenue has indeed been pursued. While that approach may provide some limited capability and undoubtedly helps identify the shortcomings of a given system, a detailed analysis of requirements and development of key performance parameters often shortens the spiral development cycle and leads to a better capability. Hence, the objectives of the research presented here are (1) explore the sensor trade space and make recommendations for a real-world operational radiation detection mission, (2) develop methods to optimize collection schemes for unmanned systems, and (3) make recommendations for future inquiries and identify areas for further investment of resources.

Remote access, coupled with radiation detection, is desirable for several reasons. First, a human being does not have to enter or remain in a potentially dangerous, harsh, or otherwise difficult to reach environment. Remotely accessing a radiation area precludes unnecessary exposure and possible contamination of personnel. Beyond avoiding potential radiological hazards, remote access also protects personnel from exposure to the elements (e.g., heat, cold, sun, and rain), as well as potential threats in a hostile or otherwise uncertain situation.

Second, remote access often denotes access to locations that are inaccessible or inhospitable to a human operator. For radiation detection, this can result in significant increases in the signal collection by (1) positioning the sensors closer to locations of interest to increase the detector solid angle, (2) approaching a location of interest from a different vantage point, including from above, to reduce the attenuation by intervening material, and (3) dwelling in a location for much longer than a human operator could remain safely or comfortably to improve statistical confidence. While there are certain locations and situations where a human operator will have better access or operational insight, many radiation detection operations could be performed just as well or better by remote means.

Third, unmanned platforms can reduce the variation in radiation measurements caused by changes in a human operator's speed and path, position and orientation of the detector, and attenuation and scattering generated by the operator's body and equipment. Integrated sensors on UAVs enable finer control of speed, path, height, and orientation. Additional sensors may also be employed to capture 3-D scene data.

Finally, the cost of remote access has dropped considerably, and access has skyrocketed. Just two decades ago, remote access was primarily limited to specialized robotic platforms designed for scientific investigation, explosive ordnance disposal, or avid hobbyists. Now, children are using smartphones to fly sophisticated UAVs in parks and neighborhoods around the world, as in Figure 1.1, which speaks directly to the cost, ease of control, and ubiquity.



Figure 1.1: 11-year-old Ryan McManus pilots a DJI Phantom 3. Source: personal photograph.

The capability to detect, locate, identify, and characterize radiological and nuclear materials using remote sensing platforms is a shared requirement across the many stakeholders in the radiation detection community. This technology has relevance to applications in homeland security and law enforcement, customs and border protection, nuclear power plant activities, nuclear waste monitoring, environmental remediation, and military operations. The primary focus for this investigation is radiation detection in support of military operations.

The choice to focus on potential military applications is threefold. The principal reason is that the author is an active duty nuclear counterproliferation officer in the U.S. Army, with specific knowledge and expertise in radiation detection requirements for the Department of Defense (DoD). His training and prior assignments have given him a robust understanding of the operational tasks, conditions, constraints, limitations, assumptions, capabilities, and risks for the employment of radiological and nuclear search assets.

Next, the overlap between military applications and the functions other entities might have for this technology are considerable. Most often, military applications will have more stringent operational requirements, whereas other governmental or private applications may have more stringent regulatory restrictions. Therefore, as a generalized assumption, operational capabilities that meet the requirements for a given military mission area will also likely meet or exceed the operational requirements of a related civil or commercial application. However, modifications to the system design or concept of operation and employment may be required. For example, law enforcement operations may have additional requirements regarding the chain of custody or privacy restrictions that might not apply to a similar military application. The bottom line is that a detection system that meets the general operational requirements for military applications will tend to meet the operational requirements of most other users as well.

Finally, military applications present the most diverse, challenging, and likely use-cases for this technology. Of interest to this author and related research projects are the following military mission areas: *directed search, battle damage assessment, consequence management, accident response, nuclear contamination avoidance, nuclear forensics, nuclear disablement, and active interrogation.*

1.2 Mission Areas

The following section introduces each military mission area, and the appendix provides further details to include: (1) a historical vignette where unmanned radiation detection assets would have provided considerable value, (2) a summary of the general operational conditions, (3) an assessment of the impact that remote detection might have on the speed, accuracy, fidelity, safety, or feasibility of a given mission, and (4) a brief consideration of the unique challenges that might arise in developing a materiel solution.

Directed Search

Directed search describes operations conducted to detect, locate, identify, characterize, and recover lost or stolen nuclear or radiological material. It is a prominent focus area in radiation detection research and development efforts for the DoD, and arguably across other government agencies as well. This mission area is the primary focus for this research endeavor, and we describe it in further detail in Section 1.3 and in the appendix.

Battle Damage Assessment

Battle damage assessment (BDA) encompasses the estimate of the damage resulting from the application of lethal or nonlethal military force. Traditionally, it is associated with assessing the damage inflicted on a target from a stand-off weapon, such as a bomb or guided missile. Assessments of the physical damage, functional damage, and effect on the targeted systems are made to inform further actions [1]. As an example, the commander's desired effect for a given strike might be physical damage to an underground hangar complex or airfield that prevents an enemy from launching fighter jets for some number of hours. In this case, verification of the depth and placement of craters provides evidence of a functional kill. While the strike has not destroyed any of the fighter jets, the ability to launch them has been delayed long enough to make their threat moot. Alternatively, if the physical damage was not achieved on-target, it may drive the commander to authorize another sortie or to adjust the plan to account for the possible employment of enemy fighter jets.

This principle can also be applied to targets with a nuclear or radiological component. An unmanned capability to detect, locate, identify, and map radioactive or nuclear material would prove useful in scenarios where facilities associated with such materials are targeted. While BDA to some extent is unique to military operations, the radiation detection requirements are likely to be quite similar to that of a civil response to an incident where radiological or nuclear material is explosively spread over an urban or industrial area, such as a dirty-bomb scenario or a nuclear device that fails to achieve a significant nuclear yield, known as a fizzle. For this reason, there is an additional incentive to develop a capability.

Consequence Management

Consequence management comprises those measures taken to protect public health and safety, restore essential government services, and provide emergency relief to governments, businesses, and individuals affected by the consequences of a chemical, biological, nuclear, or high-yield explosive incident [1]. From a DoD perspective, there are several reasons to maintain the capability to conduct nuclear consequence management operations. First, the DoD possesses, operates, and maintains nuclear reactors and weapons that could be the source of the situation. Second, DoD forces could be part of those affected by the consequences of a nuclear incident. Third, the DoD could be called to assist civil authorities with executing measures taken to protect the public, restore services, and provide emergency relief.

Accident Response

The priorities for the DoD response to U.S. nuclear weapon accidents are the location, security, and recovery of the weapon; the protection of lives and property; and remediation of the site [2]. Even though accidents involving nuclear weapons are particularly low occurrence events—just thirty-two documented U.S. “broken arrow” events since 1950—they remain a low-probability high-consequence event, even when taking modern safety design features into account [3]. While the high-alert nature of Cold War–era strategies, particularly Operation Chrome Dome, increased the probability of such events, the estimated 1,750 U.S. weapons that remain operationally deployed is a sober fact that must be taken into consideration when planning a response to mishaps involving special nuclear materials [4]. Some of the tasks where an unmanned capability could prove useful are assessing the extent of the accident site, confirming or denying the release of radioactive material, mapping the radioactive contamination, locating aircraft or missile parts, locating nuclear material or weapons components, and verifying site remediation.

Nuclear Contamination Avoidance

Limited nuclear warfare requires forces, on both sides of the conflict, to be prepared to operate in and cross through a nuclear-contaminated area. A required supporting task is to conduct a terrain-oriented zone or route reconnaissance to plan a route that minimizes the radiation exposure to forces, subject to the constraints of other competing military factors [5]. Current doctrine employs either Chemical, Biological, Nuclear, and Radiological (CBRN) reconnaissance platoons or rotary-wing aircraft outfitted with dosimeters and survey meters. Current generation M1135 Stryker Nuclear, Chemical, Biological Reconnaissance Vehicles (NBCRV) are medium armored vehicles which use readings from a vehicle-mounted beta and gamma probe—the Army-Navy Vehicle or Dismounted Radiac-meter (AN/VDR-2)—that measures dose rate and records accumulated dose [6].

Although the threat of limited nuclear warfare may not be at the top of the list of the most likely conflict scenarios, it remains possible and is a driver of validated materiel requirements within the DoD. The potential benefits of developing an unmanned reconnaissance system for contamination avoidance are numerous: (1) reduce dose to personnel, (2) increase coverage area, (3) avoid terrain limitations, (4) allow CBRN personnel to conduct other missions, (5) lower cost, and others. A UAV could even be launched from an M1135 Stryker NBCRV, as conceptualize later in Figure 5.9.

Nuclear Forensics

Nuclear forensics is the examination of nuclear and other radioactive materials, either pre- or post-detonation, using various collection methods and analytical techniques to determine the composition, origin, age, and history of a material [7, 8]. Arguably the most advanced capabilities in remote sensing of radiation reside within the field of nuclear forensics. Endeavors sponsored by government agencies to develop pre-detonation capabilities focus primarily on nonproliferation and monitoring efforts. Though a nation could decide that it is necessary and prudent to conduct atmospheric testing of their nuclear weapons—which makes forensic collection much easier—the source term for monitoring nuclear testing is generally located deep underground. Very little of the fission products make it out into the atmosphere unless there is a malfunction during the test. Rapidly deployable air collection and measuring systems are required to verify such tests. Such a capability has been demonstrated as a bolt-on pod integrated on a UAV [9].

With regards to post-detonation nuclear forensics, however, we do not possess an advanced capability to collect samples. Should a rogue nation-state or violent extremist organization detonate a nuclear device in the U.S. or within one of our partner-nations, our response policies dictate the collection and measurement of forensic materials from the nearby fallout area to attribute the device or fissile material to a source, especially when it is not readily evident or needs to be confirmed. An unmanned system would have many benefits to this mission area but would also likely have the most stringent constraints. Not only would it need to operate in a complex and high radiation setting, like that of a contamination avoidance mission, it would also need to be capable of excellent specificity and localization in a highly inhomogeneous environment. Current efforts are focused on using swarms of UAVs to characterize a debris field to direct follow-on forces to auspicious collection areas with lower dose rates [10].

Nuclear Disablement

Nuclear disablement includes those operations associated with the assessment and handling of supporting nuclear infrastructure that might be encountered or targeted as part of military actions in a given area of operations. Most likely, this involves the safe shutdown of enrichment or reactor facilities, securing materials not yet assembled as a weapon, and any other tasks that fall into the category of nuclear-related, excluding weaponized or deployed systems [11]. Current capabilities reside in Nuclear Disablement Teams (NDTs)—small military teams (~15 personnel) with specialized training in the operation of such facilities, and a limited amount of hand-operated or vehicle-mounted detection equipment. Due to the uncertain nature of the mission, location, and conditions, most tasks are completed by hand. However, teams usually conduct an initial survey of a facility using either a small, all-terrain vehicle, a vehicle-towed trailer system, or a helicopter, outfitted with a set of large directional gamma and thermal neutron detectors.

A small number of autonomous radiation sensors could prove invaluable for deliberately conducting exterior and interior reconnaissance of the facility. These would relieve a good portion of the NDT members from swinging a meter and free them to use their human sensors—primarily their eyes and ears—coupled with their intellect and training.

Active Interrogation

Active interrogation involves directing neutrons or high-energy photons toward a target and measuring the secondary radiation to gather information about the target. Government agencies have expended tens of millions of dollars or more on active interrogation projects since 2001. Whether the method includes a sizeable bremsstrahlung source, a pulsed neutron source, or some other novel source, such as cosmic muons or a photon beam driven by laser-wake field electron acceleration, they all suffer from one common limitation: the signal they induce, while unique and identifiable, obeys the same inverse square law as the passive signal and is therefore difficult to detect at any operationally significant range [7]. Detectors must be placed close to the target being interrogated to overcome this. One way to accomplish this is by integrating detection elements onboard small UAVs and flying them near the target [12].

1.3 Directed Search Vignette

As noted previously, radiological and nuclear search describes operations conducted to detect, locate, identify, characterize, and recover lost or stolen nuclear or radiological material. Exactly what the term “search” means and implies to different user groups is exceedingly diverse. Therefore, we use the term “directed search” and further define it here.

Directed search is a mission area triggered by a credible threat with potential high consequence. In addition to radiation sensors, search forces possess training and capability to conduct special reconnaissance and direct action. Directed search assumes that law enforcement, security forces, or intelligence functions have confirmed the loss, theft, or possession of radiological or nuclear material of concern by a rogue state or adversarial non-state actor (e.g., individuals, extremist organizations, and non-governmental entities). The type, quantity, total mass, chemical form, and geometric configuration of the material are potentially known or can be approximated. The suspected location of the material has been narrowed to a reasonable-sized search area through intelligence collection and assessment. For directed search, we define a reasonable-sized search area as less than ten square kilometers (e.g., a small town, a large neighborhood or section of a city, or several small villages). Furthermore, light industrial or commercial structures within the search area may be identified as possible sites for material storage, device fabrication, or weapons staging.

Efforts to neutralize attempts to smuggle nuclear weapons or radioactive materials into the country have been ongoing since the advent of the Atomic Age. Fortunately, there have not been any publicly confirmed attempts to locate an improvised nuclear device (IND) or radioactive dispersal device (RDD). However, search teams have been deployed to find lost

or stolen material. One example occurred in 2003 when DoD radiological search assets set out to locate two radioactive capsules stolen by looters from a nuclear testing site located at Saddam Hussein's main battlefield testing center in the desert west of Baghdad [13, 14, 15].

The site, built in the early-1980s, was used to test equipment, and possibly human subjects, in a simulated battlefield radiation environment. Technicians raised radioactive sources on towers arranged in an arc around a test pad. Small metal capsules, each initially containing approximately 370 giga-becquerels (GBq)—10 curies (Ci)—of the isotope ^{60}Co , were stored in concrete containers at the bases of each of the eight 23 m (75 ft.) testing poles [13]. By 2003, the sources had decayed to approximately 10% of their original activity but remained a significant health hazard and possible RDD threat at ~ 37 GBq (1 Ci) each.

According to those with specific knowledge of the mission, finding sources of that strength is “the slow pitch softball” variant of search operations [14, 15]. It was quickly accomplished by mounting a large detector system containing thallium-doped sodium iodide (NaI(Tl)) scintillation gamma-ray detectors and ^3He -filled proportional tube neutron detectors into a military helicopter and scanning the nearby area at low altitude and airspeed [13, 14]. The two sources were found along with remnants of the tower poles—the target of the looting—in two adjacent villages approximately 16 kilometers (10 mi.) north of the testing site [13].

Though this search and recovery operation was swift and successful, changes in the conditions could have made the mission far more difficult. For example, the source strength and primary gamma-ray energies associated with the decay of the ^{60}Co isotope allowed the material to be found from an altitude of more than 100 meters. Suppose instead it was special nuclear material (SNM), secretly hidden from inspectors, that went missing from the Baghdad Nuclear Research Facility. Depending on the material properties, including fissile isotope(s), enrichment levels, impurities, and other factors, the gamma and neutron flux produced by the material could range several orders of magnitude and be much more difficult or nearly impossible to detect from the air.

For this exemplification, assume that the material consisted of weapons-grade (WG) highly enriched uranium (HEU). The International Atomic Energy Agency (IAEA) categorizes 25 kg of HEU as a significant quantity (SQ), which denotes the approximate amount of nuclear material for which the possibility of manufacturing a nuclear explosive device cannot be excluded [16]. Prior to its removal by the IAEA after the 1991 Gulf War, Iraq possessed more than 12 kg of slightly irradiated 93%-enriched uranium fuel purchased from France as part of the Tammuz-2 reactor. They also had more than 13 kg each of both fresh and irradiated 80%-enriched uranium fuel for the Russian-supplied IRT-5000 research reactor [17].

Unlike the ^{60}Co sources, which were found lying in the yard of a house and partially buried in a field near another [13], assume that the value and hazards associated with the stolen SNM were known to the thieves and they kept it in a secure location, such as a non-descript building in Fallujah. The concept of operations calling for a helicopter to fly low and slow to locate the material fall apart quickly. First, the expected radioactive signature from the material would be undetectable above background, even at the lowest operating altitude and speed of

a helicopter, except for perhaps hovering directly above or landing on the roof. Second, the geographic area that the cobalt sources were recovered from was semi-permissive during the operation; i.e., the villagers, while not completely forthcoming with details regarding the missing material, were not actively hostile towards U.S. forces at the time. Had operations taken place later in the conflict, those villages at the southern end of the so-called Sunni triangle may have been much more hostile, thereby precluding the low and slow flight of a manned helicopter and compelling a much larger security presence. Third, the presence of a helicopter flying a search pattern over buildings would certainly trigger apprehension in the minds of those possessing the material, prompting them to flee the area or to shield the material if they were working with it at the time.

1.4 Summary

The identification of capability gaps and the prospect of filling one or more of them is the primary motivation for this research project. It appears that the technology is available and the tools to engineer a solution exist. There are several mission areas that could benefit from an unmanned approach to radiation detection. The intent is to get detectors out of the hands and off of the backs of warfighters and move them closer to the sources of interest. For one specific directed search scenario, it is a matter of systematically analyzing the threat-space and developing a solution to overmatch it. Hence, the goals of the research presented here are (1) assess current capabilities for directed search and substantiate the improvement that an unmanned approach would provide, (2) expand the understanding of the background radiation environment to include building rooftops, (3) establish system requirements and map out the trade space based on an analysis of current sensor and platform capabilities, (4) investigate and optimize search methods, and (5) identify and characterize additional mission areas for further investigation.

Given the realities discussed in this chapter, the conditions for high-consequence directed search operations involving SNM require pushing detectors as close to the source location as possible while not tipping off the adversary to one's actions. To that end, a remote sensing platform that can be flown, dropped, or launched to a location is an attractive solution to reduce the risk to personnel and equipment. As such, a modest collection of small unmanned aerial systems (sUAS) outfitted with radiation detectors coupled to contextual sensors could meet those requirements for an estimated \$2 million (see Section 5.2.4 for analysis).

UAVs can fly much closer to buildings and could perhaps land on them undetected. Reducing the distance between potential sources and sensors allows one to use smaller and more sophisticated detectors to achieve equal or better sensitivity, but with higher specificity. Moreover, the reduction in risk across-the-board is unparalleled. Not only are several warfighters and millions of dollars of equipment removed from a potentially high-risk situation, but the risk to mission compromise via adversary tip-off is conceivably reduced.

Of course, there are engineering challenges that must be overcome and trade-offs that need to be weighed when designing such a system of systems for this application. Considerations

for this mission area are the primary focus of the research conducted and presented in this work. The two chief concerns are the optimization of the sensor package and the development of the search method. The choice of detector materials, the quantity and arrangement of detector elements, and the selection of auxiliary sensors are paramount in developing a system that can detect relevant threats under a given set of conditions. Beyond that, the effective employment of a group of systems requires detailed analysis of individual search patterns, collective coverage schemes, and cooperative detection algorithms.

The other mission areas introduced in this chapter and described further in the appendix illustrate various conditions that might dictate a different approach than that of directed search. However, there are likely to be overlaps and synergies that exist between several missions that would permit adaptable or modular multipurpose design approaches that employ the same or similar unmanned platforms, sensors, search schemes, or algorithms.

2 Motivating Exemplar

The customary health physics principles for radiation protection—time, distance, and shielding—are applied inversely for most radiation detection applications. That is, one should aim to maximize the collection time, reduce the source-to-detector distance, and minimize the material between the source and the detector. With those principles in mind, this chapter compares three different detection schemes for a directed search scenario [18].

As described in Section 1.3, a directed search scenario involves tracking down radiological or nuclear material that is known to be lost, stolen, or otherwise possessed by some entity. One knows the material characteristics or can reduce it to a limited range of possibilities. Intelligence assets have narrowed the search area to a tractable-size and identified target locations within the search area. For this illustration, one can assume that analysts have identified several light industrial buildings as targets, each with a footprint of approximately 10,000 ft² or less.

2.1 Detection Schemes

The three search modes presented for this example are vehicle-mounted standoff detection, rotary-wing aerial detection, and sUAS-based remote detection. The principal goal of this comparison is to highlight the theoretical reduction in detector size possible to achieve the same signal-to-noise ratio for a given detector material. Aspects such as cost, size, availability, and complexity, which factor into the overall efficacy of a given technique, are evaluated as well.



Figure 2.1: Representative detector platforms for comparison. (left) Lawrence Berkeley National Laboratory's (LBNL) Radiological Multisensor Analysis Platform (RadMAP). Source: [19] used with permission from J. Curtis and V. Negut. (center) The National Nuclear Security Administration's (NNSA) rotary-wing Aerial Measurement System (AMS). Source: [20] used with permission from P. Wasiolek. (right) LBNL's prototype Localization and Mapping Platform (LAMP) mounted on a small, commercial unmanned aerial vehicle (UAV). Source: [21] personal photograph.

Representing mobile standoff detection is Lawrence Berkeley National Laboratory's (LBNL) specialized box truck that is known as the Radiological Multisensor Analysis Platform (RadMAP). It employs 100 square ($102 \times 102 \times 51$ mm) NaI(Tl) detectors in an imaging array, and 14 large-area ($85 \text{ } \varnothing \times 30$ mm) mechanically cooled high-purity germanium (HPGe) detectors [22]. The Naval Research Laboratory developed the original system, previously called the Mobile Imaging and Spectroscopic Threat Identification system [23]. LBNL personnel upgraded some of the detectors and contextual sensors used to reconstruct the scene as the system travels. They have collected terabytes of mobile data from the Bay Area and elsewhere [24].

The helicopter depicted in Figure 2.1 exemplifies aerial detection. It is part of the National Nuclear Security Administration's (NNSA) rotary-wing Aerial Measurement System (AMS). AMS generally employs 12 large ($51 \times 102 \times 408$ mm) NaI(Tl) detectors in the belly of the aircraft. AMS also employs fixed-wing aircraft and has experimented with advanced detectors and externally mounted pods.

The UAV depicted in Figure 2.1 is a commercially-sourced DJI Matrice 600 Pro. LBNL personnel outfitted it with a prototype payload known as the Localization and Mapping Platform (LAMP), which is a state-of-the-art system for remote detection. LAMP has a scanning laser light depth and ranging (LiDAR) sensor, several inertial measurement units (IMUs), a binocular camera, and onboard scene data fusion processing. The base platform is detector agnostic; in this case, operators mated four small ($25.4 \times 25.4 \times 51$ mm) thallium-doped cesium iodide (CsI(Tl)) detectors in a self-occluding array. In other incarnations, researchers configured LAMP with better energy resolution detectors such as cerium-doped lanthanum bromide ($\text{LaBr}_3[\text{Ce}]$), cerium-doped cesium lanthanum lithium bromo-chloride (CLLBC[Ce]), cadmium zinc telluride (CZT), and even an HPGe imager.

The key aspects that drive the signal-to-noise ratio are collection time, source-to-detector distance, and attenuation due to intervening materials. Therefore, assumptions are made to establish operational boundary conditions for this analysis. The following sections explore each technique sequentially and provide a consolidated list of attributes in Table 2.1.

2.1.1 Vehicle-mounted Standoff Detection

The vehicle-mounted standoff detection technique consists of mounting large detectors in a vehicle ranging in size from a large sport utility vehicle (SUV) up to a semi-trailer truck. Often, search teams use thermal neutron proportional tubes in conjunction with NaI(Tl) crystals coupled to photomultiplier tubes. Teams have also evaluated developmental systems consisting of several mechanically cooled HPGe semiconductor crystals. For the SUV end of the size spectrum, operators can fit several (2–8) NaI(Tl) logs ($51 \times 102 \times 408$ mm) and thermal neutron detectors; for a large box truck, on the order of 1 m^2 of NaI(Tl) detector area is reasonable. With the HPGe approach, a much smaller total detector area is achievable, though the improved energy resolution may provide an overall improved detection capability. Four to eight large-area ($85 \text{ mm } \varnothing \times 30 \text{ mm}$) HPGe detectors are feasible for a passenger vehicle,

and researchers deployed 48 detectors in a semi-trailer truck [23].

The operators of the search vehicle must investigate the building from a position as close to the building as possible without arousing suspicion. Therefore, we assume that the vehicle must drive by or around the building, or perhaps due to some ruse stop for a period near the building. From this information, we can deduce a range of distances, collection times, and intervening materials.

Regarding distance, we assume the source to be somewhere inside of the building, and the building is some minimum distance from the road. In the best-case scenario, searchers can examine the building from each side, and the source is located near an external wall. Given such a fortunate layout, the closest approach would be on the order of 5–7 m, considering the likely size of the easement between the road and the building. However, this highly favorable set of conditions is incredibly unlikely. It is more likely that the search team can only approach the building from one or two sides, and the source could be located anywhere inside. A more representative distance would be the midpoint of the building, with the worst case occurring when a source is located opposite the approachable wall of the building. Therefore, we assume the distance of closest approach ranges 5–35 m, with an expected value of 20 m.

As to the dwell time, the value depends on the speed of the vehicle and the integration time chosen. In general, an appropriate integration time is chosen to maximize the signal to background ratio. The integration time which maximizes such a ratio (see in Figure 6.4) is

$$t = \frac{2d}{|v|}, \quad (2.1)$$

where d is the distance of closest approach, and v is the speed of the vehicle. There are some factors which call for deviations from this, such as the shape of the detector (cylindrical versus parallelepiped) and arrangement scheme with regards to the source. One can assume that the vehicle will travel as slow as possible in the target area and make multiple passes or stop in locations near the building, if possible. Nominally, a slow pass by at 40 kph (25 mph) would call for a 5-second integration window. Assuming the best-case scenario, such as when the team can park near the building or one in which they employ a flat tire or similar ruse, the integration time could be considerably longer—on the order of many minutes or even hours. However, if we presume a more typical scenario, where remaining undetected by the adversary is essential, we expect the upper limit for collection time to be 60 s. Therefore, we assume the dwell time ranges 5–3600 s, with an expected value of 60 s.

Finally, we must consider the material between the source and the detector that attenuates the signal. While building construction varies considerably [25], the critical assumption we make is that target locations are most likely to be light industrial or commercial. More than 70% of buildings worldwide have exterior walls constructed from masonry [26]. Many low-rise commercial or industrial buildings are erected using concrete masonry units, also known as cinder blocks. Tilt-up concrete construction is a competing method of construction which uses poured concrete walls which are then raised to the vertical position and braced into position. Tilt-ups account for an estimated 15% of all low-rise commercial and industrial new

construction and is most common in North America, Australia, and New Zealand [27]. Regardless of the method assembly, the primary attenuating material is concrete.

While cinderblock construction generally involves reinforcement with rebar and poured concrete in the gaps, some gaps will inevitably remain, reducing the amount of attenuating material between the source and detector. Depending on the construction technique, the amount of concrete could be as little as 5 centimeters, if unfilled, all the way up to 20 cm if filled with concrete, and perhaps even more if for a custom application. Tilt-up construction tends to be slightly thinner than cinderblock construction [28].

There also may be additional attenuation by interior walls and other materials, as well as the air. However, compared to the attenuation by the concrete, the air attenuation is negligible, and the attenuation from other building materials (e.g., sheetrock, wood, metal studs) is a small fraction of the total. Note that the attenuation is a function of the energy of gamma-ray(s) emitted by the source. Because the attenuating materials have different densities and thicknesses, it is convenient to convert the attenuating factor to an effective atomic number and areal density. The effective atomic number is dependent on photon energy [29] but has a value between 9 and 10 from 100 to 3000 keV. Therefore, we assume the attenuation factor has an effective atomic number of 9.5 and a range of areal density 10–50 g cm⁻², with an expected value of 30 g cm⁻².

2.1.2 Rotary-wing Aerial Detection

The rotary-wing aerial detection technique is similar to the vehicle-mounted standoff approach in that it also consists of mounting large detectors, either inside the helicopter or attached to external pylons. The primary differences between the two methods are the source-to-detector geometry and vehicle speed. The aerial approach generally has a larger standoff and shorter collection time. However, we can expect less attenuation due to the differences between roofing and wall materials. The helicopter also presents a much larger signature to a potential adversary; i.e., helicopters flying low and slow certainly draw the attention of nearly everyone within earshot and are generally a rare event in most environments. It is also challenging to stage a ruse that would allow the helicopter to hover or repeatedly pass near a target area. That said, it remains a capability, and we will present it for the sake of comparison and completeness.

Concerning the distance of closest approach, one must assume a height above ground level (AGL) which allows the helicopter to avoid obstacles such as power lines, communication towers, and tall buildings. In aviation regulations, 150 m (500 ft.) AGL is considered a safe distance in populated areas, with that same distance measured linearly from any person, vessel, vehicle, or structure in sparsely populated areas. However, one can assume that a search situation presents exigent circumstances that would reduce this height to something much lower. For example, a target operating AGL of 90 m was published for flights in Berkeley, CA in 2012 by the NNSA's AMS team [30], and an AGL as low as 70 m was recorded in near Richmond, CA during test flights conducted in 2015 under the Airborne

Radiological Enhanced-sensor System program sponsored by the Domestic Nuclear Detection Office of the U.S. Department of Homeland Security [31, 32]. One can imagine that in actual search operations, this height could decrease to as low as possible, for the surrounding conditions near the target building. Therefore, we assume the distance of closest approach ranges 10–150 m, with an expected value of 45 m.

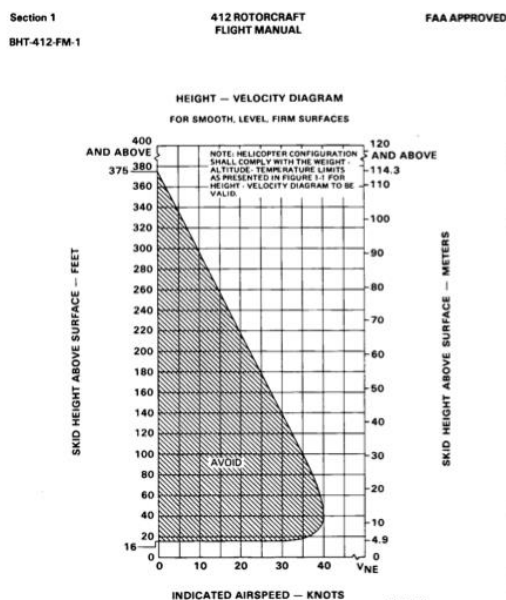


Figure 2.2: Height-Velocity diagram for Bell 412 multi-engine helicopter. Pilots must maintain a minimum velocity at a given height in order to retain the ability to land via an autorotation maneuver in the case of engine failure. Source: [33] used with permission from S. Myers and J. Sams at Bell Textron Inc.

As to collection time, the minimum safe speed of the aircraft is a function of its height. Rotorcraft have a safe height-velocity relationship known as a Deadman’s curve. As shown in Figure 2.2, pilots must avoid the shaded portion so that they can overcome a loss of power due to the failure of the engine or transmission by conducting an autorotation maneuver. Based on the expected aircraft height, the slowest airspeed safely permitted is ~30 knots, according to Figure 2.2. This airspeed gives an ideal integration time window of ~8.5 s. The ARES test consisted of flying at approximately 35 m s^{-1} (68 kts) which gives an ideal integration time window of 2–12 s, depending on the altitude. A reasonable low-end speed for a helicopter is on the order of 10 m s^{-1} (20 kts), which would expand the integration time window to more than 40 seconds. This low-speed does not include the possibility of a hover maneuver, which could push the collection time up to several minutes or longer, though at that point any semblance of maintaining a low profile has undoubtedly been forfeited. Therefore, we assume the collection time ranges 2–300 s with an expected value of 7 s.

Regarding attenuating material, this approach is much different from the vehicle-mounted approach since most roofs are not made of concrete. Most light industrial and commercial buildings have thin roofs consisting of a metal deck, a layer of insulation suitable for the

climate, a layer of wood or particleboard, and a waterproofing material. At low energies (150–200 keV) the attenuation factor ranges approximately 10–50%, primarily due to the gauge of steel used and thickness of insulation. Because of the variation in roof construction, it is useful to reduce this to an effective atomic number and areal density. One must also account for the attenuation effects of air because of the considerable distance. Consequently, we assumed the attenuation factor has an effective atomic number of 6.33 and areal density range 2–15 g cm⁻², with an expected value of 10 g cm⁻².

2.1.3 sUAS-based Remote Detection

The sUAS-based approach is quite different from the other two approaches because of the limited detector size and weight that can be employed. Large format NaI(Tl) crystals, as well as most mechanically-cooled HPGe detectors, are too massive to be carried by a typical multi-rotor unmanned aerial vehicle. While there are oversized UAVs that can carry additional weight and specialized systems that make use of small HPGe detectors, we assume that much smaller detectors are necessary for this approach. However, we can overcome some of the shortcomings in detector size by using arrays of high-resolution, room-temperature semiconductor detectors, such as coplanar grid CZT. Moreover, we expect the overall gain in the source signal—due to increased collection time, reduced source-to-distance, and reduced shielding—to outweigh the losses in efficiency due to smaller detectors.

In terms of distance, an sUAS-based detector can inspect a suspected source location from the shortest distance of all three methods. It can take measurements from just outside the walls of the building as well as at locations on the rooftop. Since the rooftop presents a much lower observable signature, it is the preferred inspection location, and we will use its height to determine source-to-detector distances.

In general, most light industrial and commercial buildings are single-story and ~5 m tall. Less than 20% of the buildings worldwide are more than four-stories tall. Therefore, assuming the source is located inside the building, the minimum source-to-detector distance from the roof is no more than the roof height. The distance between measurement locations drives the maximum source-to-detector distance. A general rule of thumb for this spacing is twice the height of the building. This grid distance would give a maximum source-to-detector distance equal to the building height scaled by the square root of two. Therefore, we assume the source-to-detector distance ranges 3–17 meters, with an expected value of 5 meters.

The collection time is also very advantageous for this scheme. While there are indeed power constraints both for the detectors and sUAS platform, a system could surely collect for minutes to hours on the roof during a period of darkness. The limiting factor is the number of measurement locations for a given building, which we could partially overcome by using multiple systems or even a suite of emplaced detectors. Therefore, for reasonable coverage of a representative-sized building, 30-minute measurements are possible. Moving to multiple platforms (e.g., six systems) runs the collection time up to 180 minutes per location. Furthermore, if the detector systems were designed to be delivered to, left on the roof, and

perhaps recovered by the sUAS, then that collection time could be expanded to multiple days. Assuming one period of darkness to collect and make a decision, we assume the collection time be 15–180 minutes, with an expected value of 30 minutes.

Like the rotary-wing aerial detection technique, this concept takes advantage of the path with least unintentional shielding between the detector and the potential source. Like the previous method, the roof construction will vary and consists of the same heterogeneous layers. Therefore, the assumed attenuation factor has an effective atomic number of 6.33 and areal density range 2–15 g cm⁻², with an expected value of 8 g cm⁻². The primary differences from the rotary-wing aerial detection technique are the improved source-to-detector distance, coupled with the reduction in air attenuation.

Although not treated in this example, the addition of external shielding to a source is certainly a possibility and is expected for most threat sources, either because of their high value and requirement to shield from detection, or because of the hazard to health that they pose. Though not a rule, shielding is often thickest in the horizontal direction and least effective in the vertical direction. That is, shielding is applied to reduce the flux to occupants in a room or would-be searchers in the same two-dimensional plane. However, shielding in the vertical direction is often a secondary consideration, which could benefit measurements taken from above.

Summary Boundary Conditions for Detection Schemes

Table 2.1: Estimated attributes for three possible detection schemes employed to interrogate a targeted light industrial building for the presence of radiological or nuclear material.

Attribute	Standoff Detection (Box Truck)	Aerial Detection (Helicopter)	Remote Detection (sUAS)
Dwell Time	Tens of seconds (5–3600 sec)	Seconds (2–300 sec)	Hours (up to 8 hrs)
Distance of Closest Approach	Meters (5–35 m)	Tens of meters (10–150 m)	Meters (3–17 m)
Unintentional Shielding	Z=9.5 $\mu/\rho=10\text{--}50\text{ g cm}^{-2}$ Concrete (5–20 cm)	Z=6.33 $\mu/\rho=2\text{--}15\text{ g cm}^{-2}$ Steel (1– 2 mm) Wood (~1 cm) Insulation (5–10 cm)	Z=6.33 $\mu/\rho=2\text{--}15\text{ g cm}^{-2}$ Steel (1– 2 mm) Wood (~1 cm) Insulation (5–10 cm)
Cost	Millions (\$1–3.5M)	Millions (>\$7.5M)	Tens of thousands (~\$50k)
Size	10 m length	17 m length	< 1 m diameter
Weight	Tons (>13,000 kg)	Tons (3300 kg)	Kilograms (1.5–25 kg)
Detector Area	> 1 m ²	$\sim\frac{1}{2}$ m ²	50 cm ²

2.2 Theoretical Performance for Notional Conditions

Minimum detectable activity (MDA) is a useful figure of merit to compare these three methods. Using the MDA attainable with the biggest and best detectors in vehicle-mounted standoff detection technique, one can extrapolate to an approximate size detector to achieve the same MDA associated with the conditions expected in the other two methods. Static collection scenarios with ^{137}Cs as the source (i.e., a stationary vehicle, hovering helicopter, and rooftop sUAS) and standard NaI(Tl) detectors are used to simplify the calculation and facilitate a comparison using simulation.

We used a form of the often-quoted ‘‘Currie Equation’’ [34] to calculate the MDA

$$\alpha = \frac{4.653\sqrt{Bt} + 2.706}{f \epsilon_{int} \frac{A}{4\pi d^2} t}, \quad (2.2)$$

where α is the minimum detectable activity in becquerels, B is the background count rate, t is the collection time, f is the radiation yield per disintegration, ϵ_{int} is the intrinsic detection efficiency at a given gamma-ray energy, A is the detector plane frontal area visible to the source, and d is the source-to-detector distance.

Table 2.2: Calculated minimum detectable activity (MDA) of ^{137}Cs based on thallium-doped sodium iodide NaI(Tl) scintillation gamma-ray detectors and assumed parameters for three different detection schemes.

<i>Detection Method</i>	<i>Detector distance (m)</i>	<i>Collection time (s)</i>	<i>Transmission factor</i>	<i>Detector Area (cm²)</i>	<i>Intrinsic efficiency</i>	<i>Background counts near peak (s⁻¹)</i>	<i>MDA (μCi)</i>
Vehicle-borne	20	60	0.25	10,000	0.10	300	67
Rotary-wing	45	60	0.90	5,000	0.10	150	133
sUAS-based	5	1800	0.90	50	0.10	1.5	3

While it should not come as a surprise, it is strikingly evident just how much improvement comes with pushing detection capability as close to the likely source location as possible. Moreover, the approach that achieves the closest source-to-detector distance also permits the longest signal collection time through the least amount of attenuating material.

In general, energy resolution provides significant improvement in detection sensitivity by reducing the width of the full-energy peak. Sharper peaks stand out above the average background count rate, which reduces the MDA further. Though advanced approaches take the full-spectrum into account, an improved energy resolution will also improve performance by enhancing the capability to identify characteristics of the scattering environment.

Solid-state material such as CZT and HPGe provide excellent energy resolution for a cost. Switching to HPGe detectors from NaI(Tl) in the vehicle-borne system would cost a factor of 25 times more for the same detector area. However, if we assume that we are willing to spend twice the cost of the NaI(Tl) detectors, approximately 14 HPGe detectors could be employed, improving the MDA by ~40%. However, as seen in Figure 2.3, diminishing returns are quickly realized for this specific scenario; 5 detectors are required to achieve the same MDA, and 14 almost buys only a twofold improvement at twice the cost. Since the MDA is proportional to the inverse square root of the number of detectors, another twofold reduction in MDA will require four times the number detectors.

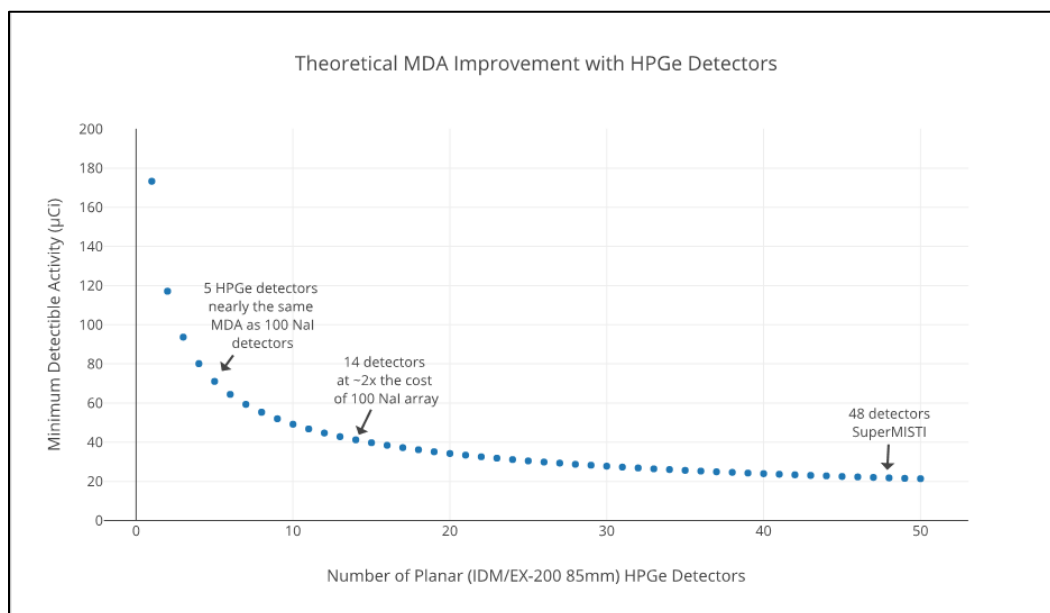


Figure 2.3: Effect of additional high-purity germanium detectors on the minimum detectable activity (MDA) of ^{137}Cs source in a vehicle-borne scenario.

As seen in Table 2.3, achieving the same MDA as fourteen large, HPGe detectors in the vehicle-mounted standoff detection method—which costs on the order of \$1M—is accomplished in just 400 seconds with only one cubic centimeter of CZT—costing about \$10k—in the sUAS-based remote detection concept. Furthermore, one could array several CPG CZT detectors together to push the MDA down even further.

Table 2.3: Calculated minimum detectable activity (MDA) for ^{137}Cs based on fourteen high-purity germanium (HPGe) detectors in vehicle-borne scheme versus one cadmium zinc telluride (CZT) detector in a small unmanned aerial system-based scheme.

<i>Detection Method</i>	<i>Detector distance (m)</i>	<i>Collection time (s)</i>	<i>Transmission factor</i>	<i>Detector Area (cm²)</i>	<i>Intrinsic efficiency</i>	<i>Background counts near peak (s⁻¹)</i>	<i>MDA (μCi)</i>
Vehicle-borne HPGe	20	60	0.25	800	0.2	2.5	42
sUAS-based CZT	5	400	0.90	1	0.08	0.25	42

2.3 Summary

This chapter explored the effects of time, distance, and shielding on radiation detection using the best-in-breed NaI(Tl) systems for three different approaches to directed search. We developed boundary conditions for each of the factors affecting signal collection pertaining to each method and suggested expected values based on our analysis of the environment and system attributes. We compared theoretical performance for these notional conditions by calculating an MDA for ^{137}Cs . Then we expanded the analysis to semiconductor detectors to estimate the realm of the possible. Though moving to HPGe required just $1/20^{\text{th}}$ of the number of NaI(Tl) detectors for the same MDA, we found that improving the MDA to levels commensurate with the sUAS-based approach was not achievable even with an exorbitant number of detectors. Furthermore, we demonstrated the relative effectiveness of a small amount of high-resolution CZT placed close to the source compared to a much larger amount of HPGe at a greater distance.

Even so, the goal of the research presented here is not to replicate the capabilities of a given detection system and its associated concept of operation. Rather, it is to explore the ways and means to optimize the capabilities of a system of systems, which include a suite of radiation detectors, auxiliary sensors, unmanned vehicles, and an associated concept of operations, to meet or exceed the requirements of a given radiation detection mission area. The assessment presented here merely serves as a proof of concept to demonstrate the feasibility and potential utility of the approach within a set of expected boundary conditions. The remaining chapters add further detail and stretch those conditions in order to maximize the operational value of a future system.

3 Radiological and Nuclear Threat Detection

Designing a tool to aid in the search for lost or stolen radiological or nuclear material requires a systematic decomposition of the expected operational environment. We described the mission and general conditions in Section 1.3 and further explored the target building in Section 2.1.3. From that information, one can then predict background signals, identify relevant detectable signatures, establish collection modalities, select appropriate sensors, and develop an effective employment strategy. This chapter aims to compile and classify the radioactive and alternative signatures associated with radiological and nuclear threat materials and outline various methods to detect those signatures.

3.1 Radioactive Signatures

Any effort to remotely sense radiological or nuclear material—for detection, localization, mapping or otherwise—requires knowledge of the signatures exhibited by the material of interest as well as the background and nuisance signatures that are found in the environment. This section explores the radioactive signatures emitted by background sources and threat materials.

3.1.1 Background radiation

Background radiation is found everywhere and varies by location based on factors such as geology, altitude, and latitude. The sources of natural background radiation are often divided into two categories: cosmic and terrestrial. There are also artificial sources of radiation found in the environment from human activities that are considered part of the background. This section contains a brief description of the three primary sources of background radiation and the effects each has on field-detection.

Cosmogenic

Stars—including our sun—supernovae, and other galactic objects produce charged ions called cosmic-rays that continuously bombard the Earth’s atmosphere. Cosmic-rays are the primary source of neutrons found in the background environment [35] and also create cosmogenic radionuclides, such as ^{14}C , ^3H , ^7Be and others, in the air and ground [7]. Proximity to dense, large masses of metal—such as bridges, buildings, and ships—can deliver an enhanced production of cosmic-ray-induced spallation neutrons that is 2–4 higher than usual, through a phenomenon known as the ship effect [35, 36].

Latitude and altitude are the two main factors that influence the intensity of cosmic background radiation for a given location [35]. It also varies temporally with diurnal time, earth’s sidereal position, and the solar cycle [37]. Cosmic-ray intensity increases from the equator to the poles by about a factor of two. The variance is most significant at 20–50°

geomagnetic latitude and is nearly constant over 0–15° and 60–90° [38]. As discovered in the early 20th century by Erich Regener and Georg Pfozter, the cosmic-ray flux increases exponentially with altitude, up to a maximum at about 15 km above sea level [39]. The similarities between the maps in Figure 3.1, depicting cosmic-ray exposure and topography, indicate a strong correlation with elevation.

High-energy primary cosmic-rays—predominantly protons (>85%), some alpha particles (5–12%), few electrons and positrons (~2%), and very few heavier nuclei (~0.5%)—collide with atoms while traveling through the atmosphere, thereby ejecting high-energy neutrons and protons, electrons and photons, and other exotic cascade particles such as pions and muons [37, 40, 41]. Primary cosmic-rays and the cascade particles they liberate that reach the surface of the earth are known as terrestrial cosmic-rays. The typical threshold energy to produce terrestrial cosmic-rays is above 1 GeV. Primary particles comprise fewer than 1% of the total shower of particles that reach the ground; rather, third- to seventh-generation cascade particles dominate the terrestrial cosmic-ray flux. By sea level, cascading collisions convert 97% of the primary cosmic-ray flux into cosmogenic neutrons [37].

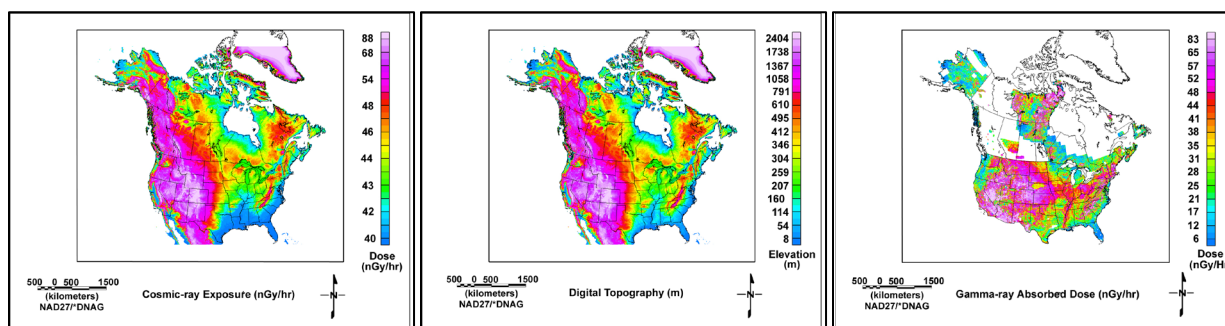


Figure 3.1: Side-by-side comparison of (left) cosmic-ray exposure, (middle) elevation, and (right) absorbed dose from terrestrial sources. Source: [42] U.S Geological Survey in the public domain.

Terrestrial

Terrestrial radiation primarily comes from three elements formed in primordial synthesis; they are potassium, thorium, and uranium—commonly referred to as KUT [43]. Those three elements have four long-lived isotopes that have been decaying since the formation of the Earth but are still present in large quantities because of their long half-lives [44]. The primordial radionuclides are ^{40}K , ^{235}U , ^{238}U , and ^{232}Th .

The decay of these radionuclides and their progeny contributes to more than 90% of the radiation exposure due to natural sources and comprises roughly half of the equivalent annual dose to people in the United States [45, 46]. Most of the dose comes from the daughter products radon and thoron, which are gases that can seep from ores into the air or water and then are taken up into the body through inhalation or ingestion [47].

Anthropogenic

Artificial background radiation from human activity comes primarily from four sources: nuclear weapons, nuclear reactors, industrial sources, and medical applications. The information presented in this section is summarized from [48]. Atmospheric nuclear testing introduced a significant amount of radioactive contamination into the environment while it took place in the mid-20th century. At its peak in the 1960s, the gamma-ray dose in Richmond, CA, as estimated from fission product deposition from the fall-out, was more than 0.14 mSv yr⁻¹ [49]. This has since dropped to less than 5% percent of that (~0.006 mSv yr⁻¹) principally due to the decay of the shorter-lived isotopes. The estimated total effective dose commitment worldwide from atmospheric nuclear testing is 3.5 mSv [50]. In the U.S., the estimated cumulative deposition of global fallout of ¹³⁷Cs ranges 1000–10,000 Bq m⁻² with most locations falling somewhere in the middle of that range [51].

The operation of nuclear reactors introduces radiation into the environment through four main pathways: normal discharges from power plants, spent fuel storage and waste disposal, nuclear fuel production, and nuclear accidents. Discharges from power plants give rise to low radiation doses and contribute less than 0.005% to annual public exposure by radiation sources. Spent fuel storage and waste disposal are isolated and contained. Exposure from them should not extend beyond the perimeter of a facility unless there is an accident or improper disposal. The nuclear fuel cycle causes increased background radiation from uranium mining and milling operations. The residual tailings contain elevated levels of natural radionuclides at higher concentrations than when they resided in the ground as ore.

Nuclear reactor accidents, including Three Mile Island, Chernobyl, and Fukushima, have contributed a collective effective dose of almost 450,000 person-Sv. Some studies estimate Chernobyl fallout to have contaminated more than 162,000 km² in Europe with ¹³⁷Cs to a level above 37,000 Bq m⁻², and an area approximately 19,000 km² in Belarus, Russia, and Ukraine to a level > 185,000 Bq m⁻² [50]. The discharge of ¹³⁷Cs from the Fukushima Nuclear Power Plant significantly contaminated the soil around the facility and neighboring prefectures to levels greater than 100,000 and 10,000 Bq m⁻², respectively [52]. However, the relative contribution of global fallout from nuclear testing and nuclear accidents to background radiation in most locations is minor. Long dwell measurements using high-energy-resolution instruments are required to detect it.

Industrial sources are employed for a wide array of applications including sterilization, radiography, instrument illumination, geological characterization, and measurement gauges. These sources are usually contained within significant shielding when not in use. Some consumer goods like smoke detectors and watch dials contain small-activity sources as well. Certain industrial processes produce increased concentrations of naturally occurring radioactive material in their products, by-products, and waste. These include several activities related to the extraction and processing of ores, coal, oil, gas, metal mining, ceramics, phosphates, and other industries. The fly ash from the burning of coal for electricity is a prime example; it has ten times the concentration of uranium and thorium found in coal and ends up

in roads, buildings, and landfills [53].

Medical applications include radiology, nuclear medicine, and radiation therapy. Sources from medical applications contribute to the background environment via the patients receiving treatment or during transportation to and from hospitals and clinics. Some short-lived isotopes are ingested for functional imaging, while others can be used to treat diseases. A few radiation therapy treatments involve placing sealed sources in a patient for some time. In many cases, radiation levels near the patient are noticeably above the background for days or weeks.

Orphaned sources from medical and industrial uses sometimes end up in the scrap metal trade and have been detected in construction materials as well as some consumer goods. On a few occasions, large-activity orphaned sources have been the cause of extensive contamination and exposure to the public because they were not stored or disposed of properly and were later mishandled by untrained and unsuspecting personnel.

3.1.2 Threat Materials

The signatures that are of most interest for directed search operations are the gamma-ray and neutron radiation associated with threat materials. Threat materials include fissile isotopes that could be fabricated into a nuclear device or large-activity industrial sources which could be employed in a radiological dispersal or radiological exposure device (RED) [54].

Fissile Threats

Uranium and plutonium are the two primary nuclear materials of interest because they are the most common materials found in nuclear devices as well as nuclear reactor fuel. There are also novel threat materials such as americium and neptunium, but their scarcity and cost make them far less likely to be encountered as a threat material. The most measurable signatures of each element include gamma-rays associated with the radioactive decay of the substance and daughter isotopes, neutrons released in spontaneous fission, gamma-rays resulting from the capture of neutrons in surrounding materials, and impurities inherent to the material or due to processing. Each signature will be further explored and defined with the associated threat material.

Uranium

Uranium is found everywhere throughout the world in the earth's crust, at an average concentration of 2.8 parts per million. It is mined or chemically leached from areas where the formation of uraninite, also known as pitchblende ore, is high or often as a by-product of mining other metals, such as copper, gold, silver, and vanadium. The ore is mined, milled, and chemically converted into a compound that is suitable for enrichment, normally uranium hexafluoride, and then further converted into a different compound for use as a nuclear fuel or weapon component [55]. The radiation signature of uranium depends on the isotopic composition, compound form (e.g., metal, oxide, fluoride, ceramic), and geometry (e.g., ball,

foil, pellet, rod). Natural uranium is predominantly ^{238}U (99.275%) with a small percentage of ^{235}U (0.720%) and a trace amount of ^{234}U (0.005%) [56].

Though ^{238}U is a chief component of background radiation, substantial quantities could present a detectable signature and possibly indicate the development, fabrication, or assembly of an IND. Depleted uranium, also known as DU or enrichment tails, is the by-product material from a ^{235}U -enrichment process and is typically 99.78% or more ^{238}U . It is a very dense material (1.7 times that of lead) and is used in armor plating, armor-piercing munitions, ballast in aircraft and ships, radiation shielding, and as a component of nuclear weapons [56]. ^{238}U ($t_{1/2}=4.468$ billion years) has associated gamma-rays with energies 742.81, 766.36, 786.27, and 1001.03 keV that result from the decay of $^{234\text{m}}\text{Pa}$, a meta-stable daughter in the uranium decay chain, shown in Figure 3.2 [57]. The key signature is the gamma-ray emission at 1001.03 keV resulting with an effective branching ratio of 0.837% and an intensity of 73.4 photons $\text{s}^{-1} \text{g}^{-1}$ of ^{238}U , assuming $^{234\text{m}}\text{Pa}$ is in secular equilibrium with ^{238}U [58].

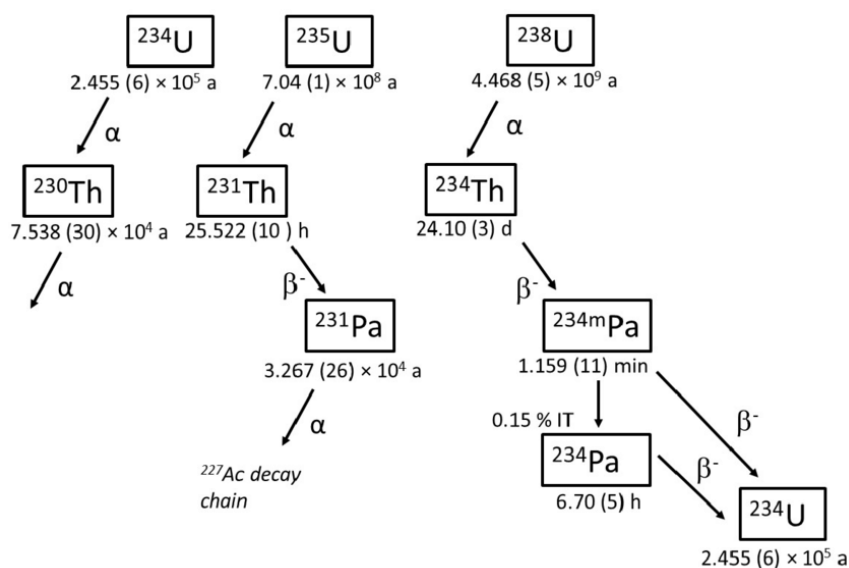


Figure 3.2: Simplified decay chain of naturally occurring uranium isotopes. The short decay times of ^{234}Th , $^{234\text{m}}\text{Pa}$, and ^{234}Pa give rise to secular equilibrium conditions with the parent isotope ^{238}U . Source: [59] open access <https://doi.org/10.6028/jres.122.044>.

The distinctive gamma-ray at 1001 keV is useful in that its energy is high enough that a significant fraction of photons produced will penetrate typical thicknesses of conventional construction materials. The mean free path, or the average length a photon of this energy will travel before interacting with and depositing energy in a substance, is 5–7 cm for various types of concrete [60]. As demonstrated below, the intensity of uncollided 1001 keV photons passing through a typical concrete wall, on the order of six inches thick, is $\sim 10\%$. This signal could be enough to indicate the presence of threat material, depending on the detection scheme (i.e., collection time, source-to-detector distance, detector size and type). Likewise, a foot or more of concrete is required to attenuate $>99\%$ of the 1001 keV gamma-rays.

The attenuation law for gamma-rays takes the form

$$I = I_0 e^{-(\mu/\rho)\rho \cdot x}, \quad (3.1)$$

where I is the intensity of the uncollided photons, I_0 is the initial intensity of the photon source, μ/ρ is the mass attenuation coefficient measured in $\text{cm}^2 \text{g}^{-1}$, ρ is the density of the attenuating media, and x is the thickness of the material. Solving for I/I_0 and substituting values from the National Institute for Standards and Technology (NIST) Standard Reference Database 126 [61] yields

$$I/I_0 = e^{-(0.06495 \text{ cm}^2/\text{g}) \cdot 2.3 \text{ g/cm}^3 \cdot 15.25 \text{ cm}} = 0.103 \pm 0.002. \quad (3.2)$$

while solving for x and substituting values yields

$$x = \frac{-\ln\left(\frac{1}{100}\right)}{(0.06495 \text{ cm}^2/\text{g}) \cdot 2.3 \text{ g/cm}^3} = (30.83 \pm 0.14) \text{ cm or } (12.2 \pm 0.3) \text{ in} \quad (3.3)$$

The 1001 keV gamma also has relatively low interference from nearby peaks from other background or nuisance sources. The only isotopes with significant nearby peaks are extremely rare (^{172}Lu and ^{133}Te) or have many other tell-tale peaks that preclude one from identifying it as uranium (^{152}Eu). Though uranium and its progeny are present in the background, a concentrated amount of DU, perhaps used in an IND tamper, would stand out relatively well in a medium to high-resolution energy spectrum, as illustrated in Figure 3.3.

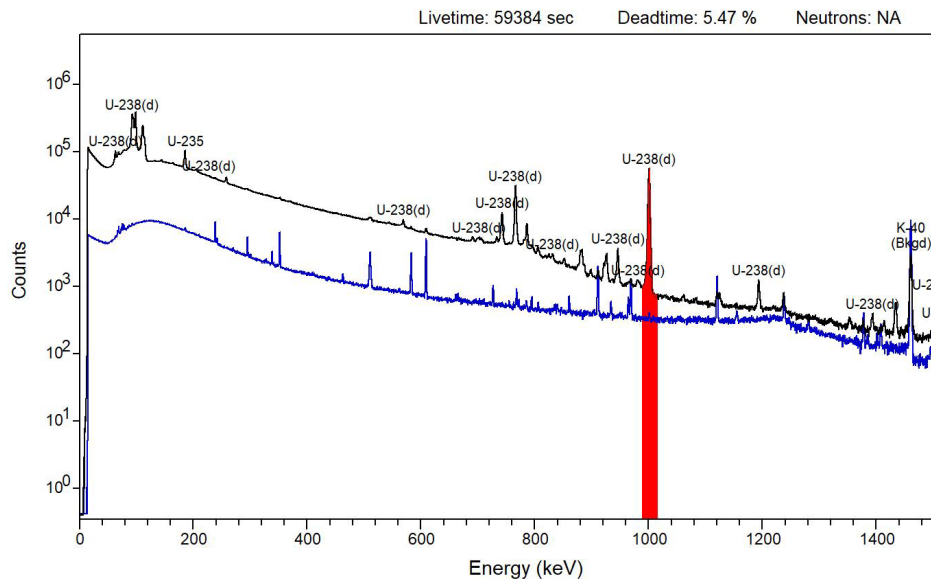


Figure 3.3: Representative high-purity germanium gamma-ray spectrum of 17 kg depleted uranium plates measured at 135 cm (black) compared with nominal background (blue). The red illustrates the significant peak at 1001 keV. Created using PeakEasy computer software with depleted uranium spectra from PeakEasyLib(3.0) [62].

Conversely, the gamma-ray signatures attributed to the decay of ^{235}U ($t_{1/2}=703.8$ million years), the chief fissile isotope of uranium, are much less illuminating and not nearly as distinguishable as the 1001 keV gamma-ray. Though they are more plentiful on a per-atom basis, due to a shorter half-life and larger branching ratios, they are relatively low energy at 143.76, 163.33, 185.72, 202.11, and 205.31 keV. The 185.72 keV gamma-ray is the most prominent of the group, radiating at 4.3×10^4 photons $\text{s}^{-1} \text{g}^{-1}$ of ^{235}U , and it is the most frequently used signature to measure enrichment levels of a sample [58, 63]. Because of their low energy, just six inches of concrete—the average thickness of an exterior wall in a commercial building—attenuates 99% of these photons.

Worse yet, the low energy of the gamma-rays implies that a significant portion of the photons emitted will be attenuated in the high-density material itself unless the geometric form has a high surface-area-to-volume ratio. Because of self-attenuation, only the outer surface of a mass of enriched uranium emits a gamma signature to the surrounding environment. Based on the infinite thickness criterion, the so-called “skin depth” for the 185.72 keV photon in a uranium metal sample is just 2.6 mm. The infinite thickness criterion is defined as seven mean free paths of a given energy photon in a material [58]. Essentially, a half-centimeter plate of enriched uranium presents the same 185.72 keV gamma signature as an infinitely thick plate of the same planar dimensions when measured normal to the face of the plate.

Not only is the signal attenuation of the 185.72 keV photon problematical, but the background interference from other sources exacerbates the situation. Even though intrinsic detection efficiency at low energies is very good, counts from down-scattered Compton events from natural background dominate the low energy region of the energy spectrum. This elevated Compton continuum, coupled with the fact that other naturally occurring radioactive materials emit gamma-rays with remarkably similar energy, complicates the energy spectrum. Indeed, ^{226}Ra ($t_{1/2}=1,600.2$ years), an isotope in the decay chain of ^{238}U , emits a gamma-ray at 186.21 keV. The two peaks are only distinguishable in high-resolution detectors or with significant count rates in other associated energy regions. Other interferants include $^{166\text{m}}\text{Ho}$ ($t_{1/2}=1,200$ years)—which is synthetically produced and used as a calibration source— ^{67}Ga ($t_{1/2}=3.26$ days)—an injectable radiopharmaceutical used in medical imaging—and radiative capture gamma-rays from absorption of neutrons on copper and germanium found in gamma-ray detectors.

A significant quantity of highly enriched uranium also poses a slight radiation hazard to those working with or around it. While we expect such material to be well-guarded and highly controlled, it will also likely be stored in a shielded container when it is not being manipulated. Using a dose calculator based on the ANSI/ANS-6.1.1-1991 historical standard found in the tools of Gamma Detector Response and Analysis Software (GADRAS), the equivalent dose rate for an unshielded 25 kg sphere of oralloy (U.S. origin 93%-enriched HEU) at 30 cm is estimated at $300 \mu\text{rem hr}^{-1}$ with a gross leakage of roughly 10 million photons per second [64]. This dose rate is hardly a radiation health concern in that form. If formed into a thin plate or shell, the dose rate and leakage from the same quantity of material would increase by

more than an order of magnitude and could perhaps warrant some further control measures.

Uranium also has two other isotopes of interest that are produced in a nuclear reactor and have unique signatures. ^{233}U ($t_{1/2}=1.6 \times 10^5$ years) is a fissile isotope that is generated slowly from the decay of ^{237}Np , which is produced in a uranium fuel cycle either by successive neutron capture (n, γ) on ^{235}U and again by ^{236}U , or via fast neutron knockout ($n, 2n$) on ^{238}U . ^{233}U can also be bred quickly from ^{232}Th in a fast or thermal reactor using the thorium fuel cycle. It has potential uses as nuclear fuel or possible weapons material. The isotope ^{232}U ($t_{1/2} = 68.9$ years) is produced in trace quantities as well by ($n, 2n$) reactions on ^{233}U , ^{232}Pr , and ^{232}Th , as well as (n, γ) reactions on ^{230}Th —though to a much smaller extent because of its small fractional abundance in the thorium fuel. The decay chain of ^{232}U joins the thorium decay chain at ^{228}Th , and, because of its short half-life, quickly yields strong gamma emissions, namely the 2614 keV (99.16%) gamma associated with the beta decay of ^{208}Tl . The co-presence of ^{232}U makes ^{233}U very difficult and dangerous to work with and very easy to detect [65].

It is somewhat fortunate that nearly all HEU contains some small quantity of ^{232}U because often some of the feedstock uranium was used first in a plutonium production reactor. The bulk of HEU stocks found in the U.S. were irradiated in reactors at Hanford and Savannah River; similar operations took place in the former Soviet Union as well. The absence of ^{232}U and ^{236}U in a sample of HEU is known as “virgin” HEU and is indicative of a concealed small-scale or well-funded program [66], especially one employing centrifuge enrichment.

Plutonium

Plutonium, the other primary threat material, is produced in nuclear reactors either by design or as a by-product depending on the reactor type, fuel, and operating conditions. It also occurs in nature, in trace quantities, due to neutron capture on uranium from cosmic sources. The principal isotope of interest is ^{239}Pu , though many of the distinguishing signatures of plutonium come from the presence of the even-numbered isotopes ^{240}Pu , ^{242}Pu , and to a small extent ^{238}Pu . ^{239}Pu ($t_{1/2}=24,110$ years) decays predominantly by alpha emission to $^{235\text{m}}\text{U}$, or by spontaneous fission at a meager ten fissions $\text{s}^{-1} \text{kg}^{-1}$. Although it belongs to the actinium series, the decay of ^{239}Pu produces a more distinct gamma signature than ^{235}U . The gamma-rays associated with its decay occur at slightly higher in energies, 375.05 and 413.71 keV respectively, and the greater specific activity of ^{239}Pu results in higher normalized count rate. Additionally, because of the higher energies and much smaller mass required to achieve criticality, the self-attenuation aspect is of less significance since the surface-area-to-volume goes up as the volume decreases.

The truly undeniable signatures of plutonium result, however, from the unavoidable byproducts that accompany its production—the most revealing being the presence of elevated levels of neutrons generated by the spontaneous fission, primarily from ^{240}Pu and ^{242}Pu . Both isotopes result from neutron capture events that occur after the initial cycle of neutron capture on ^{238}U and sequential beta decay to ^{239}Pu . While ^{239}Pu is fissile—with an even higher thermal fission cross-section than ^{235}U —it absorbs a thermal neutron about twenty-five percent of the

time. These radiative capture interactions lead to higher mass isotopes of plutonium as well as other transuranic isotopes of americium, curium, berkelium, californium, and others.

The spontaneous fission rate of ^{240}Pu is approximately $415,000 \text{ fissions s}^{-1} \text{ kg}^{-1}$, while that of ^{242}Pu is more than double that at $840,000 \text{ fissions s}^{-1} \text{ kg}^{-1}$. However, the ^{242}Pu content of typical WG Pu is less than 0.05%, compared to a ^{240}Pu content typically ranging 3–7%. Even at the super grade level of 4.5%, the neutron emission from a 4 kg solid sphere would be on the order of $4 \times 10^5 \text{ n s}^{-1}$. Even a small (1.65 cm \varnothing \times 13.0 cm) ^3He -filled proportional counter located 20 meters from the source would register a count rate more than twice the background.

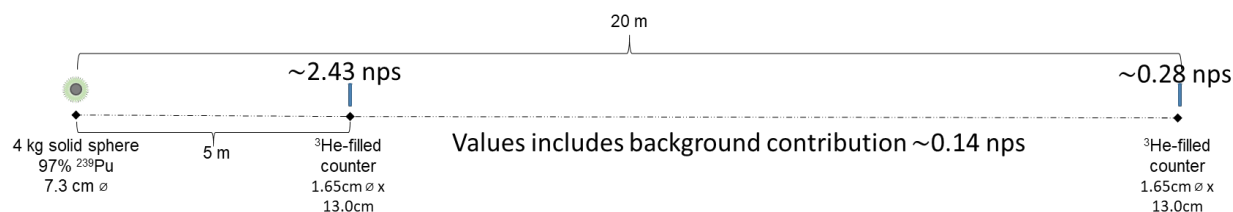


Figure 3.4: Diagram of detection scheme for 4 kg of super-grade plutonium. Detection is unambiguous at expected operational distances. Expected response based on neutron background in the San Francisco Bay Area, ^3He -filled polyethylene-moderated neutron detector in ORTEC Detective-EX-100, and plutonium model created in GADRAS Version 18.7.9.0 [64].

Another source of neutrons, though usually far less significant, comes about from interaction of the alpha particles, produced from the decay plutonium isotopes, and low- Z materials that may be present as impurities, coatings, or in nearby weapons components. The (α, n) reaction is commonly associated with engineered mixtures that couple strong alpha emitters with low- Z elements that have a high cross-section for alpha absorption, such as lithium and beryllium, as in Am-Be or Pu-Be sources. These reactions can also take place with other low- Z elements such as boron, carbon, oxygen, and fluorine as well as light metals such as magnesium and aluminum. This pathway for neutron production becomes more significant depending on the method for preparing plutonium metal or when the plutonium is in a non-metallic form, such as an oxide or fluoride. Nearly 45% of the neutrons produced in an 8 kg sample of plutonium oxide ($\sim 6\%$ ^{240}Pu) are the result of (α, n) reactions on oxygen from the decay of ^{241}Pu , whereas in a metal (α, n) reactions only comprise 1.3% of the total. We base these calculations on values for reported in [58, 67] for spontaneous fission and (α, n) reactions in plutonium metals and oxides.

Not only are the neutrons a distinct signature, but they also induce additional gamma signatures by their capture on low- Z materials such as hydrogen, lithium, beryllium, carbon, nitrogen, aluminum, and others. These materials are likely to be present in other weapon components such as high explosives, reflectors, and casings. The capture reaction often generates high-energy gamma-rays, ranging from 500 keV to several MeV. Many even exceed the 3 MeV energy scale employed by most field gamma-ray detectors. However, a common gamma-ray indicating the presence of neutrons does occur at 2223 keV; it is released

by the excited deuterium nucleus formed in the capture of thermal neutrons by hydrogen present in the water vapor in the air.

Radiological Threat Materials

Nearly any radioisotope of sufficient activity could be considered a threat material for an RDD or RED. However, the specific activity, half-life, decay chain, chemical form, availability make certain isotopes much more viable as threat source material. The IAEA and the U.S. Nuclear Regulatory Commission, in conjunction with an interagency task force, has made recommendations on the radionuclides of interest as well as activity action levels that trigger enhanced security measures [68].

The activity action level for many radionuclides is 37–370 GBq (1–10 Ci). As an example, the specific activity of natural uranium is 25,280 Bq g⁻¹; in order to have enough material to approach the low end of this threshold, one would need nearly 1500 kg of natural uranium [69]. That amount of material is entirely unsuitable for dispersion as a radiological hazard. On the other hand, isotopes such as ¹³⁷Cs and ⁶⁰Co have specific activities on the order of TBq g⁻¹, thereby requiring just milligrams of material to comprise a threat amount. One can find these materials in significant quantity quite easily in the industrial and medical sectors.

While the specific activity of an isotope is a function of its half-life, the decay rate of a particular isotope is of interest for other reasons as well. A material that decays away too rapidly has less appeal as a source term for an RDD, particularly since the aims of detonating such a device often include long-term uninhabitability or costly cleanup. However, for a RED, there might be advantages to sources with high specific activity and short half-lives. Therefore, in general half-lives on the order of years to tens of years are most common for RDD/RED threats. Isotopes that fall outside of that time frame should not be excluded, especially if other factors make them appealing, such as availability or chemical form.

The chemical form of a potential RDD radioisotope is useful to understand for possible distribution methods, such as dissolution or aerosolization. With such high-activity sources, manipulation of the radioisotope and fabrication of a device becomes difficult and may have to be performed remotely or with significant shielding. Certain isotopes used in medical and industrial applications are better suited than others for making a device.

Cesium-137

The isotope ¹³⁷Cs is a beta emitter but has a unique gamma signature that is associated with the decay of its metastable daughter product ^{137m}Ba ($t_{1/2}$ =2.552 minutes), an isomer it populates 95% of the time. The short half-life of ^{137m}Ba put it in secular equilibrium with its parent isotope and is the reason that the gamma-ray emission at 662 keV (85.1%) is often mistakenly attributed to the decay of the ¹³⁷Cs isotope.

¹³⁷Cs is commonly used in blood irradiators, radiation therapy devices, and various industrial gauges for measuring flow rates, thicknesses, and moisture density. It is an isotope of particular concern as a threat RDD material because it is often packaged in a sintered powdered chloride form and can be dissolved in strong acids for dispersion.

Cobalt-60

^{60}Co has a unique and high-energy signature consisting of two cascading gamma-rays at 1173 (99.97%) and 1332 (99.99%) keV following beta minus decay to stable ^{60}Ni . Its decay results in two distinguishable photo-peaks with very little interference from background since the Compton edge of the 1460 keV gamma associated with the decay of naturally occurring ^{40}K falls between the two peaks. Also, under certain conditions, summation peaks are expected to stand out above 2.5 MeV. Given those signatures, any detector of reasonable size and sufficient energy resolution would be able to identify a high-activity quantity of ^{60}Co at operational distances.

^{60}Co has a high specific activity and is found in large quantities in teletherapy cancer treatment devices such as GammaKnife [70]. It is also used in industrial radiography, equipment sterilization, food and blood irradiation, and industrial gauges. Over 170 large-scale gamma irradiation facilities are currently in operation worldwide containing over 11 exabecquerel (300 million curies) of ^{60}Co [71]. An estimated 2.2 EBq (60 MCi) is produced annually to replenish sources used in hospitals, clinics, and industries worldwide [72]. Companies that produce and fabricate the source material for these devices frequently ship source activities in the 7.4–13.3 TBq (200–360 kCi) range. It is a common belief these shipments are self-limiting in that their weight inside their protective shielding prevents theft, and removing the material would incapacitate or kill an aspiring thief in minutes. However, a sophisticated actor could intercept a shipment and possibly use the material in an RDD or RED.

Indeed, there have been several incidents whereby ^{60}Co sources have been out of regulatory control and have resulted in radiation sickness and even deaths. In 2013, indeed opportunistic thieves in Mexico carjacked a cargo truck containing ^{60}Co sources for a teletherapy machine amounting to 111 TBq (3000 Ci) [73]. Mexican authorities found the truck with the source outside of its shielding 40 km (25 mi.) from the gas station where thieves stole it at gunpoint [74].

In 2000, thieves stole an out-of-use teletherapy machine stored by a medical device distributor in an unused parking lot. Scrap collectors purchased the material from the unknown strangers and attempted to separate the head to recover material for salvage. They were only partially successful and took the treatment head, containing approximately 15.7 TBq (425 Ci), to a nearby scrapyards outside of Bangkok, Thailand. Workers there inadvertently exposed the source while disassembling the machine with a torch to recover useful materials. Ten people received high doses from the source, three of which died within two months from their exposure [75].

Neutron Sources

Mixed alpha-neutron sources and spontaneous fission sources are primarily found in industrial gauges used to measure density and moisture in soils, well logging instruments, or portable neutron activation analysis systems. These sources generally have an activity on the order of a curie or less and produce roughly a million neutrons per second isotropically.

Materials of this nature could be used in a RED but would not be expected to be used effectively as an RDD. Because the neutron background level is considered low, detection of these sources above background is relatively easy. They do, however, often give rise to nuisance alarms when encountered in the environment.

3.2 Radiation Detection

When radioactive isotopes decay they release of some form of ionizing radiation. There are two categories of ionizing radiation—direct and indirectly ionizing—that give rise to four main radiation types: alpha, beta, gamma-ray, and neutron.

Charged particles ejected from the nucleus, such as alpha and beta particles, are classified as directly ionizing. Both their charge and mass dictate their range in matter. Alpha particles, consisting of two protons and two neutrons (equivalent to a fully ionized helium atom), have charge +2 and significant mass when compared to the electrons and positrons associated with beta decay. Consequently, alpha particles have a very short range, only a few centimeters in air, and are easily stopped by a material as thin as a sheet of paper.

Beta particles have charge ± 1 and are roughly 7,300 times lighter than alpha particles. Beta-decay is a three-body problem consisting of a beta particle, an (anti)neutrino, and the daughter nucleus. This allows the kinetic energy of the beta particle to have a continuous range up to the entire Q-value of the decay. Even at the maximum end-point energy, beta particles still only have a range on the order of a few meters in air, and most average energy beta particles are entirely stopped by tissue as thin as the dead-layer of human skin.

Detection of directly ionizing radiation is generally not useful for standoff detection applications because of its short range and weak penetration. However, there are requirements for detecting directly ionizing radiations in some contamination, assessment, remediation, and forensics missions. Indirectly ionizing radiation, however, has a much larger range and is the focus of the detection methods outlined here.

Neutral particles ejected or otherwise liberated from the nucleus or atom, such as gamma-rays, x-rays, neutrons, and muons, are classified as indirectly ionizing radiation. Because they are neutral, they interact far less with surrounding matter than alpha or beta particles and have ranges on the order of meters to kilometers. The two types of neutral particles that are of primary interest in detecting threat materials are gamma-rays and neutrons. To detect them, they must interact with detector materials and liberate information carriers that are collected and converted into a signal that correlates to the original neutral particle's interaction.

Gamma-rays are penetrating photons that result from gamma decay. Gamma decay usually occurs after other forms of radioactive decay have taken place but have left the daughter nucleus in an excited state. Gamma-rays are electromagnetic waves, like x-rays, that carry away this excess energy. Gamma-rays are the result of the nucleus transitioning to a lower energy state, whereas x-rays result from electronic transitions in the atom.

Neutrons are much less common in the environment than gamma-rays. Cosmic-ray production is the primary source of background neutrons in the environment. Both fast and thermal neutrons have flux on the order of $1\text{--}5 \times 10^{-3} \text{ cm}^{-2} \text{ s}^{-1}$ at sea level [7, 35], whereas the gamma-ray background at 40–3000 keV is on the order of $25\text{--}50 \text{ cm}^{-2} \text{ s}^{-1}$ [64]. Neutron rates are affected by altitude (pressure), latitude (geomagnetic rigidity), and solar activity. The following sections detail how photons and neutrons interact with matter and by what methods they are detected.

3.2.1 Gamma-ray Interactions with Matter

Gamma-rays and x-rays interact with matter in the same manner. They are both high-frequency photons emitted to rid an atom of excess energy. Gamma-rays are emitted due to changes in nuclear structure, whereas x-rays are the result of the rearrangement of electrons. In general, gamma-rays tend to be higher in energy than x-rays; however, synchrotron radiation sources produce high-energy x-rays above 100 keV. The information presented in this section is derived primarily from [76].

The principal energies of interest for standoff gamma-ray and x-ray detection range from 20 keV to 3 MeV, though some valuable signatures occur in the 3–8 MeV range as well. These higher energy signatures are used primarily for characterization rather than detection and usually require close proximity and unobstructed access to the material of interest due to the low efficiency at these energies and the limited flux of gamma-rays from these reactions.

While there are several mechanisms for gamma-rays to interaction with matter, there are three primary means by which photons deposit energy that are relevant to radiation detection. They are photoelectric absorption, Compton scattering, and pair production. These processes, either individually or collectively, lead to the full or partial conversion of a gamma-ray photon's energy into an electronic signal within a detection medium.

Photoelectric Absorption

Photoelectric absorption is the process by which a photon is absorbed by an atom, and an energetic photoelectron is ejected. The ejected electron most often comes from the tightly bound K-shell but can occur from any bound state where the gamma-ray energy is above the binding energy. The release of a tightly bound electron is followed by either the capture of a free electron or a cascade of outer shell electrons to fill the inner shell vacancy. This rearrangement of electron results in one or more low-energy characteristic x-rays or Auger electrons being emitted to carry away the resulting atomic excitation energy. Most often, the energy of these x-rays is deposited locally, though escaping from the detector is a possibility. These subsequent emissions impact the overall energy response since the combination of the energy of the photoelectron, x-rays, and any Auger electrons amount to the total energy of the incident gamma-ray photon, known as the full-energy peak.

This process is dominant for all materials at lower energies, and the interaction probability is a strong function of the atomic number as well as the energy of the incident photon. There is no single analytic function for the probability over all energies, but a rough approximation valid over the gamma-ray energy region of interest is

$$\tau(E) \cong \text{constant} \times \frac{Z^n}{E_\gamma^m}, \quad (3.4)$$

where τ is the cross-sectional probability per atom, Z is the atomic number, E_γ is the energy of the incident gamma-ray, and the exponent n varies between 4 and 5 while the exponent m decreases from 3.5 to 1 going from low to high energies respectively [77]. The effect of Z can readily be seen in Figure 3.5 where more than a tenfold increase in cross-section occurs when going from Al to Fe and a hundredfold when going from Fe to Pb at energies above 100 keV.

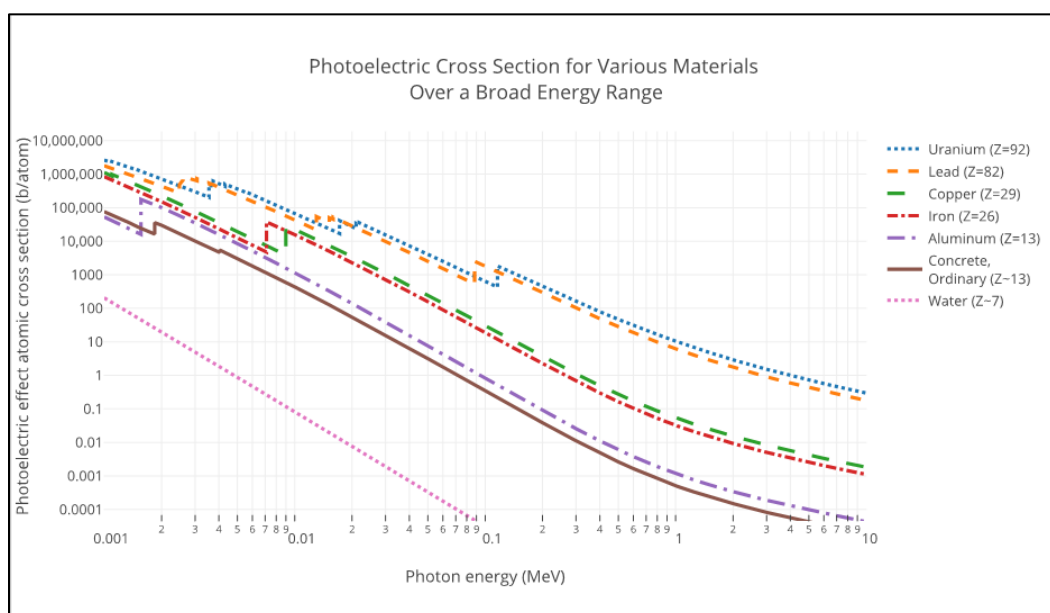


Figure 3.5: Photoelectric cross-section for various materials over a broad energy range. Adapted from [78] with data from NIST XCOM: Photon Cross-sections Database [79].

The plot in Figure 3.6 illustrates the energy dependence of the photoelectric absorption cross-section. The two gamma-ray emissions from ^{60}Co have nearly the same branching ratio, but the peak at 1173 keV is more pronounced due to the higher cross-section for photoelectric absorption at that energy.

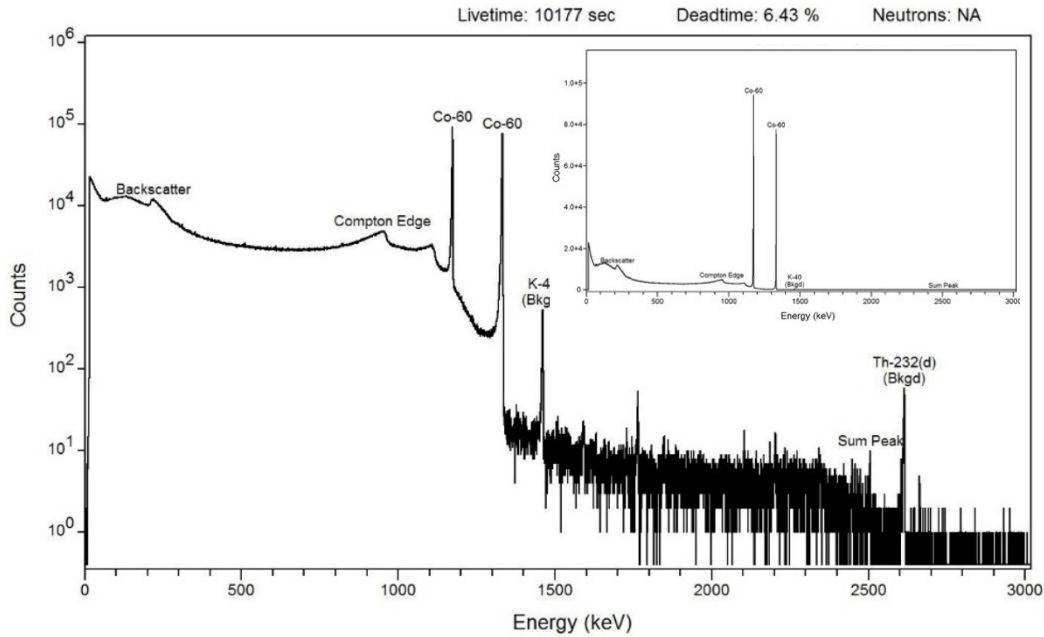


Figure 3.6: Measured spectrum for 158 μCi ^{60}Co taken at 100 cm with an ORTEC Detective-EX-100 from PeakEasyLib(3.0) taken at an unknown location in 2004 [62]. (inset) The same spectrum on a linear scale to highlight the difference in peak heights for 1173 and 1332 keV.

Compton Scattering

Compton scattering events are inelastic collisions whereby an incident photon strikes a bound or unbound electron. The incident photon transfers some portion of its energy and momentum to the recoiling electron and continues moving in some new direction with respect to its original path. Compton scattering is an incoherent process, as the phase of the incident photon is not preserved. Using relativistic kinematics, the fraction of the incident energy transferred to the recoil electron, as well as the portion retained by the scattered photon, can be closely approximated by treating the interaction as an elastic collision between a photon and an unbound electron at rest. By simultaneously solving conservation of mass and energy equations, under these simplifying assumptions, the following relationship is derived

$$hv' = \frac{hv}{1 + (hv/m_0c^2)(1 - \cos \theta)}, \quad (3.5)$$

where hv' is the energy of the scattered photon, hv is the energy of the incident photon, m_0 is the rest mass of the electron, and θ is the scattering angle of the photon measured with respect to the incident path in the lab frame of reference, as depicted in Figure 3.7. This equation implies a transfer of energy ranging from zero to some maximum at $\theta=180$ degrees.

A transfer of zero energy corresponds to Thompson scattering for which a phase change may still take place because the interaction is with a single electron, which contrasts with coherent scattering—also known as Rayleigh scattering—where there is little or no phase shift

because the interaction is with all of the electrons in an atom. The maximum energy transfer occurs at 180° , but due to the requirement to abide by the conservation laws of energy and momentum, the scattered photon will still retain some energy.

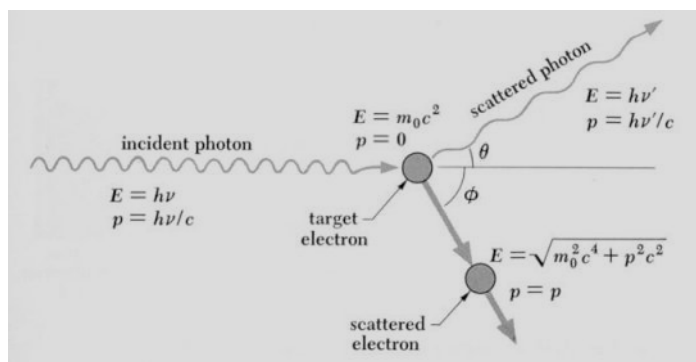
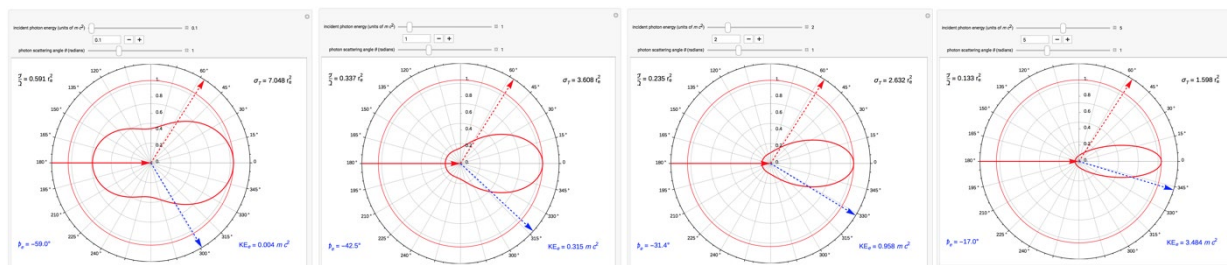


Figure 3.7: Diagram of Compton scattering with a target electron assumed at rest. Source: [80] in the public domain.

This difference in energy for a complete backscatter ($\theta=180^\circ$) event corresponds to a feature in gamma-ray spectroscopy known as the Compton edge, above which there are much fewer counts between it and the full energy peak. The counts that fall between the Compton edge and the full energy peak are caused by multiple scatter events occurring in a detector or from some higher energy gamma-ray. Below the Compton edge is the Compton continuum that arises from the range of scattering angles, and therefore a range of energy deposited in a detector. This continuum continues down to roughly 200–250 keV

The angular distribution of photons scattered from a free electron is given by the Klein-Nishina equation, which is not included here, but predicts forward peaked scattering for energies of interest to this study, as seen in Figure 3.8.



S.M. Blinder, (<http://demonstrations.wolfram.com/KleinNishinaFormulaForComptonEffect/>), “Klein-Nishina Formula for Compton Effect” <https://creativecommons.org/licenses/by-sa/3.0/legalcode>

Figure 3.8: Polar plots of the differential scattering cross-section for a 51, 511, 1022, and 2555 keV incident photons. Source: [81] open content licensed under CC BY-NC-SA 3.0.

Compton scattering is the dominant interaction process above roughly 100–300 keV for most detector materials and the majority of radioisotopes found in the field. Since collisions take place with electrons, the cross-section for Compton scattering is proportional to the number of electrons, or the atomic number for a neutral atom. The probability for Compton

scattering falls off gradually with increasing gamma-ray energy. The pile-up of Compton events at lower energies from various sources contributes to the spectral shape which tails off at higher energies, as seen in Figure 4.14. This phenomenon is compounded by the decrease in detector efficiency with increasing energy.

Pair Production

The creation of a subatomic particle and its antiparticle from a neutron boson is known as pair production. In most cases, it involves a photon in the vicinity of an atomic nucleus or electron creating an electron-positron pair. It is a threshold reaction whereby the incoming photon must have a minimum energy equivalent to the rest mass energy of the particles created, but the probability of such an interaction is low except for photons with several MeV of energy. The probability rises with photon energy and increases approximately as the square of the Z of the absorber. A simplified approximation for the cross-section for pair production in the vicinity of a nucleus the cross-section is

$$\sigma_n^{pair}(E) \approx \alpha Z^2 r_e^2 \ln E_\gamma, \quad (3.6)$$

where σ_n^{pair} is the cross-sectional probability, α is the fine-structure constant, Z is the atomic number of the absorber, r_e is the classical electron radius, and E_γ is the energy of the incident photon.

Pair production manifests itself in radiation detection in two primary ways, depending on whether the interaction takes place inside or outside of the detector. Inside a detector volume, the electron-positron pair produced begin interacting with other particles. The kinetic energy of the electron is deposited just as it would be from a photoelectric or Compton scattering event. The positron will travel some distance, join with an electron, and then annihilate creating two 511 keV photons traveling approximately the opposite direction as one another. One or both photons may escape the detector volume, or they may deposit a portion or all their energy via Compton scattering and the photoelectric effect. The result spectra will show a full energy peak equal to the energy of the incident photon, whereby all the kinetic energy from the electron and the pair of photons is converted to information carriers (e.g., ion pairs, electron-hole pairs, scintillation photons) in the detector. Alternatively, it may record a single or double escape peak, where the electron energy is captured, but one or both annihilation photons escape the detector, respectively.

An incident photon with energy greater than the threshold may also interact outside of the detector and undergo pair production with some other material. The same sequence of interactions detailed above can take place. However, one of the resultant annihilation photons can then interact within the detector volume and deposit its energy via Compton scattering and the photoelectric effect. This phenomenon often results in a slightly broadened peak at 511 keV with incident photons that exceed the threshold for pair production.

Attenuation

The intervening material between a source and a detector is a significant factor inhibiting the detection of threat sources. Not only is the signal from characteristic gamma-rays reduced but signatures that found at lower energies can be overwhelmed by down-scattered gamma-rays from background sources that undergo Compton scattering in the intervening material. Intervening materials are not limited to common shielding materials such as lead bricks; even air itself attenuates gamma-rays to varying degrees depending on the energy. The purpose of this section is to outline the conditions for expected threat building roofs to ascertain the impacts that attenuation will have on detector requirements used in search operations.

The improved signal expected due to limited attenuation through the roof is a strong motivation when compared with methods that require detection through exterior walls. A misconception with regards to rooftop measurements is that it is likely to be just as difficult to detect through the roof as it is through the wall. After all, one can usually walk on a roof and often it is primarily composed of metal, which is much more difficult to for gamma-rays to penetrate than concrete. Though the half-value layer of steel for a 1 MeV gamma-ray is a factor of three smaller than that of concrete, concrete exterior walls have an attenuation factor nearly twenty times greater than the roof because of they are much thicker.

Roofs are designed to have a high strength-to-weight ratio and do not have the same requirements for static loading as structural walls. A typical building practice for light industrial buildings worldwide is to build walls with cinder blocks, or tilt-up poured concrete that is nominally 6–8 inches thick, whereas the steel decking used in the roof is 18–22 gauge (roughly 1–2mm). One can usually assume that the walls of a building are not likely to be any less attenuating than the roof. Counterexamples would be something like a warehouse where conditions such as cold and snow require stronger and thicker roof materials, but the exterior walls are thin corrugated steel or wood. The attenuation of photons through the roof is addressed further in Section 4.1.2.

3.2.2 Gamma-ray Detectors

While there are classes of detectors that can be used to detect the presence gamma-rays, namely gas proportional counters, the focus of this treatment will be on those that are capable of spectroscopy. That is, rather than relying solely on gross counts above a given threshold to detected elevated levels of radiation, directed search requires further information about the energy of the gamma-rays deposited in the detector to differentiate threats from elevated background levels or nuisance sources. The content of this section is derived largely from [34].

The two most common classes of spectroscopic detectors are scintillators and semiconductors. Much like the two categorizes of ionizing radiation, indirectly and directly ionizing, the processes by which the energy deposited into these two classes of materials is converted and collected are also dissimilar.

Scintillation Detectors

Scintillators are materials that exhibit the property of luminescence in which the energy deposited by incident gamma-rays is converted to visible or ultraviolet light through the de-excitation of electrons involved in the slowing down of the primary ions liberated by one of the aforementioned interaction mechanisms. The light is then guided to a sensor which converts and amplifies the light into a measurable electronic signal.

Scintillators are typically grouped into two categories, organic and inorganic, and can be found in gaseous, liquid, or solid phase depending on the application. Organic scintillators are usually comprised of aromatic hydrocarbons. They typically have fast timing and are inexpensive to produce. Some organic liquid scintillators are used as neutron detectors and newer plastic scintillators, loaded with conversion materials such as boron or lithium, can detect and differentiate both gamma-rays and neutrons.

Inorganic scintillators are usually crystalline structures grown in high-temperature furnaces. They are often doped with an activator material that creates luminescence centers within the crystal lattice. These recombination sites provide access to intermediate energy levels that are otherwise forbidden in a pure crystal. These states allow for a more efficient de-excitation from the conduction band to the valence band and give rise to visible light rather than the higher energy photon that would be associated with a transition across the full bandgap.

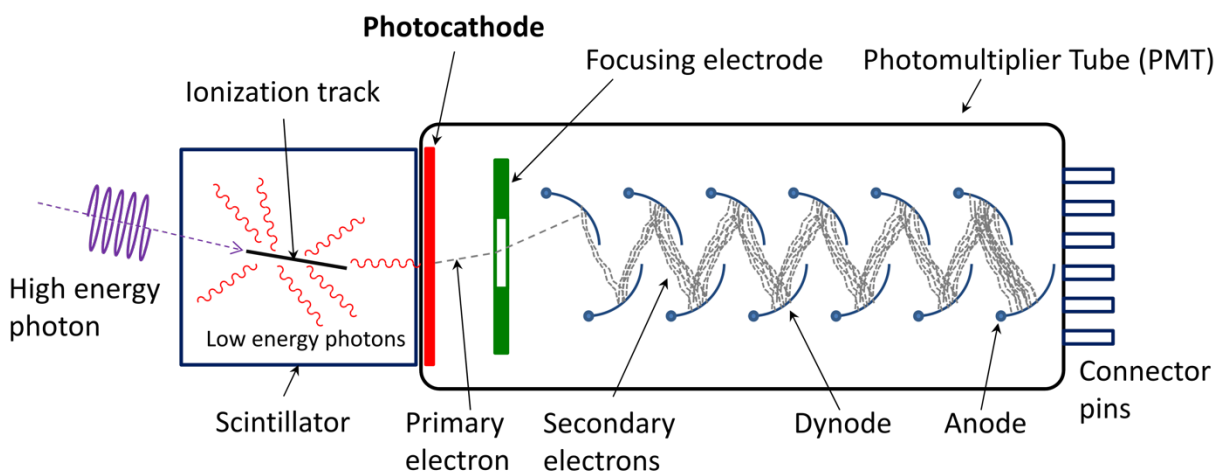
One can find a list of common inorganic scintillating materials used as gamma-ray detectors and their properties in [34]. Many common detectors are found in the alkali halide family with a small amount of activator impurity. Of those, NaI(Tl) is the workhorse material for most search applications, primarily due to its size, availability, and cost. Newer materials with better energy resolution are available and are often found in small handheld systems. Users often bypass them for applications requiring larger efficiency detectors because of their limited size and high cost.

The critical features that determine the usefulness of a scintillator material are abundant light output, linear response across a range of energies, fast rise times and short decay times, and self-transparency to the scintillation light generated. Physical features such as a large effective atomic number, high density, and manufacturability in bulk sizes affect the efficiency of the detector. Additional properties such as ruggedness, temperature insensitivity, and cost also play into the trade space in choosing a scintillator best fit for a given detection application.

The method of collecting and amplifying the light generated in the scintillator is critical to the resolution of the detector system. The electronic light sensor is often the limiting factor, or quantum sink, for the energy resolution of a detector. The three most commonly used light sensors are photomultiplier tubes (PMT), photodiodes, and silicon photomultipliers (SiPM)

In a PMT, light from the scintillator is coupled to a photocathode where it is converted back to electrons via the familiar photoelectric effect. These photoelectrons are directed by a focusing electrode to a series of dynodes which serve to amplify the signal. They multiply

the number of electrons by way of secondary emissions from collisions with each dynode. The resulting stream of electrons is measured as a current striking the anode. The PMT gain is a strong function of the operating voltage. The number of secondary electrons produced in collisions with the dynode depends on the kinetic energy of the incident electrons, which is a function of the potential difference between dynodes. For normal detection operations, the gain is usually set to cover a wide range of flux environments, from low background up to high-activity sources. Measurements over long time intervals require some form of gain stabilization due to temperature changes in the scintillator or electronics, gradual changes in the voltage levels, or variations in the gain of the elements in the signal chain.



Qwerty123uiop (<https://commons.wikimedia.org/wiki/File:PhotoMultiplierTubeAndScintillator.svg>),
 “PhotoMultiplierTubeAndScintillator”, <https://creativecommons.org/licenses/by-sa/3.0/legalcode>

Figure 3.9: Schematic showing incident high-energy photon hitting a scintillating crystal, triggering the release of low-energy photons, which are then converted into photoelectrons and multiplied in the photomultiplier. Source: [82] open content licensed under CC BY-NC-SA 3.0.

Photodiodes are semiconductor devices that convert light to electric current and are used with some scintillating detectors. Compared to PMTs, they have small areas, low sensitivity, slow response time, and lack internal gain. However, they are often used in search detection systems for non-spectroscopic gross counting because they are low cost, lightweight, compact, rugged, low noise, low voltage, and have excellent linearity, spectral sensitivity, and high quantum efficiency [83].

Avalanche photodiodes (APD) are a highly sensitive form of a photodiode because they operate at a large reverse bias voltage near the breakdown voltage and result in a built-in single-stage gain on the order of 10^2 – 10^3 due to avalanche multiplication. APDs have detection applications primarily in positron emission tomography and particle physics, as well as commercial applications in laser rangefinders and fiber-optic telecommunications [83].

Advances in photodiode technology over the past two decades are the basis for electronic light sensors known as multi-pixel photon counters, more commonly called SiPMs. These

devices consist of arrays of APDs, as many as 1,000 in a mm^2 , that are operated in single-photon Geiger-mode. Each pixel is kept a few volts above the breakdown voltage, and a gain of up to 10^6 can be achieved for 1–1000 incident photons on the nanosecond time scale. Advantages of SiPMs include high gain with low operating voltage, insensitivity to magnetic fields, and high photon detection efficiency in a compact, rugged, and low-cost form factor [83, 84, 85]. However, current SiPMs also have significant disadvantages, including relatively small areas and issues with noise and nonlinearity at high energies.

Detectors larger than 1 cm^2 suffer from degraded energy resolution over implementation with PMTs because of the losses that occur in guiding the light from the scintillator to the SiPM. There are also nonlinearities at higher energies because the number of scintillation photons striking the pixels in the device exceeds the number of pixels. There is approximately a 10 ns dead-time per pixel once triggered by a photon. At higher incident gamma energies, the current generated from the struck pixels is missing the contribution of those scintillation photons which impinged on an already fired APD [86].

Semiconductor Detectors

Detectors made from semiconductor material do not require the same arduous steps as scintillators do in converting gamma-ray photons into a measurable signal. Instead, energy is deposited in the depleted layer of a semiconductor where a gamma-ray interaction liberates both electrons and holes. Both information carriers can be collected and translated into a signal, depending on the type and arrangement of the detector. However, the electrons in certain semiconductors travel much faster than the holes; in those cases, often only the electron component of the signal is captured.

The most common semiconductor detector materials are silicon, germanium, cadmium telluride, and cadmium zinc telluride. The critical feature that determines the usefulness of a semiconductor for gamma spectroscopy is the energy bandgap. A small bandgap, such as that of germanium (0.67 eV at room temperature) is a suitable trait for superior energy resolution because more information carriers are created for a given amount of energy deposited. However, such a small bandgap is a double-edged sword. Germaniums' bandgap is on the same order as the thermal energy of its electrons. This near-parity leads to unsurmountable noise issues at room temperature and requires cooling germanium to liquid nitrogen temperatures ($\sim 77\text{--}100 \text{ K}$) using cryogenic or mechanical means. Even detectors that can operate at room temperature tend to have improved energy resolution at colder temperatures.

Silicon detectors have been used since the early 1960's and are still prevalent today for application such as charged particle and x-ray spectroscopy as well as electronic personnel dosimeters. As discussed previously in the scintillator section, they are finding an increasing role as solid-state replacements for PMTs. Their application to standoff gamma-ray detection is limited to dosimetry and is not considered here.

High-purity germanium detectors are known as the gold standard for gamma-ray spectroscopy. HPGe detectors are the best resolution available for field-deployable detectors

with energy resolution on the order of 1.6 keV (0.25% FWHM at 662 keV). In the past two decades, HPGe detectors have been pushed into field use more than ever before because of mechanical coolers replacing liquid nitrogen cooling. There are man-portable systems in the field that can operate on batteries for up to 8 hours and weigh under 10 pounds. There are also segmented systems which use the position information of interaction to image sources of radiation.

CZT is being used to a greater extent for high-resolution spectroscopy. Its main advantage is that it can be operated at room temperature. It is also fairly low power and can be segmented or arrayed to provide position information for imaging. Its energy resolution is not as good (~1–1.5% FWHM at 662 keV) as that of HPGe, and it has proven difficult to manufacture in sizes larger than ~6 cm³. Yet, systems of comparable performance to HPGe are being developed without the need for cryogenic cooling.

3.2.3 Neutron Interactions with Matter

Neutrons can undergo a variety of interactions with surrounding materials, and the likelihood of any one of those occurring is a strong function of the kinetic energy of the incident neutron; hence, neutrons are often classified by their speed. The number of groups and associated energy bins varies by application and sub-discipline, but the most common categories are thermal, epithermal, slow, fast, and high-energy. Thermal neutrons are defined as having an energy that is in equilibrium with their surroundings—they are equally as likely to gain energy in a collision as they are to lose energy. Thermal neutrons have energies that follow the Maxwell-Boltzmann distribution, where the most probable energy is 0.025 eV. Epithermal neutrons have energies above 0.025 eV up to a few hundred eV. Slow neutrons generally range from one keV to several hundreds of keV. Fast neutrons are generally considered to have a kinetic energy of more than 0.5 MeV up to 10–20 MeV. High-energy neutrons have energies above 20 MeV and require relativistic effects to be taken into consideration [87]. When more precision is required, the number of bins and energy windows are refined to suit the application.

As discussed in Section 3.1.1, neutrons that are found in the environment are most often products of reactions from cosmic-rays in our atmosphere. The other primary sources of neutrons are those produced by spontaneous fission isotopes, mixed alpha-neutron reactions, or small accelerator-based fusion devices. ²⁵²Ca (SF), ²⁴¹AmBe (α , n), and D-D or D-T fusion devices are licensed sources that are often found in the operational environment. Licensed users often employ them in road construction, petroleum exploration, and portable neutron activation analysis. For example, prompt gamma neutron activation analysis is used in soil density gauges that are driven with a neutron source or neutron generator [88].

Neutrons are “born” fast and thermalize through collision with matter. Collisions, especially with light elements such as hydrogen, are the most effective means to thermalize neutrons. Neutrons transfer a significant portion of it in a grazing collision with a nucleus that is near the same mass and up to all of it in a head-on collision with hydrogen [34].

Conversely, collisions with high-Z materials contribute very little to the energy loss of a neutron because of the mismatch in mass. A high-speed golf ball striking a bowling ball provides an illuminating comparison, where the mass difference is on the same order to that of a fast neutron striking tungsten.

3.2.4 Neutron Detectors

Neutron detectors are generally classified by the speed of the neutron, fast or thermal, and further by the type of interaction, scattering or absorption, that produces the measurable signal indicating a detection of the elusive neutral particle.

Thermal Neutron Detectors

Table 3.1 catalogs the most common reactions used to detect thermal neutrons. The most prolific and straightforward thermal neutron detector is a gas-filled detector, containing either ^3He or BF_3 , operated in the proportional region. Such detectors are easy to manufacture, and the Q-value of the reaction allows for pulse-height discrimination to be employed for gamma rejection. Boron can also be embedded into a gas detector by coating the inner wall of the gas cylinder with a boron layer. Bundles of boron-coated copper straws have also been employed to increase the surface area of boron for neutrons to interact with and create charged ions [89].

Table 3.1: Nuclear reactions of interest in thermal neutron detection (adapted from [34])

Reaction	Thermal Cross-section [b]	Q-value [MeV]	Natural Isotopic Abundance [%]	Notes
$^{10}_5\text{B} + ^1_0\text{n}$ $\rightarrow \begin{cases} ^7_3\text{Li} + ^1_1\text{p} & 6\% \\ ^7_3\text{Li}^* + ^1_1\text{p} & 94\% \end{cases}$	3840	2.792 2.310	19.8	Enriched ^{10}B (99%) is readily available
$^6_3\text{Li} + ^1_0\text{n} \rightarrow ^3_1\text{H} + 2^4_2\alpha$	940	4.780	7.40	Enriched (95%) ^6Li is controlled but available
$^3_2\text{He} + ^1_0\text{n} \rightarrow ^3_1\text{H} + ^1_1\text{p}$	5330	0.764	0.000137	Enriched ^3He is a by-product of tritium production

Fission counters are another type of thermal neutron detector that could be employed. They operate similarly to a boron-lined detector but instead are lined with a layer of highly-enriched ^{235}U . One should swiftly recognize the drawback to using such a detector for directed search operations—it will certainly interfere with the gamma detection scheme if the target material is ^{235}U as well. Furthermore, the efficiency of a typical fission counter is orders of magnitude less than that of a BF_3 or ^3He tube [34].

Scintillator and semiconductors are also employed as neutron detectors. For the case of scintillators, materials such as boron, lithium, or gadolinium are implanted into glass or plastic

and extruded as scintillating fibers, loaded into bulk scintillating plastics or organic liquids, coated onto scintillating screens, or grown as crystals. The capture of a thermal neutron by one of these materials liberates ions which cause ionizations in the nearby material and leads to excited states which fluoresce when they de-excite. These visible photons are collected, either by a traditional PMT or solid-state photomultiplier and generate a signal that is characteristic of a neutron interaction.

Semiconductor neutrons detectors employ a similar strategy as scintillators by etching ${}^6\text{Li}$ into silicon wafers [90]. However, the resulting charged particles from neutron capture create electron-hole pairs directly in the silicon. These devices can be operated at extremely low power and have achieved modest efficiency. They can be tiled to achieve sufficient sensitivity for an application.

While each method has unique considerations and characteristics, the underlying principle is to capture a thermal neutron, produce ions, generate information carriers (electron-ion pairs, electron-hole pairs, photons), transport and collect the information carriers, and generate a signal that is indicative of a neutron interaction.

Fast Neutron Detectors

There are three primary methods to detect fast neutrons: (1) moderate to thermal energies and measure energy from thermal absorption, (2) measure energy from fast absorption, and (3) measure recoil energy from collisions with atoms and molecules. There are several reasons and strategies for moderating neutrons down to thermal energies for detection in a thermal neutron detector. The two primary applications are the spherical dosimeter and the long counter, neither of which are relevant to this effort. However, we do anticipate making use of UAV components as neutron reflectors or moderators to thermalize or otherwise deflect neutrons into a thermal detector.

As for direct absorption, most materials do not readily absorb fast neutrons; some exceptions are ${}^3\text{He}$, ${}^6\text{Li}$, and fissionable materials like ${}^{238}\text{U}$. The primary reason to absorb the fast neutrons directly is to gather information about the energy distribution of the neutrons, which would be of some value to this effort. Because the kinetic energy of the neutron is no longer dwarfed by the Q-value of reaction, one can simply subtract the Q-value from the energy deposited by the reaction products to estimate the incident neutron energy. This would be useful information to differentiate between (α , n), D-D or D-T, and fission sources. Elpasolite detectors, such as CLLBC(Ce), have intrinsic efficiencies for fast neutrons on the order of a percent [91, 92].

Another mechanism to detect fast neutrons relies on collisions with atoms and molecules instead of absorptions. Neutrons deposit energy with each scattering event, and it is the momentum transferred to a given material, primarily protons, that is measured. Common target materials are hydrogen, deuterium, and helium. Many applications use organic scintillators, employing some form of pulse-shape discrimination to differentiate between gamma-rays and neutrons. There are also applications which use gas proportional counters.

While we recognize that several candidate target materials emit a substantial and detectable number of fast neutrons, we expect that a significant fraction of those will be moderated by the time they reach the rooftop. Several possible materials such as explosives, low-Z shielding, room clutter, air moisture, and roof constituents may contribute to the slowing down of neutrons emitted by the source. Therefore, we do not expect to employ a standalone fast neutron detector in an sUAS-based approach for directed search. However, we will consider employing methods to extract fast neutron information from detectors selected for gamma-ray or thermal neutron detection, if applicable. That is, if CLLBC(Ce), or some other elpasolite material sensitive to fast neutrons, is chosen, and the means to extract fast neutron information is worth that additional size, weight, power, and complexity, we would consider implementing such a detector.

3.3 Alternative Signatures, Indicators, and Other Sensors

The term alternative signatures, when applied to radiological and nuclear threats, generally indicates signatures that are not associated with gamma or neutron emissions. Alternative signatures for this mission area include indications of explosives, firing devices, dense materials, specialized machining equipment, and unusual human activity. Sensors deployed either alongside the radiation detectors or as separate systems could also gather ancillary information that could improve both the collection and analysis of the radiation data. These requirements include the location and pose of the detector; an estimate of the background radiation levels and variation; the density, thickness, and composition of intervening roof material and other characteristics of the scattering environment.

Orthogonal sensors are desirable in that they can reduce the false alarm rate of the overall system and increase the sensitivity to specific threats. We do not intend to cover these alternative signatures and their associated sensing modalities in great detail or specificity. Rather, we present a general overview of them because their inclusion in the larger system would impact the size, weight, and power (SWaP), and could possibly force tradeoffs in the radiation detection components.

Explosives Detection

Explosives are an integral component of INDs and RDDs. The quantity and type of explosives required depend on the design of the device. Some example components include detonators, propellants, and bulk high explosives. The presence of explosives or precursor chemicals is a reliable indicator of nefarious activity. The mere presence of explosives does not indicate that activity to produce an IND or RDD is taking place; nor does its absence remove that possibility. However, the presence of explosives does render substantial probable cause to compel further investigation and may warrant raising the threshold required to absolve a target building of suspicion.

There are multiple techniques for sensing explosives that are orthogonal to one another.

The information presented here is summarized from [93, 94, 95]. Technologies generally focus on either bulk and trace explosive detection, and the two areas are quite different in their approaches. Standoff detection of explosives is generally defined as distances of 10 m or greater. Standoff detection of bulk explosives is possible through imaging techniques used to indirectly identify characteristic shapes of explosives, detonators, or wires; or to directly detect chemical composition, dielectric properties, or other physical characteristics. Various X-ray, gamma-ray, neutron, infrared, terahertz, microwave, radar, and other electro-magnetic techniques have been explored and operationalized. However, these techniques normally require line-of-sight to the material or control of the container being interrogated. Therefore, it is unlikely that one could employ any of these methods for bulk detection in a typical directed search scenario. For this treatment, we assume that line-of-sight is not possible, and trace detection is the most viable means available for remote detection.

Trace explosives detection at standoff distances is based on sample collection and analysis of residual particles or vapors. The most common explosives trace detection methods include colorimetric, chemical luminescence, gas chromatography, mass spectrometry, ion mobility spectrometry, field ion spectrometry, surface acoustic wave, amplifying fluorescent polymer, Fourier transform infrared, electron capture detectors, and photoionization detectors (PID). Some of these techniques are coupled together, as in a gas chromatography-mass spectrometry, thereby using orthogonal techniques in series on the same sample. While each technology and particular device varies in the manner in which samples are collected and analyzed, the broad approaches are sniffing, swiping, or sorbing residual vapors, liquids, or particles.

It is beyond the scope of this work to describe in detail the specific aspects of each of these methods. Rather, it is sufficient to note that we must consider employing one or more of these technologies in conjunction with a radiation detection system. We also recognize that remote sample collection and detection of explosives has operational value outside of nuclear and radiological search missions and is undoubtedly being pursued in several other mission areas. The key factors determining which technologies we should evaluate for this mission area include sensitivity, specificity, SWaP, sample collection and preparation, and orthogonality.

With regards to sensitivity and specificity, a variety of explosive types may be employed in a device, spanning a range of vapor pressures and chemical signatures. The detection of machined explosives manufactured off-site and brought to the target building is unlikely at any standoff. However, the case in which the explosives were either manufactured or machined on-site increases the viability of trace detection. A system that is sensitive to a wide range of indicator compounds and can distinguish between contaminants, military-grade explosives, and improvised or homemade explosives is desirable.

Like radiation detection, there often is a background level of indicator molecules present in the environment, especially in areas around the world that have been involved in recent military, de-mining, or blasting activities. In those cases, samples from nearby locations not associated with the target building may also be required to provide a reference measurement.

Dense, High-Z materials

Dense, high-Z materials are used both in shielding radioactive sources and as potential components of INDs. Materials such as lead, tungsten, and depleted uranium are effective shields for high-energy photons, or they might be used as a tamper or neutron reflector in an IND. Such dense materials are detectable by imaging systems, such as x-ray backscatter, dual-energy megavoltage radiography, muon tomography, and nuclear resonance fluorescence [12]. These systems are very large; one would have to employ them from a vehicle in a directed search operation. While these methods are not likely to be deployed from a UAV, the detection of characteristic gamma-rays or neutrons could be performed remotely as part of an unmanned system. This concept has overlap with active interrogation applications and should be further explored. However, the methods to detect dense, high-Z materials is currently outside of the scope of this study.

Detector Location and Pose

Knowledge of the location and pose of the detector allows one to develop proximity imaging maps for the areas measured by the system. Moreover, one could apply a directional efficiency calibration when trying to reconstruct counts from a well-characterized system that employs either self-occluding detector arrays or more advanced modulation concepts. Sensors that would provide location and pose information include standard and differential global navigation satellite systems, inertial measurement units, visual and stereo cameras, structured light RGB-D devices, light detection and ranging scanners, and perhaps other electro-optical instruments. Often, one or more these systems function together to provide a capability that builds a map of the scene and tracks the position of the sensor as it moves through it, otherwise known as simultaneous location and mapping. The ability to track radiation detectors as they move through a scene, as well as provide context to what is around the sensors in a given area, enables near real-time volumetric (3-D) imaging of gamma-ray and neutron sources through an approach known as scene data fusion [96].

Background Radiation Estimation

The background radiation intensity is likely to be a strong function of the building materials and the surrounding area. For example, if the building is erected on a poured concrete slab, we find strong evidence (see Chapter 4) to suggest that the contributions from the concrete will dominate the background radiation levels. There are efforts to semantically segment scenes and make estimates on the contribution of materials found in the scene to background. Some form of an electro-optic sensor (visual, hyperspectral, multispectral, thermal) could provide enough non-radiation data input to give a reasonable estimate of the background. However, an actual measurement of the local background from a nearby location is likely to provide more accurate information. This technique could be relevant to isolated target locations or areas where no previous measurement data available.

Intervening Material and Building Contents

A measurement or estimate of the amount of intervening material, such as the thickness and composition of the roof material, would inform the shape of the resulting spectrum as well as the reduction in full-energy peak signal due to the scattering and attenuation that take place in the material. Moreover, knowledge of the location of structural supports (e.g., arches, beams, trusses, columns, stretchers) can inform the best locations to make measurements for a given area. One could garner this information from architectural blueprints or collect it in situ using one or more sensor modalities.

For example, one can obtain limited but useful information from LiDAR scans through the windows of a building. Other technologies such as capacitive sensors, ultra-wideband radar, thermal infrared radiation (IR) cameras, and ultrasonic radar are approaches that could provide data on near-field material characteristics and possible occupancy and room clutter information as well, depending on the building construction.

From the perspective of other sensing modalities, the data on the building contents and clutter inform several lines of analysis. First, with regards to radiation detection, it can help with modeling efforts to characterize sources of interest by taking scattering in the environment into account for gamma and x-rays, as well as the production, scattering, and moderation of neutrons. Second, it can improve imaging efforts by providing information to voxelize the interior of the building as well as indicate regions from which gamma emissions from a potential source are either very likely or unlikely to reach the detector, as in the case of thick interior walls, large equipment, or intentional shielding. Third, the confirmation of industrial equipment (e.g., machine shop tools, chemical mixing tanks, processing cells, glove boxes) could inform high-priority measurement locations or might be strong enough of an indicator to warrant a full-scale building raid.

The knowledge of building occupancy is valuable for several reasons. It could inform decisions on whether to proceed with further measurements at different locations on or around the building or whether to deploy additional remote sensing vehicles to the building. Moreover, the detection of human activity, especially at certain times, particular work cycles, or within specific locations might be indicators of nefarious activity which may raise the threat assessment level of a target location. Finally, combined with other intelligence, surveillance, and reconnaissance (ISR) streams, it could point to the presence of a threat person or group which may trigger a response without the deployment of remote radiation sensing platforms.

3.4 Summary

In this chapter, we explored the radioactive and alternative signatures associated with lost or stolen nuclear or radiological material. We discussed the sources of background radiation present in the environment, and we examined typical threat materials that might trigger the deployment of a search force and the unique signatures they emit. Then we turned to the properties of the detectable radiations they emit. We explored the ways in which gamma-rays

and neutrons interact with material and expanded further into the mechanisms by which we can detect them. Along the way, we looked at the impact of attenuating materials as well as the impact that background radiation has on the signal-to-noise ratio in detecting threats. In the next chapter, we delve deeper into the background encountered on buildings and explore the limits of detection from the rooftop.

Regarding alternative signatures, we briefly introduced some modalities that do not involve the measurement of radiation but would prove valuable if they could answer questions regarding the presence of explosives, high-Z materials, specialized equipment, or human activity. We also looked at the benefits of contextual sensors as they apply to improve the radiation detection scheme. Many of these sensors are worth considering for a system of systems approach to the problem. Some may even be deployable on the same platform as the radiation detection sensor package.

However, with the layering of sensing modalities and reconnaissance objectives, there is a risk that the complexity of the system will grow too cumbersome and unruly. One does not want to overburden a search team with dozens of sensors, each of which will have their quirks, logistical burdens, and failure modes. Moreover, assuming everything works, the goal is not to overwhelm the commander with technical data that may or may not indicate a threat. Instead, it is to provide a scalable toolset to the commander so that they can make the best decision possible given the information available. There certainly are operational conditions and decision points where a commander might choose to conduct a raid on a building or compound or order a cordon and search of the entire area instead of deploying an extensive suite of sensor platforms. After all, a substantial amount of direct information can be obtained by kicking down the door and looking inside rather than piecing together a number of indirect measurements taken from outside.

4 Background Radiation and Source Measurements

In nuclear and radiological search operations, a reasonable estimate of the distribution of background radiation is required for most detection and identification algorithms. The variation in the background across the search area influences the probability of detection for a given false-alarm rate. Different search modes may have unique background features and signal collection considerations. For example, vehicle-borne search operations are characterized by rapidly changing background conditions with short signal integration windows. Dismounted search activities feature more gradually changing background conditions with longer integration times. Vehicle portal operations have longer fixed signal collection intervals under a relatively constant background, though the background rate decreases as the ground near the detector is partially obscured or shielded by the vehicles and contents being screened. sUAS-based reconnaissance of buildings resembles dismounted search, in that the detector moves in the environment, but also shares similarities with portal operations, in that collection times are usually long and can be fixed.

For this study's first thrust area, we conducted a measurement campaign on representative light industrial buildings to address two primary questions: (1) What does the background radiation environment look like from the rooftop of a building? (2) Are radioactive threat sources detectable from the roof? This chapter presents the results of the investigation into the composition, range, variation, and attenuation of background radiation measured from the rooftop of buildings. It also addresses the detection of limited-activity radioactive sources using a variety of detector types.

4.1 Background Radiation

For a search area on the order of 10 km^2 , one can expect minimal variation from the cosmic sources of background radiation unless there is a significant change in altitude or geomagnetic rigidity. Therefore, the contribution to the background from cosmic sources is likely constant across a building. Local geological conditions determine the terrestrial background component on a coarse-scale. As discussed previously, the KUT content in the soil and surrounding materials is the most prominent factor in the terrestrial background. In open and rural areas, this is relatively constant over sizable distances. However, in an urban setting, variation in the buildings and roads have a significant impact on the background levels.

Since this approach takes place on buildings, we must consider the alteration to terrestrial background caused by construction materials. Digging a foundation or grading the land may expose soil which has different ratios of KUT than the surrounding land. Modern building construction often uses materials obtained from beyond the local area. Soil or crushed stone may be trucked in to level or grade the site. Materials used in foundations and walls often come from distant quarries that have different levels of KUT than the surrounding area. Some concrete or concrete blocks may contain fly ash as a substitute for Portland cement. Fly ash

is a by-product of burning coal and contains concentrated uranium and thorium that is up to ten times the level found in coal [53]. Rebar and other structural steel components may contain trace radioactive impurities, either from atmospheric nuclear testing or the inadvertent addition of orphaned radioactive sources from scrap recycling during the manufacturing process. It should not be surprising that the background radiation measured on the rooftop of a building is considerably different from the surrounding area because of the contribution from the materials used in its construction.

As previously discussed in Section 1.3, the expected location of a target building is in a light industrial or commercial district, which points to slab foundations with corrugated metal, reinforced cinderblock, or tilt-up concrete walls. A set of buildings with these characteristics were examined at several locations: Richmond, CA; Tracy, CA; and Fort Belvoir, VA. Detailed measurements were taken to sample the variation of background levels across a building, at different rooftop heights, amongst different nearby buildings, at different locations within a region, and from locations on opposite coasts.

4.1.1 Methods

Primary background measurements were taken using an ORTEC Detective-DX-100 mechanically-cooled HPGe detector. The detector was initially self-calibrated using the prevalent background peak at 1460.83 keV from ^{40}K and further calibrated with an $8.031\ \mu\text{Ci}$ ^{152}Eu source. We placed the detector into a field-expedient stand fabricated from a shipping pallet for measurements. This stand positioned the detector in a vertical orientation, such that the axis of the coaxial crystal was perpendicular to the plane of the rooftop, as seen in Figure 4.1. Interior building measurements were raised from the floor approximately 30 cm, using a five-gallon plastic bucket, to reduce scatter.



Figure 4.1 (left) An inverted ORTEC DX-100 high-purity germanium (HPGe) detector on an improvised stand. (middle) The HPGe detector raised from the floor with a bucket. (right) The contents of the bag include various prototype detectors on loan from the Defense Threat Reduction Agency (DTRA). Source: personal photographs.

A collection of small prototype detectors, on loan from the Defense Threat Reduction Agency (DTRA), were also employed to measure the background with different detector types. They included cerium-doped lanthanum bromide ($\text{LaBr}_3[\text{Ce}]$), cerium-doped cesium lithium yttrium chloride ($\text{CLYC}[\text{Ce}]$), and strontium iodide ($\text{SrI}_2[\text{Eu}]$) scintillators, a small solid-state cadmium zinc telluride (CZT) crystal, as well as boron line tubes and straws for thermal neutron detection.

We took initial measurements at the approximate midpoint of each building, on both the rooftop and above the concrete slab floor within the building. These measurements were taken for 4,000 seconds to ensure suitable statistics for rooftop attenuation analysis. Subsequent measurements across the rooftops were taken for 900 seconds at separation distances from the primary location generally equivalent to the height of the building, but no more than twice that distance. The rooftop size and layout of each building constrained the locations of supplementary measurements. Most often, the configuration resembled a quincunx, or the pips representing the number five on a die or domino, as seen in Figure 4.2. We were not able to take supplementary measurements on all buildings, as our access to certain rooftops was limited, particularly at Livermore Site 300.

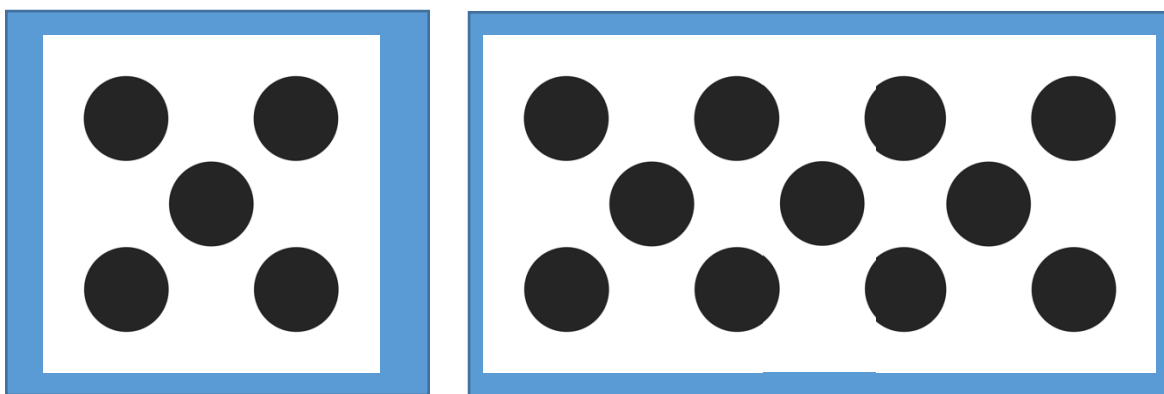


Figure 4.2: Illustration of single and repeated quincunx pattern. Source: [97] in the public domain.

The buildings chosen for this background measurement campaign were selected based on access, size, and diversity of construction materials. As seen in Figure 4.3, the buildings at Richmond Field Station varied in size, shape, height, wall construction, and roofing material. The interior construction and contents of the buildings also spanned the gamut of what one might find in an industrial setting. Figure 4.4 illustrates some of the unique elements we encountered.

Photographs of the buildings measured at Livermore Site 300 and Fort Belvoir are not included here since they are in secure areas, and the activities taking place in such buildings may be sensitive. However, these buildings exemplified the size and construction style of interest and provided a different local environment from that encountered at Richmond Field Station.



Figure 4.3 Representative light industrial buildings found at Richmond Field Station. (top left) Bldg. 486 contained tilt-up concrete exterior walls, internal cinder block masonry, I-beam structure, and steel roof decking. (top right) Bldg. 128 was built for manufacturing explosive blasting caps; it has areas with concrete walls 2 feet thick as well as corrugated steel walls and an asphalt and wood ceiling over steel trusses. (middle left) Bldg. 158 is a high-bay with an I-beam support structure and corrugated metal walls. (middle right) Bldg. 472 is a unique wooden building used for cutting cross-sections of large trees. (bottom left) Bldg. 480 contained laboratory space for analysis of concrete and asphalt road samples. (bottom middle) Bldg. 478 is a forestry products laboratory and warehouse with climate-controlled spaces. (bottom right) Bldg. 153 is used by mechanical engineering students working on small engines and contains various machining equipment. Source: [98] personal photographs.



Figure 4.4: Noteworthy characteristics of light industrial buildings. (top left) Lab in Bldg. 154 where a properly licensed and stored ^{137}Cs source was detected. Its presence was not revealed prior to our measurements. (top right) Interior view of Bldg. 158 high-bay with I-beam support structure and corrugated metal walls. (middle left) Interior view of Bldg. 486 roofing depicting steel roof decking supported by an I-beam structure. (middle right) Interior view of Bldg. 486 with concrete walls and machining equipment. (bottom left) Interior view of high-bay in Bldg. 486 with machining equipment and large rock crusher. (bottom right) Interior view of Bldg. 486 large furnace and welding equipment. Source: personal photographs.

4.1.2 Expectations

We anticipate the most significant contributions to background radiation in a light industrial building to come from the poured concrete slab and the walls. From atop the center of the roof, one can model the foundational slab as a semi-infinite half-plane with a reasonably constant source distribution. This model results in a relationship whereby the radiation field from the slab, neglecting air attenuation, is independent of distance. It is akin to applying Gauss' law to a uniform sheet of charge density σ (C m^{-2}), where the resulting electric field is uniform and independent of the distance from the sheet [99].

As shown in [7], this half-space source calculation can be useful in estimating the detector count rate from background sources if one knows or can approximate the elemental concentrations of the sources. Such information is readily available for locations in the U.S. and Canada from aerial gamma-ray data processed and maintained by the U.S. Geological Survey [42]; Table 4.1 lists data for locations germane to this study. The equation to convert the surface concentrations into a detector count rate is

$$CR(\text{min}^{-1}) = \frac{60 \ln 2 N_A BR f A_d \eta_d}{2 t_{1/2} M (\mu/\rho)}, \quad (4.1)$$

where CR is the count rate in the detector per minute, N_A is Avogadro's constant, BR is the branching ratio for the gamma-ray emission, f is the mass fraction of the emitting isotope, M is the atomic mass of the isotope, and μ/ρ is the mass attenuation coefficient for the material.

Table 4.1: Estimated surface concentrations of potassium, uranium, and thorium, based on USGS reported values [61] taken from GADRAS inject tool [64] at locations where data were taken.

Location	Potassium concentration (%)	Uranium concentration (ppm)	Thorium concentration (ppm)
Fort Belvoir, VA	0.38	1.39	4.16
Los Alamos, NM	1.68	2.49	8.38
Richmond, CA	0.60	0.83	3.59
Tracy, CA	1.21	1.64	7.12

The assumption of a semi-infinite half-plane is valid for ordinary building heights because the attenuation due to air in the energy range of the primary KUT lines is small when compared to the attenuation due to the roof material. Small thicknesses of roofing materials have the same effect on photon attenuation as several meters of air. The attenuation factor through 5 meters of air for primary KUT photons (609, 1461, and 2614 keV) ranges 2–5%. Air attenuation only becomes a factor at >50 m for gamma-ray energies above 100 keV, as illustrated in Figure 4.5. The steel, wood, insulation, and waterproofing material in the roof amount to 15–35% attenuation for the same energy photons, calculated from similar materials in the NIST X-ray Mass Attenuation Coefficients database [61].

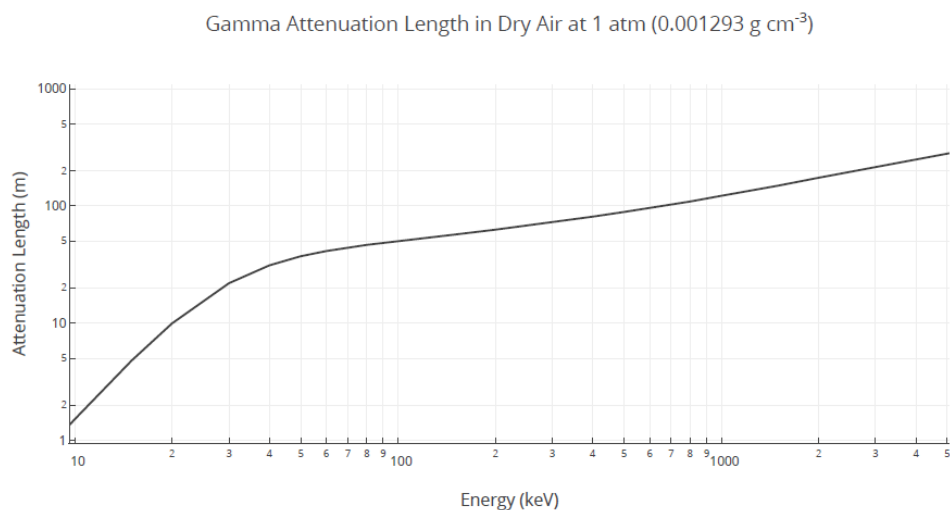


Figure 4.5: Attenuation ($1/e$) length for gamma-rays in air. Adapted from [7] with data from NIST X-ray Mass Attenuation Coefficients database [61].

Though steel contains carbon and other minor elements, we conservatively chose to use mass attenuation coefficients for pure iron. Wood has similar properties to tissue in terms of attenuating gamma-rays, though the density of plywood is nearly half that of tissue [100]. Thus, based on a review of the literature, we selected breast tissue as a suitable surrogate for plywood [101]. Roofing insulation is most often made of extruded polystyrene, and polystyrene is a material for which mass attenuation coefficients are tabulated. Ethylene propylene diene monomer (EPDM) is often used as a waterproof membrane to cover roofs. Because of its similarity in elemental composition to EPDM, we selected propane-equivalent tissue as a surrogate. The wood, insulation, and membrane material are low Z and have approximately the same effect on the gamma-ray energies of interest. The values for breast tissue, polyethylene, and propane-equivalent tissue produced nearly the same results for a material of a given thickness and density.

Table 4.2: Comparison of % attenuation of background photons by various materials [61].

<i>Material</i>	<i>Air</i>	<i>Steel</i>	<i>Plywood</i>	<i>Insulation</i>	<i>Waterproofing</i>	<i>Total</i>
<i>Thickness cm</i>	500	0.15	1.25	7.5	0.3	
<i>Density g cm⁻³</i>	1.3E-03	7.87	0.65	0.35	1.1	
<i>Source</i>						
<i>Photon energy</i>						
⁴⁰ K						
1461 keV	4.7	8.6	6.9	20.3	2.9	34
<i>U-chain</i>						
609 keV	3.1	5.7	4.6	13.8	1.9	24
<i>Th-chain</i>						
2614 keV	2.3	4.5	3.4	9.5	1.4	18

Since the material list available in the NIST database is limited, we built models in GADRAS to confirm the transmission of various energy gamma-rays through a typical roof. These models use a well-defined detector response function and are based on a combination of first-principles calculations and empirical modeling [64]. These models are in better agreement with our measured results found in Section 0.

We developed two models in GADRAS. The first was a simple 2-D layered slab geometry whereby the propagation of characteristic 1461 keV gamma-rays from the decay through layers of materials was analyzed to predict the attenuation through roof materials. First, we deposit a representative concentration of potassium in a 60 cm slab of concrete. The model produced a simulated spectrum based on this material, and then we executed an automated peak analysis to obtain an estimated count rate from ^{40}K . Next, we placed a 500 cm layer of air on to the slab and repeated the process. We continued this for all the remaining roof materials and present the results of this simulation in Table 4.3.

The second model we created was a full 3-D rendering of a building, including the concrete slab, concrete walls, and roof materials. The purpose of this model was to predict the transmission of characteristic gamma-rays from benchmark threat objects through the roof and to test the response of characterized detectors in the GADRAS library. Figure 4.6 contains a visual rendering of this model.

Table 4.3: Attenuation of the 1461 keV background peak from ^{40}K by roof materials modeled using GADRAS [64].

<i>Material</i>	<i>Void</i>	<i>Air</i>	<i>Steel 1040</i>	<i>Plywood</i>	<i>Insulation</i>	<i>Waterproofing</i>
<i>Thickness [cm]</i>		500	0.15	1.25	7.5	0.3
<i>Density [g cm⁻³]</i>		1.3E-03	7.845	0.65	0.35	1.1
Transmitted Count Rate	0.47±0.01	0.45±0.01	0.41±0.01	0.36±0.01	0.312±0.009	0.256±0.008
Layer Attenuation	—	4±3%	9±5%	11±5%	10±4%	12±4%
Total Attenuation	—	4±3%	13±3%	23±3%	34±2%	46±2%

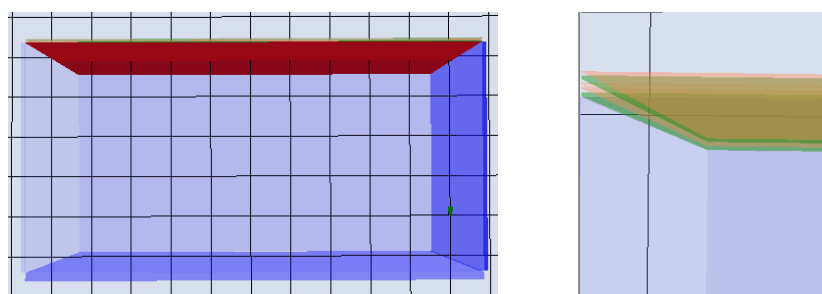


Figure 4.6: (left) 3-D model of building with a concrete slab (blue), tilt-up concrete walls (blue), steel roof decking (red), plywood decking (green), extruded polystyrene insulation (pink), and waterproof membrane (orange). (right) Zoomed in perspective to show roof layers.

4.1.3 Findings

Background radiation measurements taken on the roof looked very similar to background measured elsewhere. Still, localized conditions and diverse building materials showed higher variation than might be anticipated from surface concentration estimates listed in Table 4.1.

Although we expected local variations, the magnitude of the variation in counts from ^{40}K over short distances was unexpected. ^{40}K counts varied by as much as a factor of two across the buildings measured and by nearly that amount on the same building in one case. While unexpected, it is not so extreme when compared to the variations encountered in mobile search shown in Figure 4.10. It is also consistent with local background variations reported in [102]. Gamma-ray attenuation through the roof was consistent with predictions generated by the models in Section 4.1.2.

Gamma-ray Background Variations

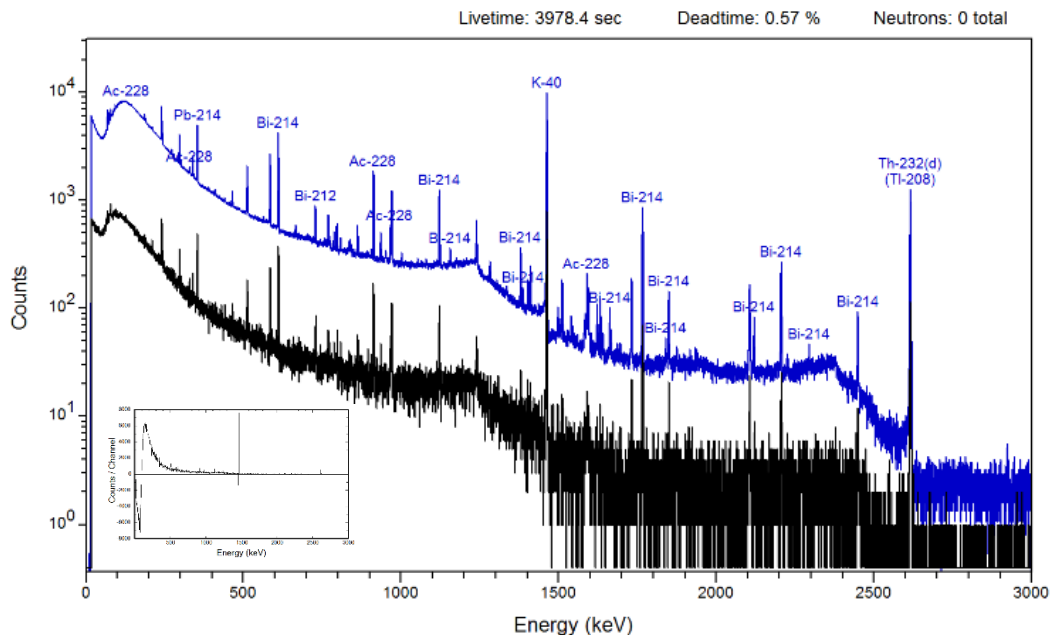


Figure 4.7: Comparison of measured background with typical long dwell background spectrum. The spectrums are not normalized to aid in visual comparison. (black) Measured ~ 4000 s background taken inside Bldg. 486, Richmond, CA. (blue) Measured 150,000 s spectrum from PeakEasyLib(3.0) taken in Los Alamos, NM in 2010 [62]. (inset) Residuals from subtracted normalized spectra.

As expected, the data are consistent with natural background radiation. Figure 4.7 shows a gamma-ray energy spectrum we measured in a building in Richmond, CA in comparison to a long-dwell background measurement taken with a similar model detector in Los Alamos, NM, distributed as part of the spectral library of PeakEasyLib(3.0) [62]. The labeled spectrum in blue highlights the dominant energy peaks for gamma-rays associated with the decay chains

of naturally occurring terrestrial isotopes. The disparity in counts per channel between the two spectra is due to a massive difference in count time (150,000 vs. 3,978 s)—this is intentionally retained to aid in the visual comparison of the peaks. When normalized and subtracted, as seen in the inset of Figure 4.7, there is undoubtedly a much higher concentration of KUT, especially potassium, in Los Alamos, NM. This finding should not be a surprise and has been measured in the past. The USGS reported values for KUT in each area are listed in Table 4.1, and Figure 4.8 visually depicts the potassium concentration in two contour maps.

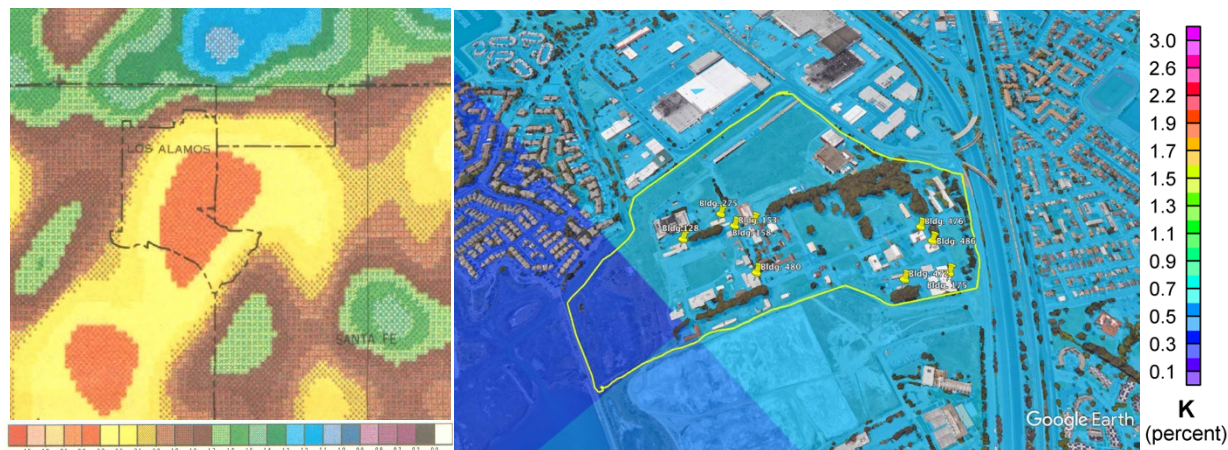


Figure 4.8: (left) Regional contour map of the estimated surface concentration of potassium zoomed into the Los Alamos region of New Mexico. Source: [103] in the public domain. (right) USGS data overlaid on ©Google Earth map of Richmond Field Station in California (yellow line). Sources: Adapted from [42, 104] with data in the public domain.

We re-calibrated spectra from ten buildings at Richmond Field Station and extracted regions of interest data to assess the variation of background across the site. We analyzed seven peaks, shown in Table 4.4, to describe the background probability distribution shown in Figure 4.9. We modeled this technique after one used by researchers analyzing background variations in mobile data collected with RadMAP, shown in Figure 4.10 [24].

Table 4.4: Background radiation peak regions of interest. Peaks were fit with a single Gaussian and a linear background using PeakEasy’s batch processing function [62].

Region of Interest	Lower Energy	Upper Energy
1	577.683	589.383
2	604.392	614.264
3	1113.780	1127.314
4	1454.190	1466.629
5	1762.659	1765.840
6	2202.503	2204.660
7	2606.239	2621.984

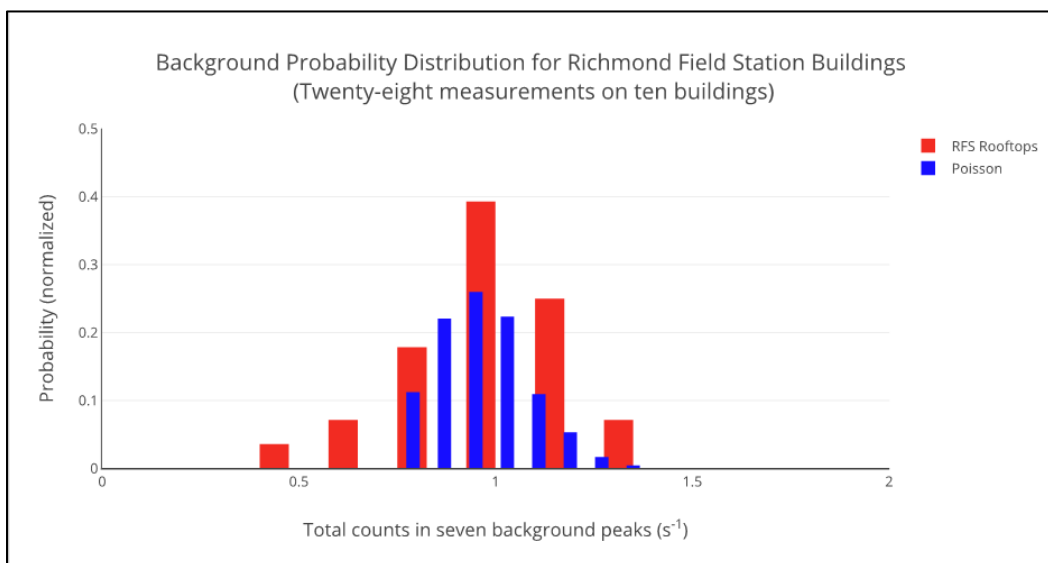


Figure 4.9: (red) Probability distribution for seven naturally occurring background energy lines measured at twenty-eight positions on the rooftops of ten light industrial buildings at the Richmond Field Station in Richmond, CA (July 2015) $\bar{x} = 0.95 s^{-1}$ (57 min^{-1}). (blue) Probability distribution of five-thousand Poisson-generated random numbers converted to cps with $\lambda = 57$.

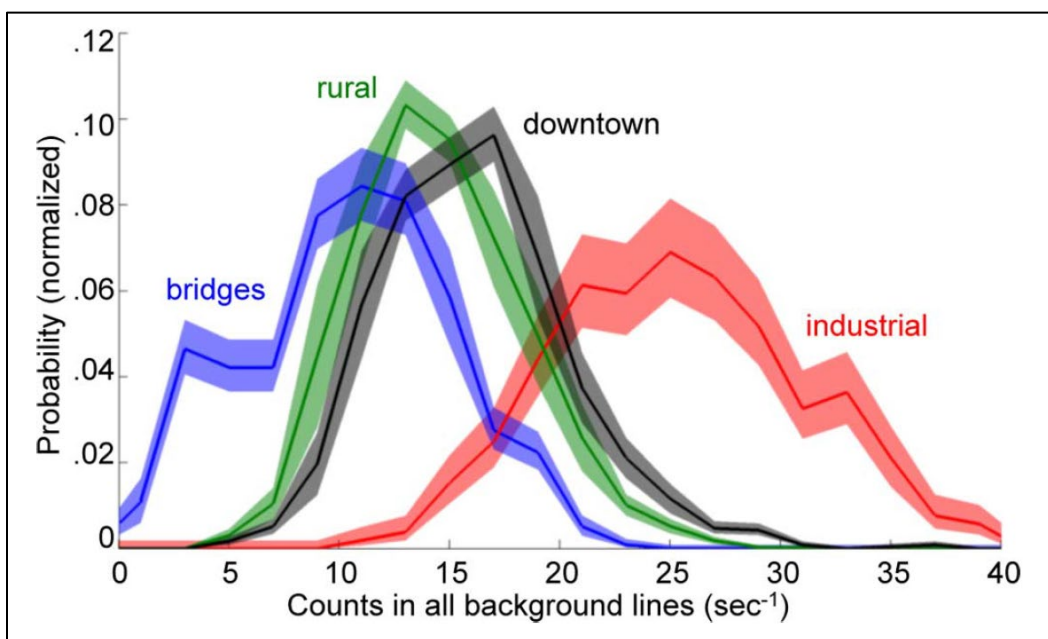


Figure 4.10: Background probability distributions for four typical environments: bridges (blue), rural areas (green), downtown Oakland (black), and the Jack London district (industrial warehouses, red). The shaded regions indicate 68% confidence intervals. Source: [24] figure is unedited and used with permission from T. Aucott.

As exhibited in Figure 4.9, the background gamma radiation levels measured across the rooftops of buildings vary beyond Poisson statistical limits. In comparison to mobile background measurements taken through four different environments in the Bay area (bridge, rural, downtown, and industrial), the normalized count rates in seven naturally occurring background energy lines most closely resemble the data taken near industrial warehouses in the Jack London district of Oakland, CA. The industrial distribution from that dataset had the highest average background count rate as well as a sizeable spread in the distribution [see Figure 4.10]. Note that the mobile data included summed spectra from twenty-four HPGe detectors with roughly $1,200 \text{ cm}^2$ of detector area, whereas we collected rooftop data using a single HPGe detector with roughly 33 cm^2 of detector area. The average rate of 0.95 peak background counts per second in the rooftop data translates to approximately 35 counts per second in a RadMAP-sized detector, which is at the high end of the industrial distribution.

While the rooftop measurements are in good agreement with the RadMAP data, there are a few plausible explanations for the elevated peak background rates from the rooftops. First, the ratio of the detector areas could be off by as much as 3%, which would translate to a difference of as much as ± 1.7 counts per second for a RadMAP-sized detector.

Second, the average source-distribution-to-detector distance was smaller for the rooftop measurements. The height of rooftops in the background measurement data ranged from 3–10 m with a mean height of 5.6 m and a median height of 5.4 m. Though the road was much closer to detectors in RadMAP, an inch of lead on the floor of the truck bed shielded the detectors from radiation entering from below. Therefore, the contribution to background peaks from KUT was from buildings, curbs, sidewalks, and other structures in the field-of-view of the detectors. These materials ranged 5–50 m from the detectors while driving, with an average distance of 10 m to the exterior walls of the closest nearby building.

Third, the peak-fitting methods used were not the same, and we may have included excess counts in the regions of interest from the rooftop data. Our rooftop data peaks were automatically analyzed with a peak-fitting routine in PeakEasy [62] using a single Gaussian fit with a linear background. The RadMAP data were analyzed using hand-selected adjacent spectral windows to estimate the background under the peak. An exaggerated estimate of the deviation between the two peak-fitting procedures could contribute to the difference. Based on the uncertainty of the net counts in the peak, this could be as high as ± 0.04 counts per second in the rooftop measurements, which translates to ± 1.5 counts per second for a RadMAP-sized detector. This extrapolation assumes that the peak-fitting routine overestimated the net peak area for each of the peaks of interest by the uncertainty of the fit.

Of note, when compiling the region of interest data, the fitting algorithm failed for some of the peaks at various measurement locations. The failure due to low statistics, especially at some of the higher energies ($>1500 \text{ keV}$), is noteworthy because the measurement device used—the ORTEC Detective-DX-100—exemplifies the ceiling of the realm of the possible for sUAS-mounted detectors. It has a relatively large active volume, is among the best for energy resolution, and the collection time for these measurements was $>900 \text{ s}$, yet some peaks were not well-enough defined for the fitting routine to automatically identify them. Many

detector options for this application will not come close to the same volume or resolution. Though longer dwell times are almost always preferred, a 300-second collection is considered an unofficial standard for presumptive field spectroscopy [105].

As seen in Figure 4.11, potassium content, which is responsible for the 1460.82 keV line, has the most significant variance by a considerable amount. As an individual peak, ^{40}K contributes the most counts to the background peak total. However, the total rate from the sum of uranium and thorium-progeny lines is on par or exceeds the average rate due to ^{40}K alone. A significant deviation in counts is observed for all seven natural background source peaks and provides strong evidence against using gross count algorithms or even energy windowing algorithms for this type of search.

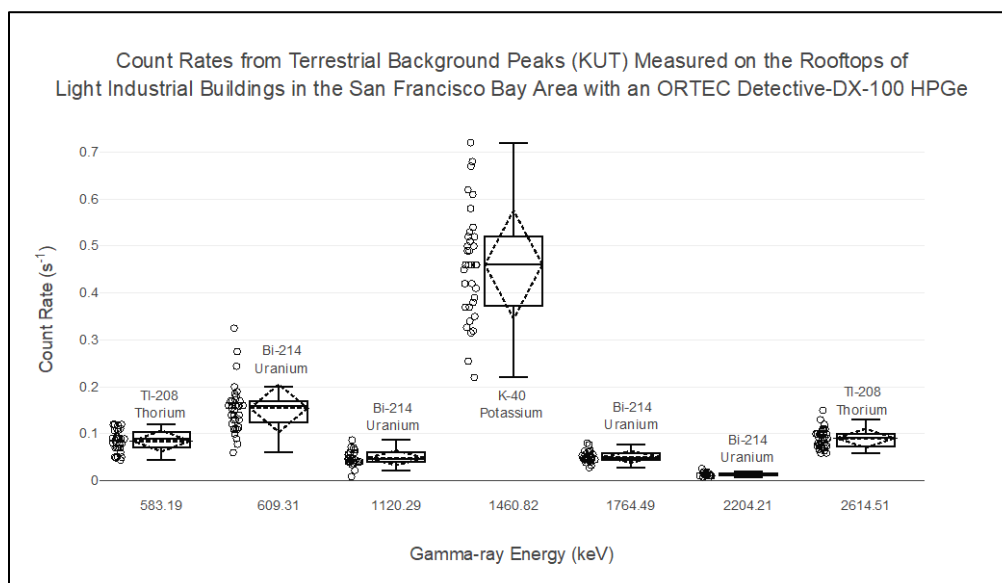


Figure 4.11: Average peak count rates for thirty-five measurements of terrestrial background measured from the rooftops of thirteen light industrial buildings in the San Francisco Bay Area using an ORTEC Detective-DX-100 HPGe detector.

The range of backgrounds encountered across different buildings at different locations is understandable. However, the variation between nearby buildings, as well as across any single building, warranted further analysis. Based on the data presented in

Figure 4.12, there is a significant amount of variation in some buildings, whereas others are relatively constant. From these measurements, it appears there is no recurrent or identifiable relationship between building height, construction, or location.

Bldg. 153 demonstrates the most substantial variation and had three different roof levels ranging 3–5.3 m. However, there is no correlation with height since pairs of locations (1&2, 3&4, and 5&6) were at the same heights, yet the most considerable variation recorded was between 3&4. Bldg. 158/158A showed little variation in background levels. The roof did have different heights, which supports the infinite half-plane conclusion that height does not impact the background when air attenuation can be considered negligible.

A noteworthy feature is seen in the data for Bldg. 486. Location 2, which is almost twice as high (10.7 m) as locations 1 and 3 (5.4 m), has a background rate 28% lower than location 1, suggesting a decreasing rate at an increased height. However, location 3, which is at the same height as location 1 but in a different section of the building, has an even lower rate (32% lower than location 1). This discrepancy contradicts any perceived correlation between height and background level.

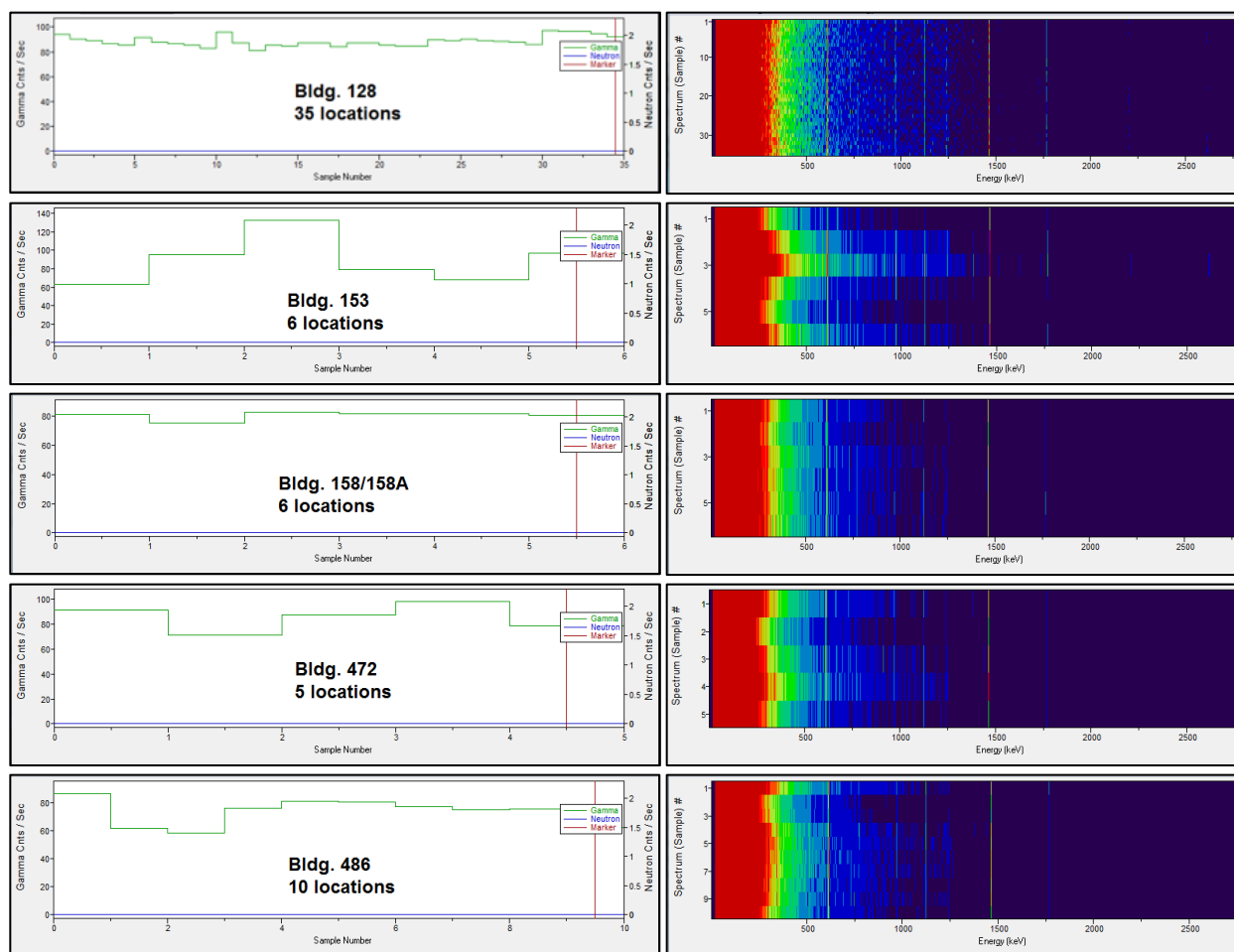


Figure 4.12: Count rate charts and waterfall plots for background measurements on Bldgs. 128, 153, 158/158A, 472, and 486.

In consideration of the impact that background variation might have on the search of a designated target, we chose to make detailed measurements at a finer pitch on Bldg. 128. We measured the background at thirty-five locations across the rooftop on a rectangular pitch. This arrangement was chosen to simulate a simple raster search pattern. We analyzed the variation of the background to inform the level of confidence required to confirm or deny the presence of threat material. Figure 4.13 illustrates the variation for the thirty-five sample locations using a color scheme that is neutral at the mean and ranges up and down three standard deviations using interpolation and smoothing algorithms.

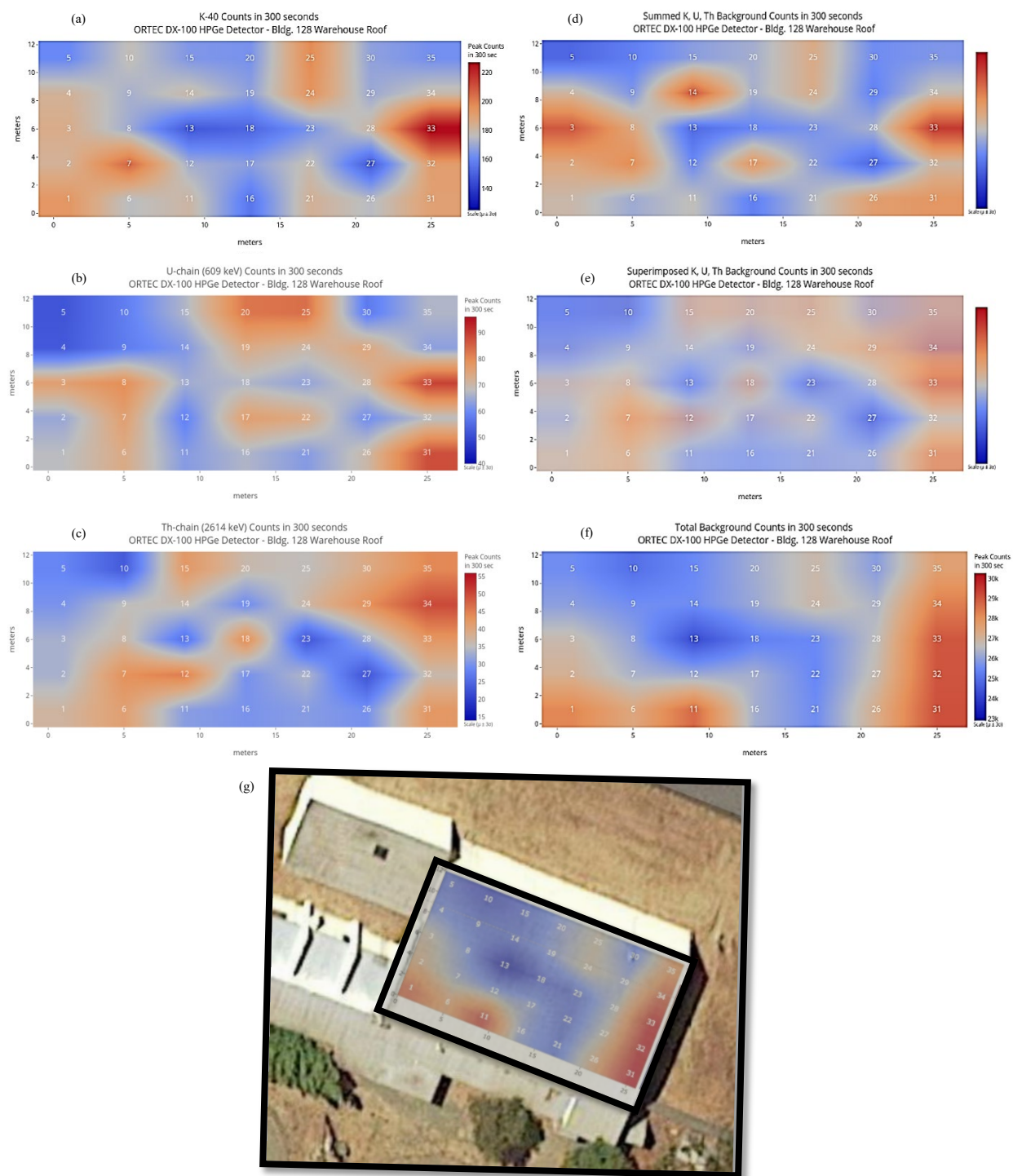


Figure 4.13: Variation of terrestrial background measured across a single building (300-second measurements at 35 locations). Counts in (a) 1461 keV peak (b) 609 keV peak (c) 2614 keV peak (d) raw sum of 609, 1461, 2614 keV peaks (e) equally weighted sum of KUT peaks (f) total counts from the full spectrum, and (g) total counts photo stitched onto an aerial photo of Bldg. 128. The color scheme is neutral at the mean and ranges \pm three standard deviations.

We analyzed the measurements of Bldg. 128 by each of the individual KUT components, the weighted and unweighted sum of primary KUT lines, and the total background counts. The spread of peak counts from potassium was about half that of the building to building comparison seen in Figure 4.11 but still amounted to a range of counts that varied by $\pm 25\%$. The sum of uranium lines was similar at $\pm 28\%$, and the spread of the sum of the thorium lines was higher at $\pm 39\%$. Table 4.5 lists summary statistics for the individual KUT contributions as well as the total background counts.

Measurements of Bldg. 128 were the most detailed and showed a rather high amount of variation for a single building. However, the nature of the construction of this building was unique. It was previously used for the fabrication of blasting caps and explosives, prior to its current use as a storage building. Some interior walls were built over two feet thick to aid in the protection of workers. They were designed to localize the effects of a blast, should an accident have occurred with the handling of the extremely sensitive primary explosive, mercury fulminate. These blast walls may have contributed to the elevated and varying background levels that were measured.

Table 4.5: Summary statistics for the variation of terrestrial background on Bldg. 128.

<i>300 s collection</i>	⁴⁰ K <i>1461 keV</i>	<i>U-chain</i> <i>609 keV</i>	<i>Th-chain</i> <i>2614 keV</i>	<i>Total</i> <i>Counts</i>
Mean counts	177.8	68.4	35.3	26612
Standard Error	2.7	1.6	1.2	187
Median	178.4	66.7	36.0	26338
Mode	182.7	67.7	29.9	27114
Standard Deviation	16.9	9.4	7.1	1168
Sample Variance	287.2	89.0	50.7	1363145
Range	83.6	37.7	27.7	4887
Minimum	146.8	51.5	22.4	24235
Maximum	230.4	89.2	50.1	29122
Sum	6934.1	2325.5	1165.9	1037870

The background variation will impact the dwell time required to adjudicate each location of the building. The dwell time per measurement location is the free parameter that can be adjusted since the source-to-detector distance and incidental shielding are fixed for a given building. The source-to-detector distance has a minimum equal to the height of the building minus the height of the source from the ground. The signal attenuation from the roofing materials is fixed, aside from the added effect of the angle of incidence (discussed later in Section 4.2.2) and possible interference from structural materials such as beams and supports.

For a background that is twice as large, it could take up to twice as long to detect the same source activity level at a 95% confidence level. For example, using data collected with a ¹³⁷Cs source present with an initial counting time of 1,800 sec, and measured background levels in the 662 keV regions with a Detective-DX-100 HPGe detector, doubling the background

would require at least 3,370 seconds to detect the same source. Depending on the detector resolution and threat source activity, the dwell time scaling can be significant. Sharp peaks associated with sub-0.2% energy resolution detectors have a much better signal-to-noise ratio and therefore a much lower MDA.

Gamma-ray Attenuation

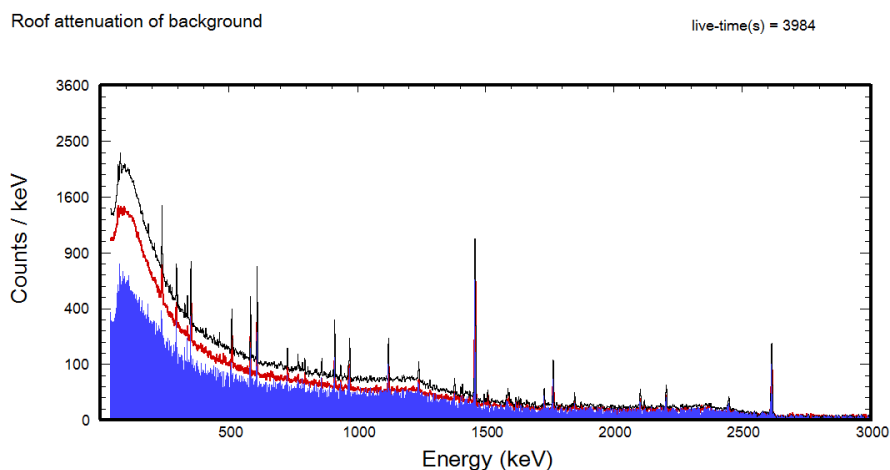


Figure 4.14: Attenuation of the background radiation by roof materials in Bldg. 486. (black) Background energy spectrum acquired in the center ± 0.5 m of the room at 30 ± 2 cm above the floor. (red) Background energy spectrum acquired in the center ± 1 m of the roof. (blue) Subtracted spectrum denoting attenuated signal, assuming no contribution from roof materials.

As anticipated, the attenuation of the gamma-ray signal through the roof is roughly 50%, exhibited in Figure 4.14. The three normalized spectra plotted from top to bottom are: the background spectrum measured at the approximate midpoint inside Building 486; the background spectrum measured on the roof of Building 486 nearly directly above the interior measurement; the difference between the first two spectra, which represents the gamma-rays that do not make it through the roof to the detector. The near parity between the bottom and middle spectra in the photopeaks, made more noticeable in Figure 4.15, confirms the $\sim 50\%$ attenuation of the background by the roof materials.

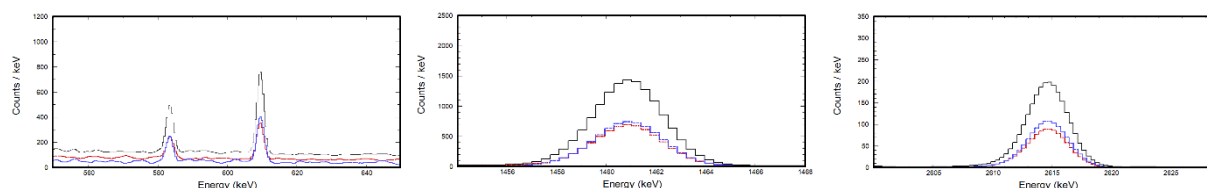


Figure 4.15: Zoomed in spectra from Figure 4.14 for representative background energies peaks (583 and 609, 1461, and 2614 keV) demonstrating roughly 50% attenuation indicated by the nearly equal roof (red) and subtracted (blue) background levels.

4.2 Source Detection

Small radioactive sources were transported to Richmond Field Station and positioned in several locations inside Bldg. 128 to test the efficacy of source detection methods from the rooftop using various types of detectors.

4.2.1 Methods

The sources we chose to conduct this investigation covered a wide range of energies and provided a varying number of identifiable peaks. Table 4.6 lists relevant properties of the sources we used.

Table 4.6: Characteristics of sources used to test the efficacy of detection from the rooftop of Building 128, Richmond Field Station, Richmond, CA 23–26 August 2016.

Isotope	Source ID UC Berkeley EH&S	Half-life (yrs)	Activity as of 22 AUG 2016 (μCi)	Primary gamma-ray energies (keV) [62]
^{57}Co	37688	0.745	2.54	122, 136
^{60}Co	872	5.3	5.59	1173, 1333
^{133}Ba	872	10.53	7.47	303, 356, 383
^{137}Cs	778–780	30.1	3 @ 8.67 ea.	662
^{152}Eu	873	13.537	7.94	122, 344, 779, 964 1086, 1112, 1408
^{241}Am	783	433.2	9.90	59.5

4.2.2 Expectations

As the detector moves off-axis from directly above a source, the projected area of the detector changes. Depending on the shape and orientation of the detector, this can have an appreciable effect. For a right circular cylinder with an end cap normal to the roof, the effective area of the detector can be calculated by

$$\textit{Effective Area} = A_{\textit{face}} \cos \theta + A_{\textit{side}} \sin \theta \quad (4.2)$$

$$= \pi r^2 \frac{H}{\sqrt{H^2 + D^2}} + 2rl \frac{D}{\sqrt{H^2 + D^2}}, \quad (4.3)$$

where $A_{\textit{face}}$ is the projected area of the end cap of the detector cylinder, $A_{\textit{side}}$ is the projected area of the side of the detector cylinder, θ is the incident angle of the gamma-ray, r is the radius and l is the length of the detector cylinder, H is the vertical source-to-detector distance, and D is the lateral source-to-detector distance. See Figure 4.16 for a depiction of the arrangement and labeling of the variables.

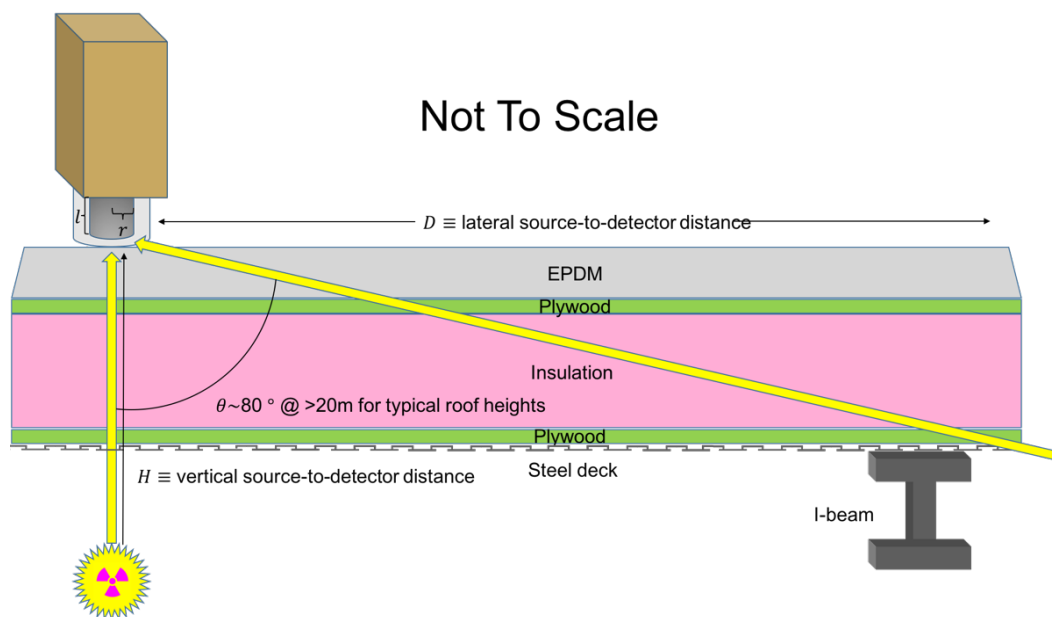


Figure 4.16: Schematic of the varying path length for attenuation through roofing materials.

Figure 4.17 shows the change in the effective area of the detector as the lateral source-to-detector distance increases. The maximum effective area occurs at a distance roughly equal to the height of the building. This projection implies that the ideal measurement location is not directly above a source for this detector shape, orientation, and building configuration. Detector area effects count rate proportionally while the source-to-detector distance has an inverse square effect. Figure 4.18 plots the effective area versus the source-to-detector distance squared and confirms a maximum at an offset location. This finding suggests that one should consider the projected area of the detector when selecting lattice spacing, a topic which is discussed further in Section 6.1.

A different detector size, shape, or orientation will influence this consideration. For example, a cylindrical detector, with its axis parallel to the roof, presents the same effective area to a source that bisects its side centerline, regardless of its lateral distance. Yet, the same detector rotated 90° to the source develops a similar profile with lateral distance as the one shown in Figure 4.18. Cuboid-shaped detectors display similar directional effects, depending on the ratio of the length of their sides. A detector which presents the largest effective area at the distance of closest approach, to a source in any direction, is desirable. Hence, a cube or ideal cylinder is a sound starting point for a detector shape, as long as the stopping power is sufficient for higher energy gamma-rays.

When the detector is off-axis from the source, the apparent cross-sectional thickness that gamma-rays penetrating the roof encounter also increases significantly. The apparent thickness of the roof is magnified by more than a factor of 4 times the actual vertical thickness when the source is 20 meters off-axis, as depicted in Figure 4.16. There is also a much higher

probability of the incident gamma-rays confronting structural supports, such as I-beams or other dense materials, on their path to the detector at high incident angles.

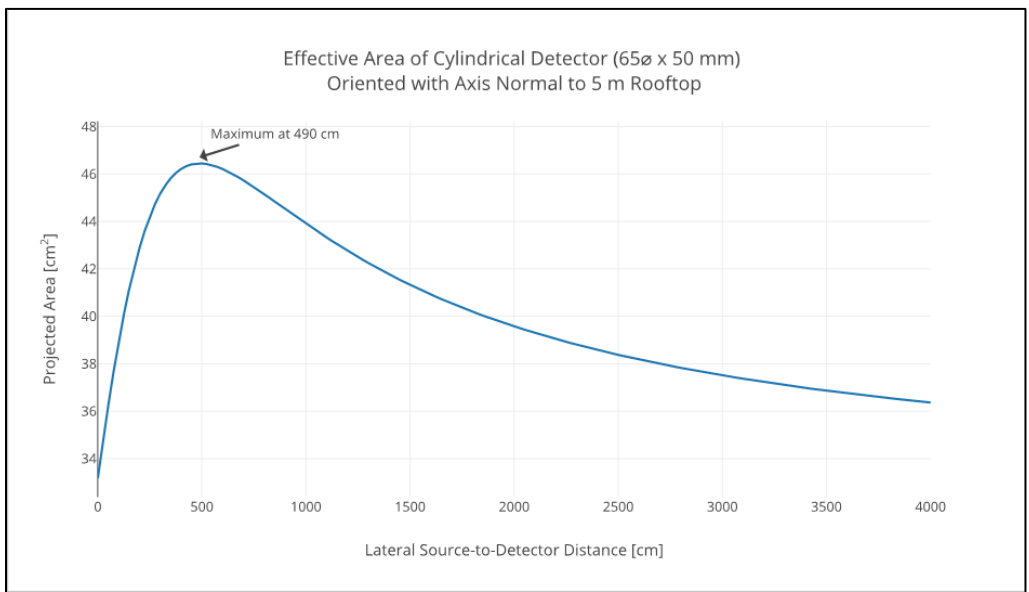


Figure 4.17: Graphical representation of the effect of lateral source-to-detector distance on the projected area of a cylindrical detector oriented normal to a horizontal surface above a source.

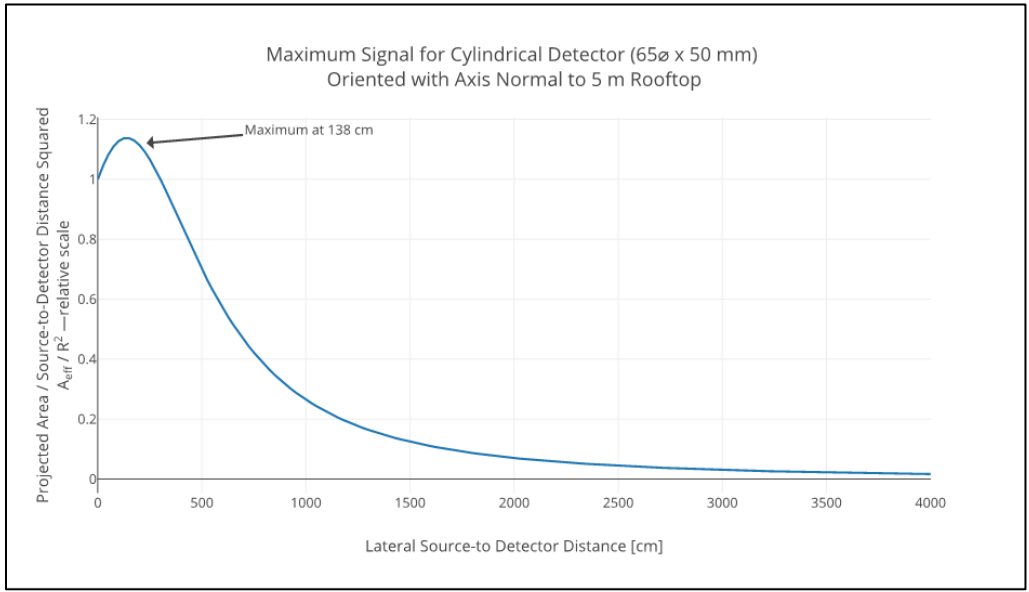


Figure 4.18: The effect of lateral source-to-detector distance on the detector count rate, illustrated by the ratio of projected detector area to the source-to-detector distance squared.

The standard counting statistics definition for the signal-to-noise ratio, as it relates to radiation detection, is

$$SNR \approx \frac{S}{\sqrt{S+B}}, \quad (4.4)$$

where S represents the counts due to the source, and B represents the counts from the background. This equation applies to count rates as well, in this application, because the source and background are taken together for the same amount of time.

Doubling the source-to-detector distance has a profound impact on the signal-to-noise ratio and the time to detect, as illustrated in Figure 4.19. In the limit with a strong source, where $s \gg b$, one should expect no more than a fourfold increase in the required counting time at the longer distance. Yet, when $s \approx b$, a doubling of the distance results in the time to detect being ten times greater. As the source strength diminishes with respect to the background, such that $s \ll b$, a doubling of the distance results in a time to detect that approaches sixteen times greater.

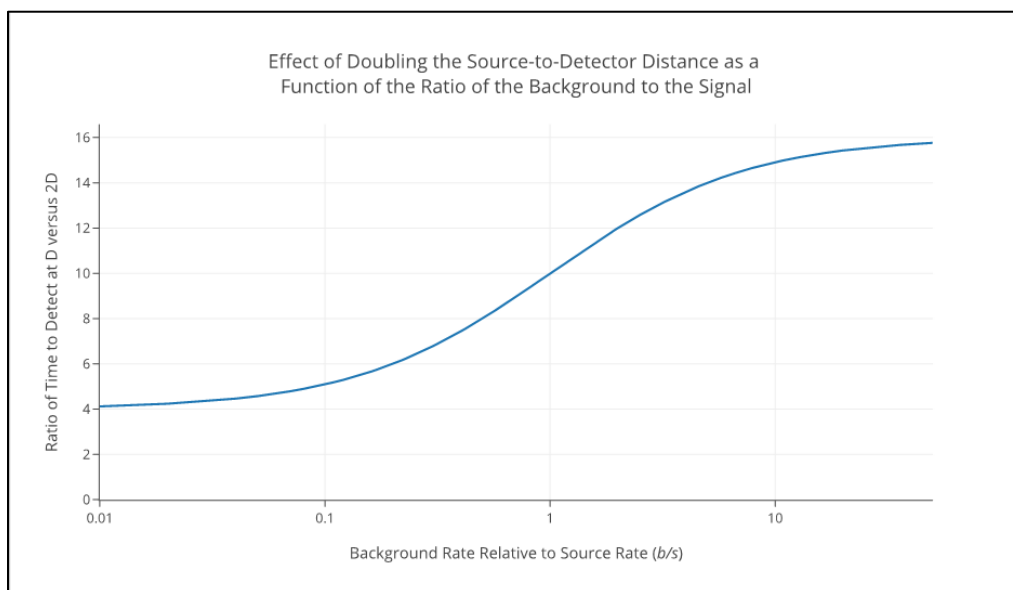


Figure 4.19: Semi-log plot illustrating the effect the doubling the source-to-detector distance has under varying background conditions with respect to source strength.

4.2.3 Findings

The time to detect 26 μCi of ^{137}Cs , at a given distance, generally followed the expected inverse power law, as shown in Figure 4.20. We acquired these data with the source in the building at a location one meter above the floor, clear of unintentional shielding and away from the walls. We initially placed the detector on the roof directly above the source and then moved it laterally along the long axis of the roof for subsequent measurements. We calculated the source-to-detector distance using the lateral distance and relative height above the source.

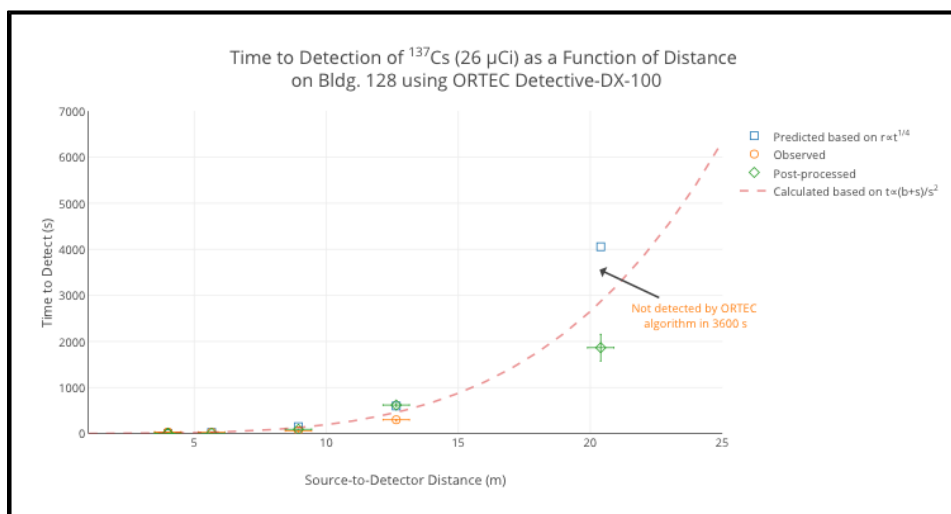


Figure 4.20: Time to detect 26 μCi of ^{137}Cs versus distance on the rooftop of Bldg. 128. The detector was approximately 4 m above three small sources located 1 m above the floor.

We determine the observed detection time based on the ORTEC Detective-DX-100 alerts when taking measurements of the cesium source. The uncertainty in the time to detect was considerable due to the use of the detector algorithm and measurement conditions. We monitored the user interface for the first 30 seconds and then every 30 seconds afterward to see if the isotope identification algorithm produced an alert. Thus, we can only narrow the time to a 30-second window.

The first few measurements show fair agreement with theoretical predictions based on changes to the source-to-detector distance alone. For these distances, the detector algorithm alarmed sooner than the predicted time. These early detections could purely be a result of the stochastic nature of the measurement, where counts in the peak stacked up above a threshold sooner than predicted by a deterministic model. Alternatively, the proprietary algorithm on the detector might have employed full spectrum analysis and observed a template match before the photopeak alone. It also could have been an adjustable sensitivity setting, set such that the detector algorithm traded off an increase in the false-positive rate for a decrease in the probability of a false negative. Regardless, the system alarmed as expected at the distances examined with one outlier. At the furthest distance, an alert was not produced in 3,600 s.

We do not know why the detector algorithm did not alarm at this distance. A calculation based on the source strength and median count rate of the background in the peak, which was previously measured, predicted a 3σ detection in under 2,870 seconds. However, a scaling calculation, based on the initial measurement directly above the source and the new source-to-detector distance, estimated the time for a 3σ detection at 4,060 seconds, which is longer than our collection time. An automated peak analysis of the measured spectrum using PeakEasy identified a peak at $>4\sigma$. A manual selection of the peak and background regions drove this up to $>7\sigma$ [62]. Automated post-processing of the spectrum using GADRAS, shown in Figure 4.21, clearly identified a peak and assessed it at $>7\sigma$ above background [64].

Trial 6 - Cs137 (26 uCi) at 20.4 m

live-time(s) = 3588

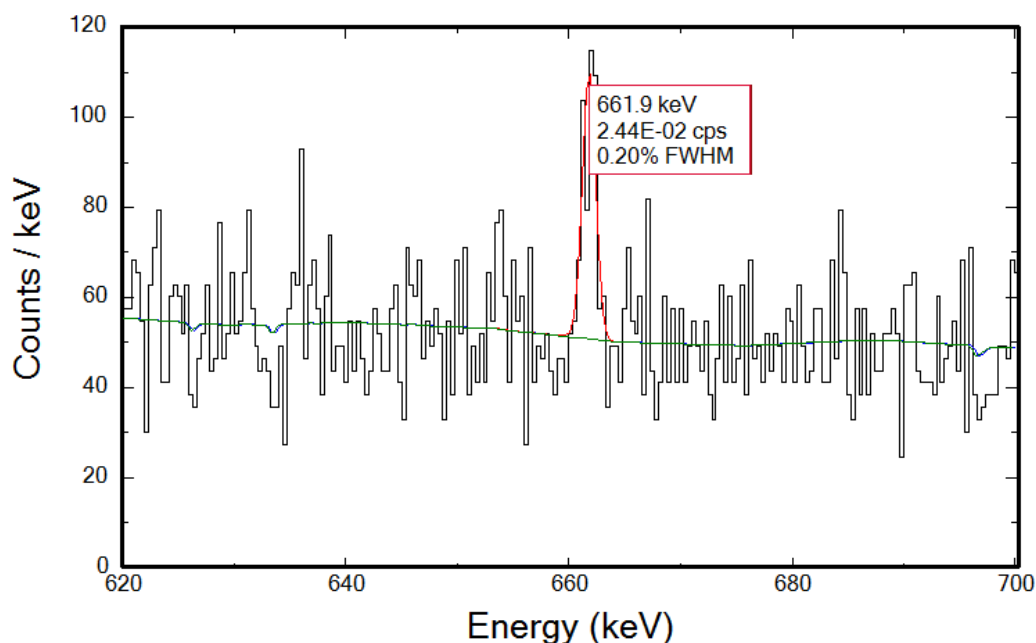


Figure 4.21: Zoomed in spectra from rooftop measurement with 26 μCi of ^{137}Cs present at 20.4 m lateral distance and 4 m relative height. The native algorithm on the ORTEC Detective-DX-100 did not trigger an alarm, but post-processing with GADRAS distinctly indicates a peak.

The deviations from the expectation at longer distances could also be a result of the amplified roof attenuation, previously discussed in Section 0, due to the increased cross-sectional thickness of the roof. The apparent thickness of the roof is magnified by more than a factor of 4 times the actual vertical thickness when the source is 20 meters off-axis, as depicted in Figure 4.16. The increased path length in effect attenuates 80% of the 662 keV photons, up from 33%.

The purpose of this data collection effort was to get a sense of the detection ranges for long-dwell rooftop collection using a relatively large detection medium with the best resolution available. We did not intend to map out a detection range versus time plot. However, if one were to repeat this type of experiment, we recommend acquiring in list mode and analyzing in post-processing to improve the uncertainty in detection time. Also, one should sample more locations at closer intervals to validate or refute the predicted results with better precision.

Three of the four prototype detectors, referred to in Section 4.1.1, were also used to collect data concerning source detection. The fourth detector, $\text{SrI}_2(\text{Eu})$, was not operable during this collection effort. Performance metrics for each of the detectors are found in Table 4.7. This assessment informed the trade space for gamma-ray detectors discussed later in Section 5.3.2. Spectra from a representative trial for each of the detectors are found in Figure 4.22.

Table 4.7: Performance of small prototype detectors on rooftop 4 m from 25 μCi of ^{137}Cs .

Detector material	Detector Size [mm]	Laboratory Energy Resolution [662 keV]	Field Trial Energy Resolution [662 keV]	Peak counts	Peak-to-Total Ratio [%]	Trials achieving 5σ in 595 sec
LaBr ₃ (Ce)	25 ϕ ×76 25 ϕ PMT	3.9%	5.97%	2350	3.80	6/6
CLYC(Ce)	25 ϕ ×25 51 ϕ PMT	4.9%	3.9%	162	1.54	5/6
CZT	10×10×10 CPG ASIC	1.4%	1.9%	36	1.08	5/6

Noticeably, there were issues with the LaBr₃(Ce) detector as it significantly underperformed its resolution potential. A review of the spectrum in Figure 4.22 suggests that the dynamic range was truncated, forcing higher energy counts into lower channels. It also shows a substantial low energy peak, which suggests that the low-level discriminator was set improperly, and excess counts were placed into low channels. As this was a custom prototype detector, we did not have access to many of the advanced settings in the controller.

The CLYC(Ce) detector seems to have under-promised and over-delivered. While its efficiency at higher energy is relatively low, it demonstrated reasonable energy resolution at 662 keV and performed adequately for the detection trials. It shows promise in that it is capable of both gamma-ray spectroscopy and neutron detection. The manufacturer did require a PMT twice the size of the crystal to ensure the best possible energy resolution.

For this test, the CZT crystal was small but mighty. With a detector area six-and-a-half times smaller than the CLYC(Ce) detectors and nineteen times smaller than the LaBr₃(Ce) detector, it was able to detect the ^{137}Cs with just 36 counts in the peak at a 5σ threshold. Though it is expensive, its energy resolution per unit total mass, which includes signal-chain-processing components such as PMTs, SiPMs, and ASIC/FPGAs, makes it a strong candidate for sUAS-based detection.

We also conducted additional trials with other isotopes and smaller activities in Bldg. 128. These data show that sources with low activity and low energy gamma-rays are indeed challenging to detect. A weak, mixed isotope source consisting of ^{241}Am , ^{133}Ba , and ^{137}Cs was used to simulate a distorted plutonium spectrum. The detection algorithm for not one of the three prototype detectors alarmed on this source in ~ 1800 s measurements. Post-processing of the spectra revealed weak peaks in the regions of interest, but not enough to indicate a clear detection. ^{57}Co , ^{60}Co , and ^{152}Eu sources were also tested but were also below the MDA.

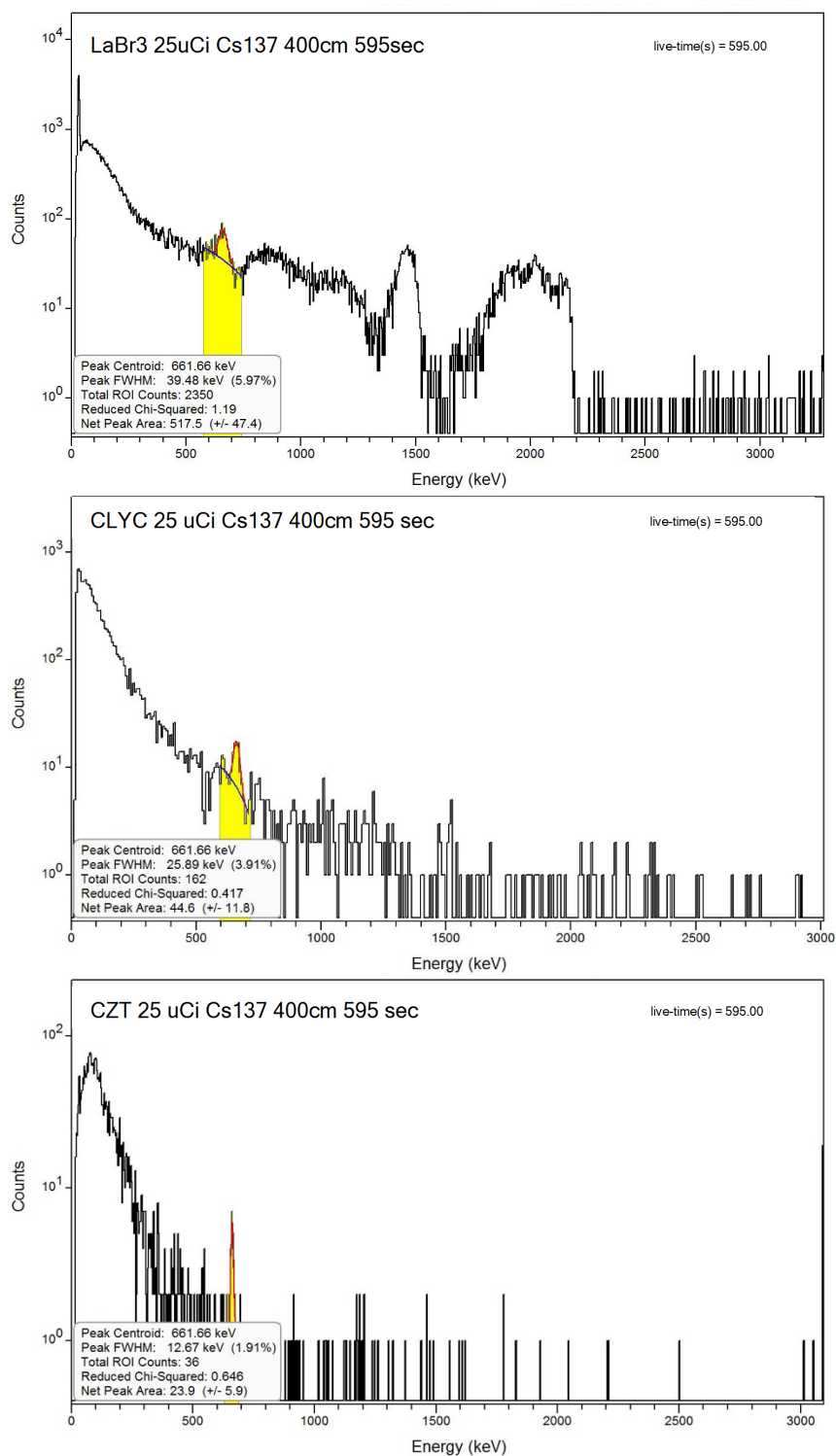


Figure 4.22: Sample spectra from three prototype detectors collected for 595 s from the rooftop of Bldg. 128 approximately 4 m above 25 μCi of ^{137}Cs .

An additional measurement campaign sponsored by DTRA took place in the summer of 2015 at the Nevada Nuclear Security Site [106]. User groups surveyed radiation test objects containing Category I quantities of SNM, as defined by Nuclear Regulatory Commission (NRC) [107], in different configurations, with an array of passive radiation detectors. We conducted this ad hoc testing under quasi-operational conditions while researchers prepared the active-interrogation system for subsequent trials. Test coordinators positioned various construction materials, including wood, steel, and adobe walls, around the source. Unfortunately, the background radiation at the test range was elevated by more than a factor three of due to activation of the ground and nearby materials from the pulsed bremsstrahlung source used for the active interrogation testing. DTRA retained the data from the measurement campaign, but they were not releasable to this study.

4.3 Summary

Understanding the background and its variation over time and space is a crucial component of any radiation detection scheme. Background levels and the associated variance have a significant impact on the MDA of a source. In this application, the collection time required to distinguish the presence or absence of a source is of most interest. From the data collected, it appears that background on top of light industrial buildings will be at the higher end of the distribution when compared to rural and urban areas. The variation does not seem to be correlated with building height or distance from exterior walls, though the dataset examined is limited. The variation across similar building types ranges ~50% when looking at the contribution from the top seven background peaks. Across a single building, this variation ranged 25–40%, depending on the particular background peak.

The extent to which roofing materials attenuate gamma-rays is of concern for this detection scheme. The limitation on detector volume imposed by the weight capacity of an individual UAV signifies an already low signal environment. Significant reduction by attenuation makes this detection strategy untenable. Fortunately, the attenuation by the air and roofing materials amounts to roughly ~50% when passing normal to the roof and continues to increase as the incident angle between the source and the detector increases.

Depending on the detector and measurement geometry, some maxima for counting occurs when the detector is not directly over the source. This occurs because the effective area projected by the detector grows when one moves off-axis, but the source-to-detector distance changes very little. This phenomenon should be taken into consideration when selecting an optimal lattice spacing for measurement locations.

Detection of small activity source is indeed possible under certain conditions, but it requires improved resolution and long dwell times. The best resolution per unit mass at the maximum size for a given UAV's weight capacity is likely the best choice for this application. Signal processing electronics, as well as any other ancillary components, such as a mechanical cooler, need to be included in the mass calculation.

5 Sensor Suite Design

A central objective of this study is to recommend a sensor suite that overmatches the broadest range of expected threats under an established set of operational conditions. Size, weight, and power are always a factor when considering a materiel solution to provide a capability. In this case, the requirement to conduct operations remotely will exclude some higher fidelity approaches.

5.1 Requirements Analysis

Several high-level requirements documents should be referenced or established to design a practical and effective sensor suite. These include a concept of operations (CONOPS); an operational mode summary and mission profile (OMS/MP); a set of constraints, limitations, and assumptions; and a list of validated performance attributes. The intent of this study is not to develop the elements of a complete acquisition strategy. However, using elements of these documents as a framework will improve the overall system design and will allow one to develop a relevant capability more efficiently.

5.1.1 Concept of Operations

A concept of operations is a verbal or graphic statement that clearly and concisely expresses what the commander intends to accomplish and how it will be done using available resources. At a minimum, the CONOPS should identify the problem being addressed, the mission, the commander's intent, an operational overview, functions or effects to be carried out or achieved, and the roles and responsibilities of affected organizations [108]. The full CONOPS for the directed search for radiological and nuclear material of concern is beyond the scope of this study, as it encompasses much more than sUAS-based detection. Therefore, we developed a limited CONOPS just for sUAS-based detection.

The problem being addressed is the expected possession of radiological or nuclear material that could potentially be used in an IND, RDD, or RED by a potential adversary. Search forces must detect, locate, and identify the presence of radiological or nuclear material of concern, or substantiate its absence with a high level of confidence, in target buildings within 12–24 hours of arriving in the vicinity, to allow assault forces to characterize and recover the material. The intent is to confirm or deny the presence of the material in a given target building with high confidence. Finding the material defines success. However, reducing the number of viable target buildings through comprehensive measurement is also valuable in that it allows intelligence assets and assault forces to concentrate on high-likelihood targets. Figure 5.1 serves as a thumbnail sketch of a potential CONOPS for the slice of the mission that is relevant to sUAS-based detection.

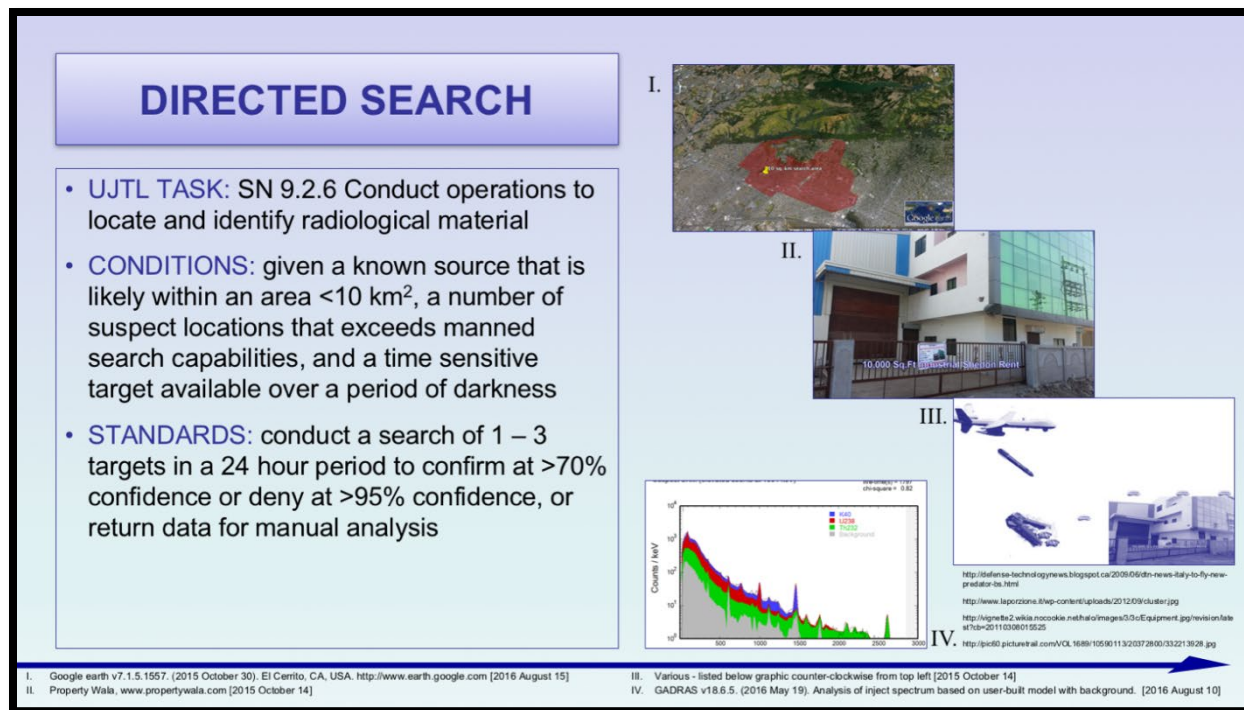


Figure 5.1: Preliminary graphical depiction of a concept of operations concerning the use of unmanned systems for the directed search for radiological and nuclear material. Source: [109]

5.1.2 Operational Mode Summary & Mission Profile

The operational mode summary and mission profile describe the operational tasks, events, duration, frequency, and environment in which a system is expected to perform each mission and each phase of a mission. The OMS/MP describes how a system will be used both in wartime and peacetime, with a focus on reliability, availability, and maintainability. It projects the mix of ways a system will be used for training and missions as well as the types of environmental conditions and terrain to which it will be exposed [108]. An abbreviated OMS/MP might include the following:

Tasks – The primary task the system must accomplish is to confirm or deny the presence of radiological and nuclear threats in a target location. Figure 5.2 contains a high-level overview of the functions, behaviors, tasks, components, and processes related to accomplishing this task.

Duration – The duration of directed search operations is likely to be more than 24 hours but less than a week.

Frequency – The frequency of use for this system is limited. It is expected that operators will conduct functional checks weekly, limited training monthly, operational training quarterly, and use it in a full-scale exercise annually. The likelihood of real-world employment is difficult to predict but is not expected to occur more than a few times during the lifecycle of the system.

Environments – The system must be able to function in all operational environments; this includes land and sea, desert and tundra, low-lying areas and mountainous terrain. The system must be capable of operating at night and in moderate precipitation. It should continue to function after exposure to dusty or sandy conditions for the duration of an operation.

Phases – An operation is likely to consist of the following phases: (1) alert, deploy, and stage, (2) gather ISR, plan, and prepare, (3) execute and assess, and (4) recover, refit, and redeploy.

Reliability – the system must always work under the stated conditions. While subsystems and components are expected to fail at times, the design of the system must factor in redundancy at all levels and prevent any common-mode failures that render the system ineffective. With regards to risk assessment, the default probability for the worst-case conditions should be equal to one. That is, engineer the solution to accommodate the worst case rather than betting that it will not happen.

Availability – A contingency capability must always be deployable for each search force. The basis of issue plan should reflect the requirement for additional systems to accommodate training, maintenance, and testing. All equipment should be rotated through the training cycle to ensure system functionality under operational conditions.

Maintainability – Maintenance of the system is expected to consist of component-level exchange; a knowledgeable electronics technician with 40 hours of training on the system should be capable of all required operational-level maintenance and calibration.

Revision control – Because of the pace at which technology in this area is moving, we expect there to be considerable spiral development in all areas of the system: hardware, sensors, software, and firmware. Any component upgrades must pass rigorous beta testing and perform as expected in an operational environment during a full mission profile before being fielded. Upgrades will take place system-wide by group; teams will not be expected to work with mixed generation equipment.

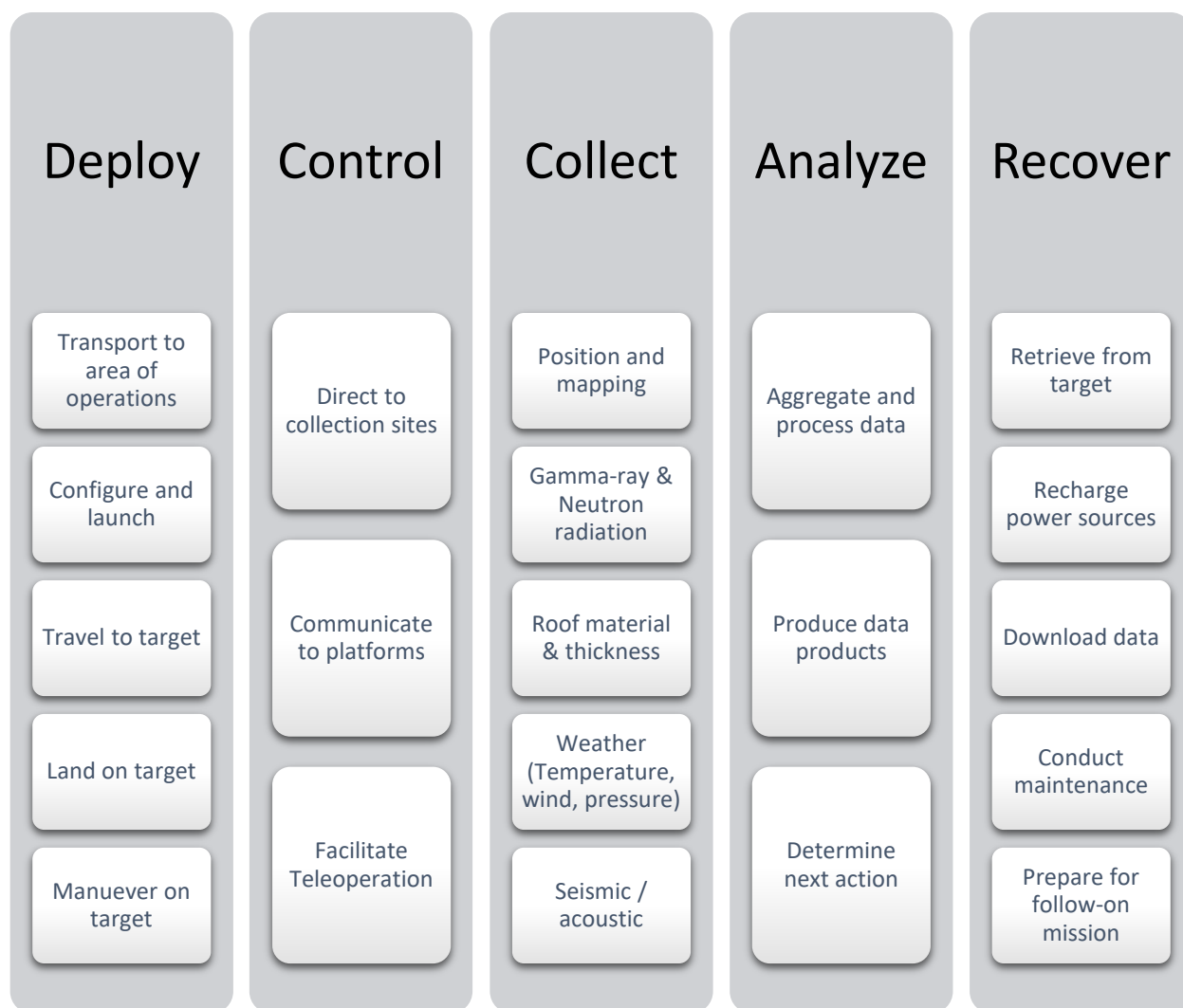


Figure 5.2: High-level block diagram illustrating the various functions, behaviors, tasks, components, and processes of the envisioned system.

5.1.3 Constraints, Limitations, and Assumptions

Whether planning a military operation or developing an analysis of alternatives, it is important to generate a set of constraints, limitations, and assumptions, generally developed in that order. The terms constraints, limitations, and assumptions have specific yet slightly different meanings in the context of operational military planning as opposed to systems analysis. Even within military planning, there is a difference in the lexicon between joint doctrine and service (e.g., Army) doctrine. Therefore, it is useful to elaborate on these terms and identify them as they might apply to a directed search scenario.

In joint military planning, a limitation is an action required or prohibited by a higher authority, such as a constraint or a restraint, and other restrictions that limit the commander's freedom of action, such as diplomatic agreements, rules of engagement, political and economic conditions in affected countries, and host nation issues. A constraint is an action

that one must take, and a restraint prohibits an action [110]. Conversely, Army doctrine refers to all restrictions placed by the higher command as constraints, whether they dictate an action or inaction [111]. In systems analysis, especially for wargaming, a constraint is a restriction imposed by the user or sponsor, whereas a limitation is usually the inability of the system to fully meet an objective or requirement [112].

In military planning, an assumption provides a supposition about the current situation or future course of events and is presumed to be true in the absence of facts. A valid assumption has three characteristics: logical, realistic, and essential for planning to continue. One must continually review assumptions to ensure their validity and must challenge them if they are unrealistic [110]. In wargaming, assumptions are usually required to accommodate a limitation and must meet the similar criteria of necessary, valid, and acceptable [112].

This study is a hybrid of military planning and systems analysis. Therefore, in this study a constraint is something that must be accomplished or achieved by the system; a limitation is something that cannot be accomplished or achieved; an assumption will meet the criteria of necessary, realistic, and acceptable. Applying these terms to a remote radiological and nuclear threat detection concept exposes the following:

Constraints

For an anticipated light industrial building, the system must:

- semi-autonomously deploy to the target from a location up to 1 km away, land on a target and collect for up to 12 hours, and extract to a retrieval location
- detect relevant, most likely threats with at least 68% confidence and confirm the absence of threats to at least 95%
- measure gamma-ray and neutron radiation on a target at a fixed location for 96 hours
- have enough capability to interrogate up to three targets simultaneously in 24 hours
- include a gamma-ray detector capable of spectroscopy
- be deployable by air within 12 hours and require no more than three aircraft pallet positions; fit as cargo in one van and three large SUV-style vehicles
- have a long-term independent means to track the location of platforms

Limitations

The system must not:

- conspicuously alert building occupants or bystanders to its presence
- require manual piloting
- require more than eighteen platforms per target building

Assumptions

- an anticipated light industrial building is 5 m high and less than 900 m²; there may be buildings with higher roofs and larger footprints
- a delivery vehicle exists or can be developed that can achieve a low enough signature (noise, visual, electromagnetic) that a commander would deploy it in a directed search scenario
- an engineering solution to achieve suitable flight characteristics, guidance control, landing retardation, and payload stabilization and preservation exists or can be developed for munition-style delivery methods
- the intelligence assessment has high confidence that the threat is credible, is of high-consequence, and is expected in the designated search area
- a relevant threat analysis will require a higher level of classification

5.1.4 Performance Attributes

Operational attributes from the CONOPS and OMS/MP inform the analysis of alternatives and help translate capability gaps into system-specific requirements. These requirements describe performance attributes which are defined by threshold and objective values. A threshold value delineates the minimum performance required to achieve the required operational effect. An objective value describes a higher level of performance that delivers significant increased operational effect or decreased operational risk; it is the desired operational goal, usually achievable at higher risk in cost, schedule, or technology [108].

Performance attributes are critical to the development of an effective capability. They are characterized in one of three ways: (1) as a Key Performance Parameter (KPP)—something critical to mission effectiveness, (2) as a Key System Attribute (KSA)—considered important to achieving a balanced solution, but not critical enough to be a KPP, or (3) as an Additional Performance Attribute—not important enough to be a KSA or KPP but still appropriate to include [108]. Currently, there are four KPPs that must be addressed for all DoD systems: system survivability, force protection, energy, and sustainment. One must either address the KPP and provide threshold and objective values for performance, or justify why a particular KPP is not appropriate for a system. Addressing these high-level KPPs is beyond the scope of this study. However, Table 5.1 provides a preliminary attempt at establishing performance attributes for one aspect of an sUAS-based directed search system—the SNM threat.

A KPP for this system is the detection of SNM threats. While an exploration of the most relevant, likely, and dangerous threats requires a higher level of classification, an example KPP can be developed using unclassified criteria. The threshold and objective values for the type of SNM can be derived from the previous discussion of signatures in Section 3.1.2. HEU at low weapons-grade enrichment levels and reactor-grade plutonium set the threshold mark, whereas virgin HEU and low-burnup-produced plutonium set the objective level. The IAEA definition of an SQ lends itself well to a threshold value for the quantity of material, and the

NRC values for Category I Strategic SNM defines the objective value [107]. The source-to-detector distance is driven by the analysis of building heights, and the shielding is indicative of a partial attempt to limit the dose to nearby personnel. Oxides may be easier to detect than metals based on their geometry and potential for increased neutron production. Figure 5.3 illustrates the signal collected by an HPGe detector located on the rooftop above 1 kg WG HEU and Pu threats.

Table 5.1: Proposed Key Performance Parameters for a small unmanned directed search system.

Threat Property Type	Threshold Value	Objective Value
		HEU (85% ^{235}U) RG Pu (>19% ^{240}Pu)
Mass of Material	25 kg 8 kg	5 kg 2 kg
Source-to-Detector Distance	5 m	15 m
Shielding	Unshielded	1 cm steel 5 cm HDPE
Chemical Form	Oxide	Metal

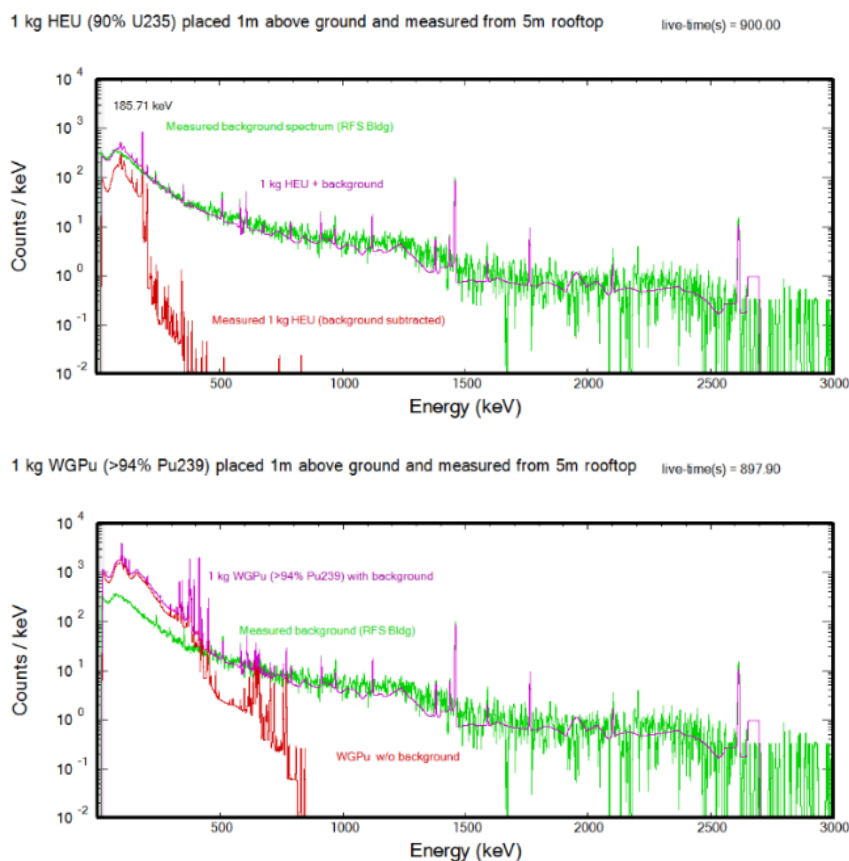


Figure 5.3: Simulated spectra of 1 kg-quantities of weapons-grade highly enriched uranium and plutonium as measured from a rooftop [64].

5.1.5 System-level Requirements

Building from the OMS/MP, we break down the high-level functional view into a system architecture found in Figure 5.4. The envisioned system currently entails four subordinate layers with at least sixteen tasks. The task-level links an exemplary purpose or behavior to a broad set of sensor types. The sensors, such as a radio, could be broken down further to their components, e.g., antenna, radio frequency transmitter/receiver, compressor/decompressor, but that level of detail and specificity is beyond the scope of this study.

Sub-System	Task	Potential Sensors/Components	
Command and Control	Communicate instructions	Low-bandwidth Receiver/transmitter	
	Communicate data	High-bandwidth Receiver/transmitter	Data storage server
	Process data	Central processing unit	Graphical processing units
	Track position and status	Situational awareness software	
Primary unmanned platform	Take-off, fly to, and land on target	Light Depth and Ranging	Barometer
		Global Navigation Satellite System	Electronic Speed Controller
		Visual Camera	Anemometer
		Inertial Measurement Unit	Ultrasonic
	Move on roof	Global Navigation Satellite System	Trace explosives collection
		Distance encoder	Light Depth and Ranging
Detect radiation	Inertial Measurement Unit		
	Gamma-ray	Geiger-Mueller counter	
Ancillary platforms	Detect human activity	Neutron	
		Ultra-wide band radar	Seismic/acoustic
	Identify structural materials	Infrared thermal-imaging	Ultra-wide band radar
	Estimate background radiation	Hyperspectral imaging	Multispectral imaging
	Detect explosives	Trace sample collection	Sample analysis techniques
Detect high-Z, dense objects	Nuclear resonance fluorescence	X-ray backscatter	
Logistics	Provide power	Spare batteries	Battery chargers
	Maintain equipment	Spare systems	Spare parts
	Calibrate system	Calibration sources	Calibration equipment
	Recover systems	Tag, track, locate beacon	Contingency payment funds

Figure 5.4: Sub-system architecture depicting the location and role of sensors within the system.

5.2 Trade Space

The term trade space has long been used in economics and systems engineering. It is also used extensively by project managers within the DoD and other government agencies. To some degree, it is synonymous with cost-benefit analysis, an approach traditionally used to provide a comparison of alternative solutions to identify the most cost-effect choice [113], whereas

the term *trade space* is the set of multidimensional outputs or outcomes of interest from a particular process or set of choices that cannot be simultaneously optimized. The trade space maps from a set of defined alternatives, or a bundle of choices, to a set of outcomes in the multiple outcome dimension of interest. The frontier (or Pareto frontier) of the trade space is the subset of outcomes corresponding to alternatives for which one cannot increase the outcome for a good or decrease the outcome for a bad by choosing another alternative without increasing or decreasing a good or bad value, respectively, in another dimension [114]

The trade space includes several components including traditional factors such as size, weight, power, and cost, as well as other factors such as noise signature, ease of deployment, shelf-life, maintenance needs, ruggedness and durability, communication bandwidth requirements, and reliability. While cost is a factor, it is not the principal criteria for making technical or operational best-value decisions in this case. One would still pursue a costly but minor improvement if it achieved overmatch in a plausible threat scenario. Other factors such as reliability and redundancy will carry significant weight and may direct technical choices that drive up cost well beyond the lowest price technically acceptable choice.

There are several paradigms for exploring trade space to inform decision-makers [115]. This section aims to outline the outcomes of interest and map a small subset of options available at the time of this study. It is by no means inclusive of all options, nor does it map all the envisioned trade space. Rather, it serves as a first-order attempt to demonstrate a viable option is achievable.

To begin, Table 5.2 provides a snapshot comparison of multi-rotor, vertical take-off and lift (VTOL) fixed-wing, and helicopter UAVs, as well as tube-launched guided vehicle systems that one could use as delivery vehicles. The UAV market moves remarkably fast, and the systems described here are merely examples of the range of capabilities achievable at a fixed point in time. Point of fact, the AV Shrike/Cube is no longer available, and production of the Pegasus III is not likely to continue.

The capacity of the vehicle system used to deliver the sensor package to the roof determines the size limit of the component sensors. Weight capacity is the more constrained resource, but the size of sensors could be an issue as well, especially if a smaller-class delivery option is required and auxiliary sensors are deemed useful and necessary.

Table 5.2: Specifications for small unmanned aerial vehicles (multi-rotors, vertical take-off and lift (VTOL) fixed-winged (FW), and helicopters) and tube-launched guided systems. * indicates data not available.

	System	Wing span [cm]	Dimensions L×W×H [cm]	Max Weight [kg]	Max Payload [kg]	Flight time [min]	Base Cost [~\$k]	Ref.
M u l t i - r o t o r	DJI Matrice 200		88×88×40	6.1	1.45	24	7.5	[116]
	DJI Matrice 600	167	167×152×73	15.5	5.5	18	5	[116]
	DJI Agras MG-1	200	200×200×42	24.5	10	10	15	[116]
	AV Qube/Shrike	92	90×90×38	2.5	< 0.5	40	50	[117] [118]
H e l i c o p t e r	Pulse Aerospace Vapor 35/55 helo	165 229	140×63×48 196×66×59	14.5 25	2.3 5	45–60	* 90	[119] [120]
	V T O L / U G V	AV Shrike 2 VTOL FW	132	83×132×25	1.2	0.3	*	*
Vertical Tech. DeltaQuad VTOL FW		235	90×235×25	6.2	1.2	110	10	[122]
Robotic Research Pegasus III UAV/UGV		102	104×102×66	20	4.5	10	125	[123] [124]
L a u n c h e d	Raytheon Pike Laser guided munition	6	4ø×43	0.7	0.3	n/a	1–10	[125] [126]
	DefendTex 40 Tube- or hand-launched rotor	~30	~4ø×20	0.18	0.11	12	1	[127]
	AV Switchblade Tube-launched FW	92	61×92×10	2.5	0.3	10	70	[128]
	DefendTex 81 Tube- or hand-launch rotor	~85	~8.1ø×65	3.1	1.1	90	*	[127]
	Raytheon Coyote Tube-launched FW	150	91×150×15	5.9	1.8	60	15	[129]

5.2.1 Size

The entire reconnaissance system, including control station, multiple vehicles, auxiliary equipment, such as maintenance items and spares, and charging stations should fit into 2-3 large SUVs. The only caveat is alternative signature systems that might require a larger vehicle or other specialized equipment in order to be employed.

The horizontal footprint of each standalone vehicle for directed search should be less than 2 m in diameter, and the height of the vehicle should be less than 1 m. Smaller is certainly preferred, but a reduction in wingspan and the number of motors will severally limit payload capacity. In general, the entire payload should be no bigger than 5,000 cm³. Some systems can accommodate upwards of 10,000 cm³, but it is more likely that the payload will exceed weight limitations before reaching the volume limit. A munition-style payload may be restricted to just 200 cm³.

5.2.2 Weight

The capacity of the delivery vehicle(s) limits the weight of the overall sensor suite. On the low end of small multi-rotor UAVs, the payload limit is approximately 500 g, whereas the high end is nearly 10 kg. Guided munitions and vehicles support payloads of 110–1,800 g. Increasing the weight of the payload reduces flight time and range, auxiliary power, and may increase the visual and acoustic signature of a UAV. A target payload of 1.5–2 kg is capable of being carried by a medium-sized multirotor UAV.

While the employment of multiple delivery vehicles, each with different sensors, is certainly possible, the distribution of various unique sensors across multiple platforms increases risk and reduces redundancy. The desire is to provide the same capability on each delivery vehicle to reduce system complexity, promote standardization, and provide the most extensive coverage. Should that not be possible, no critical sensor should be employed in quantity less than two, ascribing to the military adage “two is one, one is none.”

5.2.3 Power

The power budget is shared amongst the delivery platform, the sensors, and the control system. Each of those parts is essential at various times during an operation. Therefore, one should consider using independent power sources for all three components. For sensors that are emplaced or otherwise not mated to the delivery system, this is already a requirement.

The primary power sink is the delivery vehicle. The system must be able to transport sensors to the target building from a kilometer or more away, move or place them across the rooftop at each of the designated measurement locations, and recover the sensors when the collection is complete. Aerial movement expends roughly 20–50 times the amount of power as does ground movement for the same platform. As an example, the Pegasus III can fly only 22 minutes without a payload, yet it can drive up to 8 hours [124]. Therefore, there is a significant advantage to a system that can traverse a rooftop without having to take to the air.

A system must be able to operate for 8–96 hours. During that time, the control system, data acquisition, and radiation detection subsystems are likely to be operating. If present, a drive system will occasionally be engaged to maneuver the sensors to new measurement locations. The linear distance traveled is a function of the order in which the system travels to each measurement location. For an anticipated building size, that distance is 100–500 m.

The power required for traveling to, on, and from the target ranges is approximately 500–

1600 W for multi-rotor systems and as low as 185 W for VTOL fixed-wing systems. In comparison, a radiation sensor package and control system operating might drain a 75 W·h battery by the end of a 24-hour operation. Power is nearly as crucial as weight, and the two are entangled; a requirement for more power to operate sensors drives up the weight of the payload, which places an additional burden on the platform that requires either more stored energy or reduced flight time.

5.2.4 Cost

The target cost of a total system should be less than \$2M with a goal of under \$300k per individual platform. We base these estimates on personal knowledge of the cost of currently fielded equipment. For example, high-fidelity gamma-ray spectroscopy systems, such as the ORTEC Detective-DX-100, cost on the order of \$80–100k, and mobile systems that employ NaI(Tl) logs and ^3He tubes can cost upwards of \$250k each. Outfitting a search team with a full complement of radiation detection equipment costs well over \$500k. Therefore, the \$2M system-cost assumes that three teams are available to conduct this part of the operation with an additional team in reserve.

Looking at upper limit values found in Table 5.2 and Table 5.3 and using a factor of two times the materials cost, a goal of \$300k per platform appears to be achievable; using the same method to bound the low-end cost results in a platform cost of ~\$50k. We base this estimate solely on a rough order of magnitude cost of the components of a system and an assumed multiplier of two to assemble the system from a final approved design. This estimate does not include the cost to develop, test, and refine the design.

Table 5.3: Sensor-level Size, Weight, Power, and Cost estimates

System	Size [cm ³]	Weight [g]	Power [W]	Base Cost [\$k]	Ref.
Control	40–100	20–60	1–6	0.1–0.3	
Gamma-ray	50–200	250–500	0.150–0.750	15–40	[130] [131]
Neutron	25–200	25–150	< 0.5	1–2	[130] [132] [133] [134]
Visual	500–1500	30–600	0.5–10	1–8	[135] [136]
LiDAR	160–600	130–590	2–8	0.5–5	[137] [138]

5.2.5 Visibility Profile

One must take into consideration the visual, acoustic, electromagnetic, and other signatures that the system transmits to the environment. The size and shape of the delivery vehicles, the sensor types and modalities, and the configuration of the entire system could

present various indicators to an adversary. As noted in limitations, a commander must balance the risk to mission compromise via adversary tip-off with the probability of success given the employment of particular tools or assets. Remote radiation detection will not be the only tool a commander has in his toolkit, even in the case of lost or stolen nuclear or radiological material. Traditional methods of network analysis, pattern-of-life observation, and surveillance tracking may have a lower signature and still tip and cue forces to the correct location. Therefore, for the sensor suite to provide maximum operational value, the signatures of the entire system should be considered and reduced to the extent possible while still maintaining minimum capabilities to detect a range of threats. There are three primary windows to consider for evaluating system observables and signatures: (1) the movement to and from the target, (2) descension to and ascension from the target, and (3) movement and sensor collection on the target.

The visual signature of the system is driven primarily by the platform designed to carry the payload to the target. Generally, a smaller and lighter system presents the least signature. With regards to delivery to the target, a launched munition might present the smallest signature, depending on the launch method, the aerodynamics of the round, and the distance from the launch site to the target. However, a launched munition must be retarded in some way before impacting the roof of the target building. A winged system, or one that transforms from a winged to a VTOL configuration, offers an extended range between the launch site and target building, and can likely approach from a much higher altitude. A typical multirotor or helicopter presents the largest and most identifiable silhouette of the platforms considered.

Movement of the delivery platform is the primary source of acoustic emissions for the system. The ability of the sensors to move once on the roof is highly desirable for reasons described in more detail in Chapter 6. Movement between measurement locations can be accomplished by flying, driving, hopping, rolling, thrusting, or otherwise propelling the sensors to a new position.

The electromagnetic signature is a factor that will affect the communications architecture of the system and may limit the use of some types of active sensors. The communication between platforms as well as back to the command and control hub should either be masked in the typical background, limited in frequency and duration so as not to be detected easily, or avoided to provide the lowest signature possible. Active sensors, such as LiDAR, could also be a concern.

5.2.6 Other Considerations

Some considerations one might take into account are ease of deployment, serviceable life, routine maintenance and calibration schedule, durability, communication bandwidth requirements, and perhaps others. For example, a UAV that folds to nearly flat for storage and transport and quickly locks into a flight-ready configuration when taken out of the box is preferred to one that does not collapse and requires some tool-based assembly before a flight. A sensor which is expected to last for the lifetime of the system (5–10 years) is preferred to one that requires replacing every year or two. A radiation detector that self-calibrates and

requires little more than a functional check with a source is preferred to one that requires frequent recalibration and technician-level service. A component that still works after a UAV crashes during a training exercise is preferred over a delicate component that is guaranteed to break if dropped from a few feet. Finally, a system that can work in a bandwidth-constrained environment is preferred to one that is contingent on a large data pipe.

The point of this discussion is to illuminate additional factors to consider that may impact the trade space beyond the established size, weight, and power. It is imperative that these be explored and rank-ordered early in the system development because of the interdependency of many of these factors. Often a low-maintenance system is large; a rugged detector is heavy; a communications link is a power burden; a flight-ready system is expensive.

5.3 Functional-level Components

5.3.1 Delivery Vehicles

We considered five vehicle types for getting the sensors to the target: multi-rotor UAV, helicopter UAV, VTOL fixed-wing UAV, transforming UAV/UGV, and guided payloads.

Multi-rotor UAVs

Multi-rotors dominate the sUAS landscape for several reasons: first, they are among the most inexpensive platforms; second, they are relatively easy to fly; third, they are versatile and configurable; and finally, they can access locations that cannot be reached by a fixed-wing UAV. Figure 5.5 provides an example of a capable multi-rotor UAV for this application.



Figure 5.5: (left) Photograph of a DJI Matrice 600 Pro in flight with a prototype 3-D radiation mapping payload developed at the Lawrence Berkeley National Laboratory. Source: [139] used with permission from R. Pavlovsky. (right) The same platform with a different radiation detector payload on the rooftop of Bldg. 128. Source: personal photograph.

Helicopter UAVs

While small remotely piloted helicopters have been around for some time, only recently have they become stable enough to be flown by novice pilots using semi-automatic controls. Other than small remote-control hobbyist platforms, most helicopter UAVs have been immense (>3 m length) gasoline-powered systems, such as the Yamaha RMAX or Schiebel Camcopter S-100 [140]. However, smaller gas and battery-powered systems have entered the market and boast useful payloads and flight times for their size. Examples include the Alpha 800, UAVOS UVH-EL, and Vapor 35/55.



Figure 5.6: AeroVironment's Vapor 55, an example of a battery-powered unmanned helicopter. Source: [119] used with permission from B. Carraway of AeroVironment.

VTOL fixed-wing UAVs

VTOL fixed-wing UAVs combined the benefits of multi-rotor platforms for take-off and landing with fixed-wing endurance and range, and they can transition between the two modes during flight [141]. Current systems tend to be targeted to the agriculture sector for managing crops as well as the law enforcement and military sector for hasty ISR.



Figure 5.7: AeroVironment's Quantix, an example of a vertical takeoff and lift fixed-wing platform. This system is purpose-built for crop scouting and can cover 400 acres in a 45 m flight. Source: [142] used with permission from B. Carraway of AeroVironment.

Hybrid UAV/UGV



Figure 5.8: Pegasus III by Robotic Research (top) driving on land, (bottom left) perched on a rooftop, and (bottom right) flying up a stairwell. Source: [124] used with permission from J. Frelk of Robotic Research LLC.

Guided Payloads

One could dispense air-dropped parachute-retarded canisters to emplace sensors on a roof. The sensors may be affixed to some small UGV that could also traverse the roof. The sensors

could be employed in groups or separately. Multiple small canisters would likely be employed to provide redundancy and limit the damage or noise that might be incurred from impacting the roof with a larger canister.

One could similarly project a payload onto the roof via some tube mechanism like that of a grenade launcher or mortar. The payload for ground-launched projectiles or missiles is constrained by the diameter and range of the tube and propelling charge. Common diameters for launched grenades and mortars range from 37 to 120 mm with payloads of 100–1,800 g.



Figure 5.9: Examples of tube-launched projectiles and missiles that could deliver a detector payload to the target. (top left and right) The Pike® is a miniaturized, laser-guided weapon. Source: [125] used with permission from B. Edwards of Raytheon Company. (top middle) The Drone 40 Loitering Platform can be fitted with a small sensor payload. (bottom) The Drone 81 is in development with up to 1.1 kg payload, 45 km range, and 1.5-hour flight time. Source: [127] used with permission from T. Reddy of DefendTex.

5.3.2 Radiation Detectors

Gamma-ray

There are many candidate gamma-ray detectors available. However, for this application, the best possible energy resolution per unit mass is almost certainly the best choice. Given the level of effort required to place a sensor on the rooftop of a target building, this is not an area to scrimp on capability. The trade space for this application leans heavily toward solid-state detectors ranging from mechanically-cooled HPGe to coplanar grid or pixelated CZT.

We see that our threshold value of an unshielded SQ of WG HEU is almost instantly detectable by all detector types and is not a discriminating factor. Whether it takes ten seconds or thirty seconds has no real impact on our choice of sensor. We also see that several of the detectors have trouble detecting the threats at a distance, and they all failed to alarm on the objective quantity at the objective distance. These detections are based on a single measurement evaluated by a template-fitting algorithm. Other algorithms trained on SNM with a specific detector in a controlled environment are expected to perform better. Also, a trained spectroscopist with unique knowledge of nuclear weapons and shielded SNM should be able to discern indicators of HEU in some of these spectra that did not meet the alarm threshold for the identification algorithm.

Table 5.4: Estimated time-to-detect (± 30 s) threshold and objective highly enriched uranium threats for several detector materials based on assumed parameters for the unmanned detection scheme using a 1-D model and the IsotopeID function in GADRAS [64]. * indicates the source was not detected using the algorithm in the expected maximum mission time of 27,000 s. † indicates that an alarm was not triggered, but a spectral analysis indicated the presence of ^{235}U .

Detector Type	Type/Quantity Enrichment	25 kg HEU	5 kg HEU	25 kg HEU	5 kg HEU
		93.5%	93.5%	93.5%	93.5%
	Distance	5 m	5 m	15 m	15 m
	Shielding	Unshielded	1 cm steel	Unshielded	1 cm steel
	Area [cm^2]	[s]	[s]	[s]	[s]
1 ea. NaI(Tl) 25 ϕ \times 82 mm	21	<30	*	*	*
2 ea. CsI(Tl) 25 \times 25 \times 50 mm	26	<10	*	*	*
3 ea. CLYC(Ce) 25 ϕ \times 25 mm	19	<10	*	*	*
2 ea. LaBr ₃ (Ce) 38 ϕ \times 32 mm	24	<10	*	*	*
6 ea. CZT 20 \times 20 \times 15 mm	24	<10	600	870	*
1 ea. HPGe 60 ϕ \times 25 mm	22	<10	120	180	7,200†

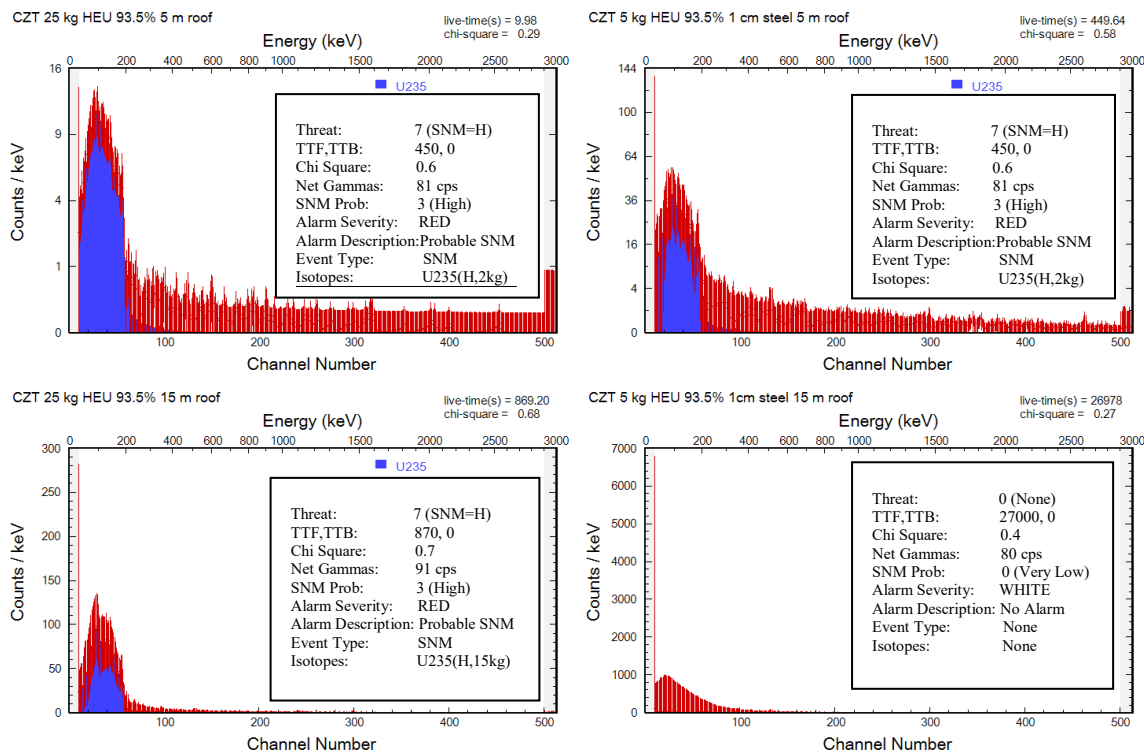


Figure 5.10: GADRAS simulated spectra for six cadmium zinc telluride (CZT) detectors [64].

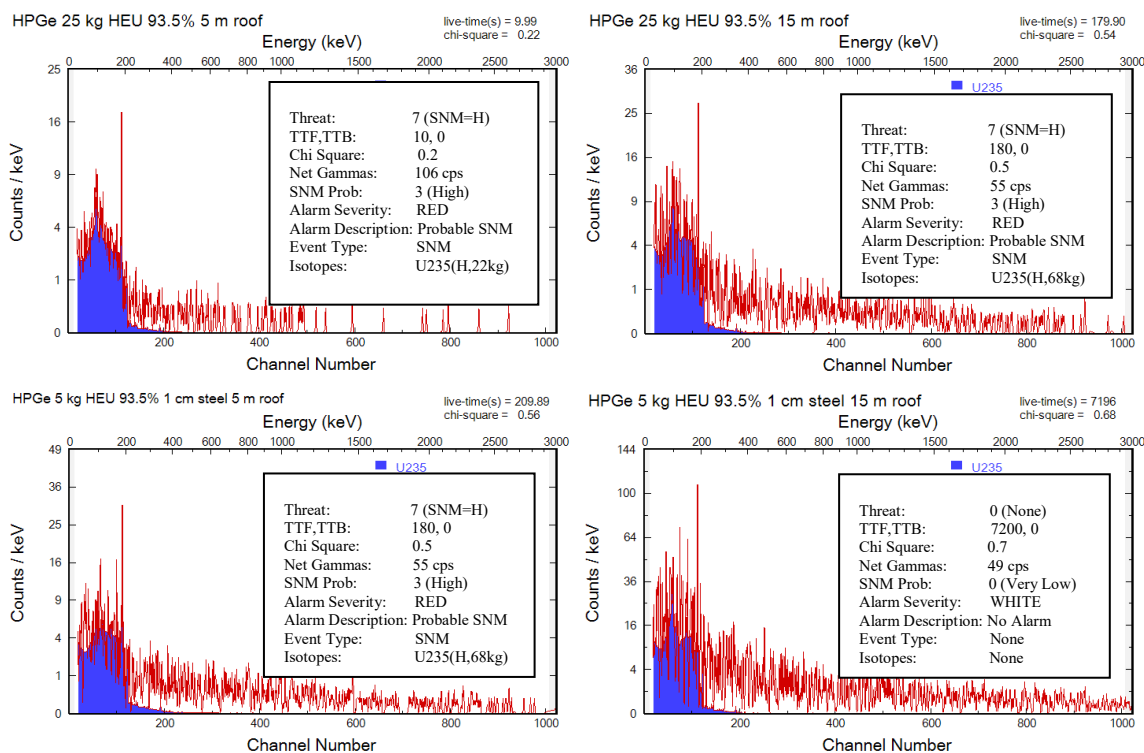


Figure 5.11: GADRAS simulated spectra for a high-purity germanium (HPGe) detector [64]. The alarm was not triggered for the bottom right trial, but the presence of ^{235}U was suggested.

Neutron

Candidate neutron detectors include traditional ^3He - and BF_3 -filled proportional tubes, ^{10}B -lined tubes and coated straws, ^6Li or ^{10}B -coated silver-doped zinc sulfide scintillators ($\text{ZnS}[\text{Ag}]$), ^6Li -scintillating fibers, ^{10}B or ^6LiF -etched micro-structured semiconductors, and dual-mode gamma-ray and neutron elpasolite scintillators, such as $\text{CLYC}(\text{Ce})$ and $\text{CLLBC}(\text{Ce})$. The key parameters are size, weight, power, and sensitivity. The baseline constraint is sensitivity, and the most valuable trade space to the overall system is weight. Therefore, the sensitivity-to-weight ratio is a reasonable attempt at establishing an initial criterion. Complexity and power are also important factors and should be evaluated for approaches that offer similar performance.

Available neutron detector data was far more limited. Only two small neutron detectors were available in the GADRAS library. A small ^3He -tube and $^6\text{Li}/\text{ZnS}$ scintillator were evaluated against relevant neutron-producing threats. The criteria used was achieving 5σ above the background in a one-minute measurement. As noted in Table 5.5, it appears that the threshold and object threat sources would be detected by nearly any neutron detector with sufficient sensitivity.

Table 5.5: Expected neutron detection distance for threshold and objective quantities of reactor- and weapons-grade plutonium evaluated for 60 seconds [64].

Detector Type	Type/Quantity	8 kg RG Pu	8 kg WG Pu	2 kg RG Pu	2 kg WP Pu
	^{240}Pu -content	18%	6%	18%	6%
	Shielding	Unshielded	Unshielded	5 cm HDPE	5 cm HPDE
	Sensitivity				
	[cps/nv]	[m]	[m]	[m]	[m]
^3He -filled HRM [143]	10.5	58	33	26	14.5
$^6\text{Li}/\text{ZnS}$ scintillator D3S [144]	12	58	33	21	11.5

Another data source came from a report on performance testing of the DTRA prototype detectors conducted by an NNSA laboratory. A figure of merit applicable to this study is the sensitivity divided by the background and mass. These results showed the ^6Li -etched silicon performing best followed by ^3He ; the boron coated straws and boron-line tubes were a bit heavier and less sensitive than the ^3He -tubes [130]. The low mass and power of the ^6Li -etched detectors are attractive for this application.

The placement within the system is a noteworthy attribute for this type of sensor. We expect neutrons that make it to the measurement location to be thermalized by collisions with the clutter in the building, the moisture in the air, and the roof materials. In that case, the best arrangement is to have a high-density, low- Z material with a low absorption cross-section behind the detector to act as a backstop and reflect neutrons into the detector. While adding heavy moderating materials to the system is not recommended, using materials that are

already part of the system to improve neutron detection makes sense. The carbon fiber UAV components are not likely to be thick enough to make a difference but should not degrade performance either. If the UAV were to use liquid fuel, placing the neutron detector between the fuel cell and the expected location of the source should be beneficial. If the power source is lithium polymer batteries, the response becomes complicated. While the batteries are mostly comprised of dense, low Z material, they also have some concentration of ${}^6\text{Li}$, which will readily absorb thermal neutrons. The extent to which the batteries help, or hinder neutron detection is left for future investigation.

5.3.3 Location and Mapping Sensors

Global Navigation Satellite System

The ability to operate in a GNSS-denied environment is necessary, but the inclusion of some level of GNSS-capability is a must. For an sUAS-based application, GNSS-antennae are likely already integrated into the system for navigation. Often, however, a more advanced solution to decrease the positional uncertainty inherent in typical GNSS solutions is desirable. The typical accuracy of GNSS is roughly 5 m for single frequency receivers found in most commercial products (e.g., smartphones, laptops, cameras, and navigation devices) even with several satellites in the field-of-view under an open sky [145]. Military systems generally employ dual-frequency receivers at the sacrifice of cost and size. The use of dual-frequency systems can improve positional accuracy to ~ 50 cm.

Augmentation systems are also available to improve the accuracy of GNSS. The most common augmentation is known as differential GNSS. It makes use of fixed ground stations or geostationary satellites to provide time corrections to signals transmitted by the GNSS constellation. The signals from the GNSS satellites encounter small delays when traveling through the atmosphere, especially the ionosphere and troposphere. Because of their known location and extended dwell, differential GNSS base stations average out the random changes from GNSS satellites and can broadcast the current delay caused by solar or terrestrial weather.

Real-time kinematic (RTK) is a technique available that provides centimeter-level positioning accuracy. It uses the number of carrier cycles between the satellite and the rover and base stations and resolves ambiguity using the difference in the number of cycles. It is more complicated and requires precise knowledge of the base station location, quality observations of the satellites in the field of view, and high-performance antennas. UAVs that employ GNSS-RTK achieve at least $1.5 \text{ cm} + 1 \text{ ppm}$ positioning accuracy [116].

Electro-optical

For most remote radiation detection applications, the inclusion of cameras, vision sensors, or other electro-optical sensors is beneficial. For a UAS-based approach, cameras are likely

already integrated into the flight control system. Camera systems can also provide enhanced situational awareness, improve navigation and mapping, and facilitate multi-system control. Binocular camera systems have been employed for computer stereo vision for navigation and mapping. Wide-angle view cameras provide immense situational awareness.

Even with all the advantages listed, the expected use-case for directed search is during a period of darkness, where a typical visible light camera is not useful. Therefore, the additional weight of the stereoscopic system is not advisable. Instead, one or more low light or thermal IR cameras would be better suited for the anticipated light conditions. A thermal IR camera could also be very useful for determining the building structure by identifying locations of material seams, I-beam locations, and any anomalous thermal activity.

For many remote radiation detection applications, the inclusion of a LiDAR sensor provides a considerable advantage. As demonstrated by Pavlovsky et al. [21], the benefit is threefold: (1) One can generate a 3-D map of the scene from the collected point cloud. (2) The position and orientation of the radiation sensors in the scene are well known and can be used in conjunction with image reconstruction algorithms to produce a high-fidelity map of the radiation field. (3) The sensor provides enhanced-ability to navigate in low-light situations, such as at night. The disadvantages are weight, power, and electromagnetic signature. Multibeam LiDAR sensors are on the order of 600 g and draw a considerable amount of power and data processing capacity. A smaller single beam LiDAR could be useful for navigation and landing, and a small, solid-state system with a limited and segmented field-of-view could possibly provide reliable position information with regards to location on the roof.

5.4 Recommended Sensor Suite

Vehicle

Movement across the roof is considered necessary unless the number of systems provides adequate and accurate coverage. Therefore, the recommended vehicle for this application is a purpose-built system that takes the best-of-breed attributes of the Pegasus III hybrid UAV/UGV. The ability to traverse the rooftop without having to take to the air is a significant advantage from both a low signature standpoint as well as a power requirement perspective. While the Pegasus III might not prove to meet all the requirements of a final design, its best attributes should be incorporated. Though a tube-launched parachute-retarded munition-style sensor package may offer a low signature, it severely restricts the sensitivity of the radiation detector package one can deploy. It would also prove challenging to incorporate radiation sensors, locomotion, parachute-retardation, laser guidance, communications and control, and enough power into a deliverable munition-sized package.

Gamma-ray Sensor

The recommended gamma-ray detector for this application is at least six 20×20×15 mm CZT detectors with an energy resolution of 1.2% at 662 keV or better. The sensitivity and

specificity of this size detector are sufficient to detect relevant threats. CZT offers the best resolution per mass when ancillary equipment such as cooling systems for HPGe crystals are considered. It has a relatively high density of $\sim 5.8 \text{ g cm}^{-3}$ and high Z_{eff} . Further study is required to determine the benefit of using pixelated CZT for this application.

Other options failed to meet threshold values for relevant threats in simulation. However, they should continue to be evaluated for actual performance in trials with physical SNM. $\text{LaBr}_3(\text{Ce})$ showed promise and was on the cusp of detecting relevant threats in simulation trials. Past experience with these detectors in the presence of NRC Category I quantities of HEU was favorable. The intrinsic radioactivity of lanthanum is a detractor for spectroscopy, but the fast decay time allows for operation in high-count-rate environments. The dual gamma/neutron detecting capability of elpasolites is attractive. However, the reliance on large traditional photomultipliers to achieve the best resolution ($\sim 3.5\%$) is a detractor. Efforts to couple them to silicon photomultipliers have resulted in degraded resolution ($\sim 5\%$).

Neutron Sensor

The recommended detector for this application is four or more RDT Domino® detectors. The compact size ($85 \times 50 \times 10 \text{ mm}$), weight (50–100 g), extremely low power (1.5 mW), reasonable efficiency (30%), and adequate sensitivity ($\sim 5 \text{ cps/nv}$) make this the best alternative for a SWaP-constrained application. We estimate the cost at \$2k for the four detector elements. Any alternative should also perform well at a slightly larger SWaP. One could achieve comparable sensitivity with a $1.9 \text{ } \varnothing \times 7.6 \text{ cm}$ ^3He -filled, boron-lined, or boron coated straw proportional tube weighing $\sim 100 \text{ g}$.

Contextual Sensors

The recommended suite of contextual sensors is still undetermined. Further investigation is suggested for GNSS-RTK, solid-state LiDAR, and thermal IR cameras. At a minimum, the platform will need some means to navigate to and land on the roof, and it must be able to operate in a GNSS-denied environment. A robust system would employ both GNSS-RTK and LiDAR. The utility of thermal IR cameras for this application is yet to be evaluated but shows promise.

6 Search Pattern Optimization

Assuming a particular sensor can detect threat sources of a specified quantity under a set of established conditions, these questions remain: How does the system go about searching? At how many locations should it take measurements? How should those locations be arranged to cover a specific building size and shape? To which location should the system go to first? How long should a sensor stay at a given location? What happens when it does not detect anything? Where does it go next? Is there an ideal path to maximize the overall value of each location? The typical, yet ineffective answer is “it depends.”

One approach is to determine a near-optimal search routine for an expected range of conditions. Such an approach requires developing a framework that allows for the adjustment of input parameters within a given set of boundary conditions to evaluate the benefit gained from a given measurement. Exploring this parameter space is the final thrust area of this research project.

Imagine a yard with a severely overgrown lawn that has not been cut in many months. A particularly valuable object is known to be missing, and it may or may not be somewhere in the lawn. The main reason for someone to cut the grass is to find the object or confirm that it is not there. The available mower can either trim off a bit at a time at a reasonable speed or cut more at a much slower speed. What is the best method to go about finding the object, or confirm that it is not there, in the shortest amount of time?

One could choose to mow the entire grass taking a little off a bit each time. They would end up having to go over the entire lawn several times to get to a level where the grass is low enough to determine whether the object was there or not. There is no guarantee that any area will be low enough to inspect before the operator gets tired of pushing the mower or the time available runs out. Instead, one could move slowly to cut each section down low enough to the ground to be sure the object was not there. This operator might not tire out as quickly because they are not pushing the mower over the lawn several times. However, they may well run out of time and not get the entire grass cut. Since the goal is to find the object, not just cut the grass, one could start with areas of the lawn where the object is more likely to be found. The allocation of time and energy across the lawn parallels the search plans described further in this section.

6.1 Measurement Location Selection

The first question we sought to address was, “Where should we take measurements?” An initial prescriptive search method was developed primarily from intuition and experience. It was initially employed for background measurements taken on rooftops before the matter of search optimization was categorically explored. Here it is considered as a baseline for comparison with more informed techniques.

Light industrial buildings are generally rectangular, with an aspect ratio ranging from 1:1 to 1:1.5. A brilliant place to start appeared to be dead center. From there, a choice was made

to take additional measurements toward the corners at distances roughly equal to the building height. This technique most often resulted in five measurements, resembling the five dots signifying the number 5 on a six-sided die, as seen in Figure 4.2. In the instance of a particularly tall or skinny building, fewer measurements were required. By-passing the corner locations is considered a best practice since measuring near a corner of a building will likely have elevated background levels from the walls, and squanders sensitivity on areas outside of the building, where a source is not expected. A buffer distance from corners, equal to half the building height, was generally followed.

On the topic of wasting sensitivity in corner measurements, consider an arbitrary spherical detector that can be placed anywhere on a plane. Furthermore, assume a point source that is located anywhere on a plane parallel to the detecting plane that is a distance h away. Ignoring the effects of attenuation for the moment, the detector's sensitivity to a given source activity forms a sphere centered on the detector. The intersection of that sphere with the source plane below defines a circle for which any source of activity equal to or larger than some value will be detected. As seen in Figure 6.1, measurements that take place close to the corners of a building project a cone of sensitivity outside of the building and therefore collect less information than a centerline measurement. This claim is based on the prevailing assumption that threat materials are not located outside of the building.

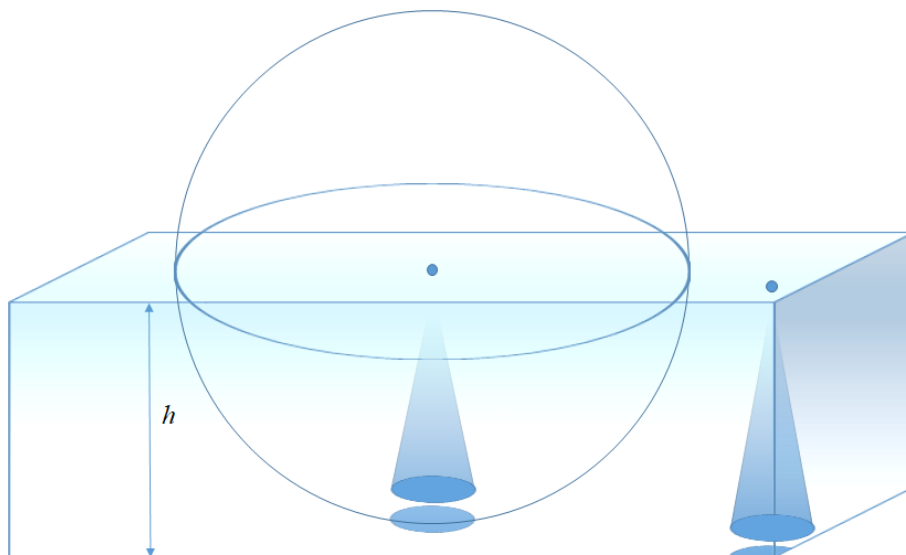


Figure 6.1: Extrapolated field-of-view for centerline and corner measurement locations.

The corners of a building also present a challenge because of the likelihood of elevated background in that area, depending on the size of the concrete pad and type of wall material. A corner represents the intersection of an infinite half-plane with two semi-infinite quarter planes, similar to what was discussed in Section 4.1.2. Elevated background near corners is evident in Figure 4.13 (f) on the right and bottom portion (locations 1,6,11, and 31–35). Areas 1 and 11 had two-foot thick concrete blast walls (see Figure 6.2) that protruded into the warehouse, and the east wall, near locations 31–35, was constructed with cinderblocks. Conversely, the north wall was constructed of corrugated metal over plywood on studs.

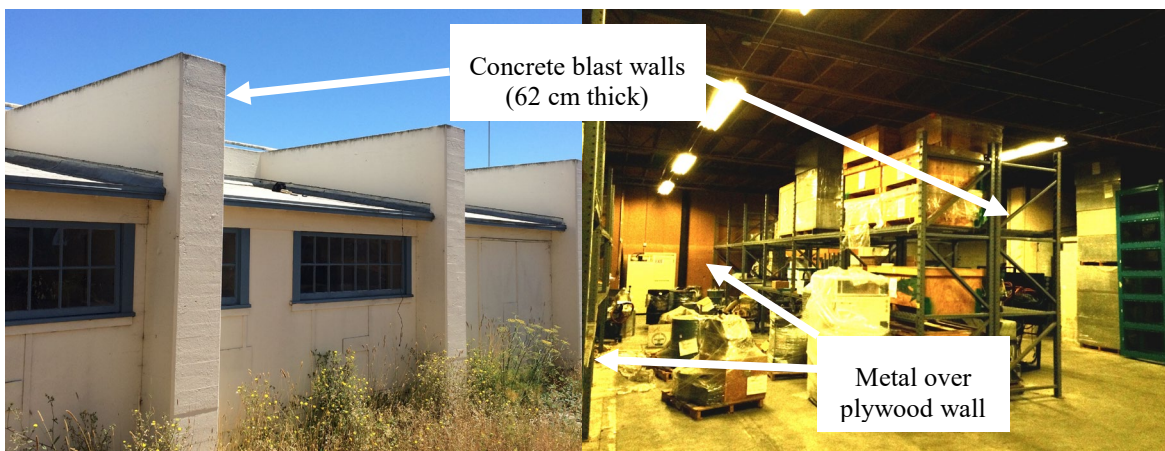


Figure 6.2: Bldg. 128 characteristics. Source: personal photographs.

Basing measurement distances on building height is taken from common search techniques for aerial measurements, as well as ground-based mobile detection systems. For aerial measurements, the goal is to determine the ideal line spacing for a raster pattern such that an area is covered sufficiently without oversampling. Most often a line spacing of twice the height above the ground is used which results in a maximum distance of closest approach that is a factor of $\sqrt{2}$ greater than the minimum distance of closest approach [20, 146].

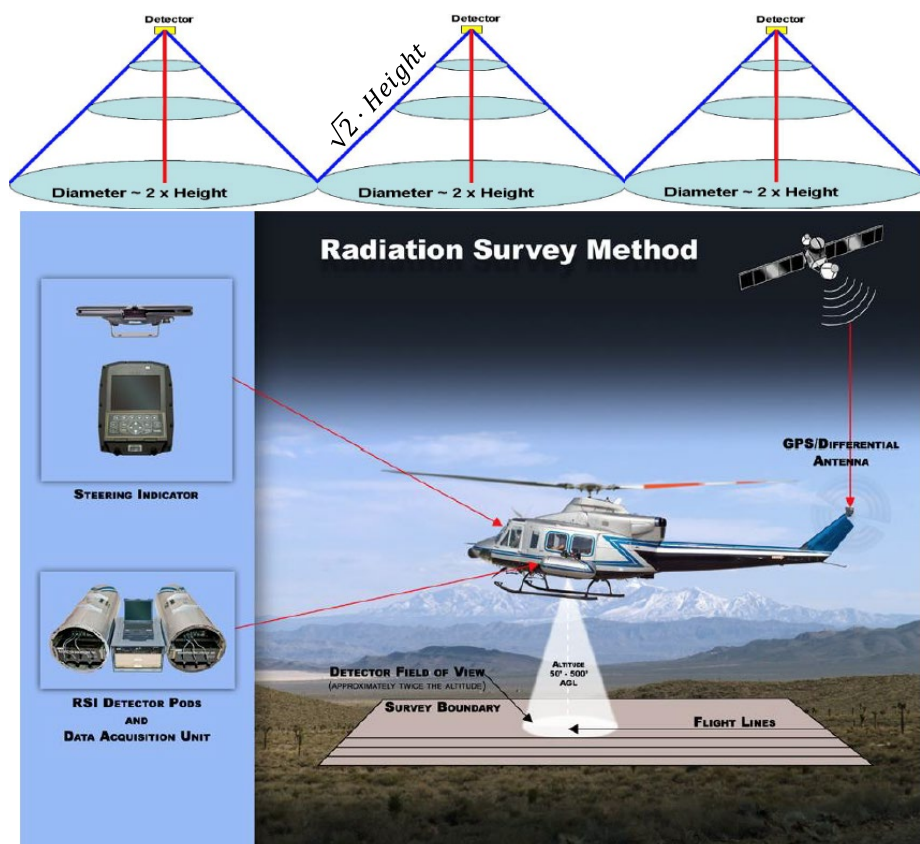


Figure 6.3: DOE's Aerial Measuring System radiation survey method Source: [146].

Correspondingly, the goal in ground-based mobile search is to establish integration time intervals to maximize the signal-to-noise ratio for the system based on the expected distance of closest approach to a source as well as anticipated vehicle speeds. For simple geometries, where the source is at the same height as a flat parallelepiped detector, the optimal integration time is a factor of two times the expected distance of closest approach. This maximization can be obtained by setting the derivative of the signal-to-noise equal to zero and solving for the distance, as seen in Figure 6.4 [147]. The integration time window can then be determined from this distance and the average speed. The optimum integration time is slightly longer when the detector is a right circular cylinder because of the uniform projected area it presents. The integration window for both shapes gets smaller when air attenuation is considered. Both differences are minor, and often detection system algorithms employ multiple integration windows to account for variations in speed or source strengths.

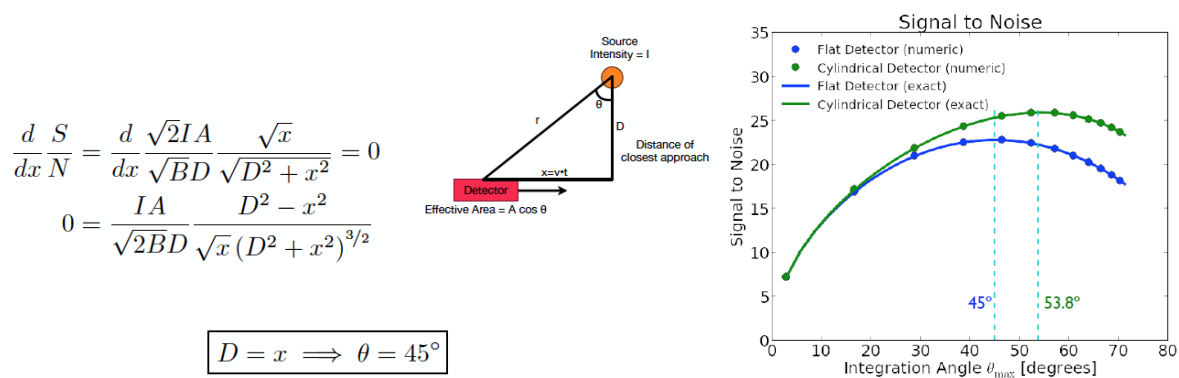


Figure 6.4: Derivation of optimal signal to noise for simple mobile search geometry. Source: [147] used with permission from B. Seilhan.

Adapting the principles of aerial measurement and ground-based mobile search techniques to a rooftop measurement scheme seems relatively straightforward. However, there are vital differences in the approach and desired outcomes that result in significant modifications to the aforementioned techniques. The first key difference is the manner in which measurements are taken. The aerial and mobile techniques are both dynamic, i.e., the detectors are moving in the environment. Conversely, the rooftop scheme is expected to consist of a series of static measurements in order to take advantage of the extended time available to make measurements and to minimize the power required for locomotion.

The second key difference is the detection geometry. Regarding the aerial technique, measurements are taken along fixed line segments in a plane, assuming the aircraft flies ostensibly straight lines across the search area. The choice of line spacing constrains the maximum distance of closest approach to the height of the aircraft added in quadrature with one-half of the line spacing distance, as shown in Figure 6.3. By the same token, ground-based measurements are even more constrained as they are taken along a single line segment—the road. Therefore, the adjustable parameters are limited to vehicle speed and detector integration time. Moreover, ground-based mobile detectors are often arranged to be most sensitive to a source located in the buildings adjacent to the direction of travel.

For the rooftop scheme, however, the path constraint relaxes from fixed line segments to any point on a plane, i.e., the rooftop. This additional spatial degree of freedom enables more optimal solutions than aerial or vehicular search. While taking measurements at points along a series of line segments spaced across the roof in a rectangular or square lattice remains a viable method, it is sub-optimal. This pattern creates repeating bands that are not sampled as well when compared to the measurement path, as seen in Figure 6.5 (left). Closer spacing is required to alleviate these bands. A smaller pitch creates overlaps, just like mowing the grass.

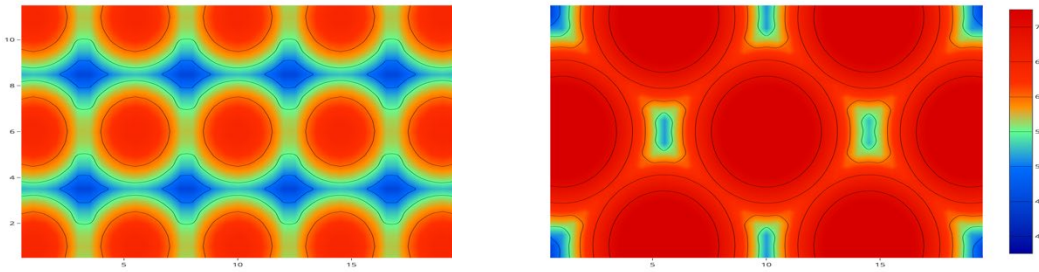


Figure 6.5: Comparison of (left) square versus (right) triangular lattice with uniform counting time at each location.

Triangular or hexagonal lattices are also commonly used. This arrangement provides more optimal coverage than a square or rectangular pitch because it implicitly overlaps rows and columns, as evident in Figure 6.5 (right). The coverage is not only better, but the overall performance is improved as well; the color and size of the contours in the right plot clearly illustrate this enhancement. Moreover, this is accomplished with less than half as many measurement locations (seven vice fifteen), which allows for approximately twice as much time to be spent at each location. A finer pitch could also be chosen, which would result in improved coverage and better overlap.

Since the detector response on a rooftop casts a circle of some minimum detectable activity for a source located below it, the spatial optimization routine becomes an exercise of circle packing on a plane. Optimal or near-optimal solutions for aspect ratios ranging from 1:0.1 to 1:1 for $N > 1$ up to several hundred, and thousands in some cases, are known to exist [148]. To first order, the general solution is a hexagonal lattice. In 1773, J.L. Lagrange ascertained the hexagonal lattice to have the highest-density lattice arrangement of circles in two-dimensional Euclidean space. This was later proven maximal by C.F. Gauss for lattice arrangements in 1831 and optimal for regular and irregular packings by A. Thue in 1890. The first rigorous proof is attributed to L.F. Tóth in 1940 [149].

However, exact optimal packing solutions in bounded shapes, for a given aspect ratio and chosen number of points, are often non-symmetric, since the goal of the packing algorithm is to maximize the diameter of N circles. For example, the solution for $N=32$ circles on 1:0.5 aspect ratio rectangle looks mostly like a hexagonal lattice, as seen in Figure 6.6. Even so, there can be a large amount of unused space if a hexagonal pattern is continued throughout without adjustment. Therefore, to maximize the circle diameter, some rows are shifted, which throws off the lattice structure ($N=19$). Surprisingly, a rectangular lattice gives the optimal

solution in some special cases ($N=18$), while other conditions exploit a mix of rectangular and hexagonal-like lattices to achieve an optimal packing arrangement ($N=33$).

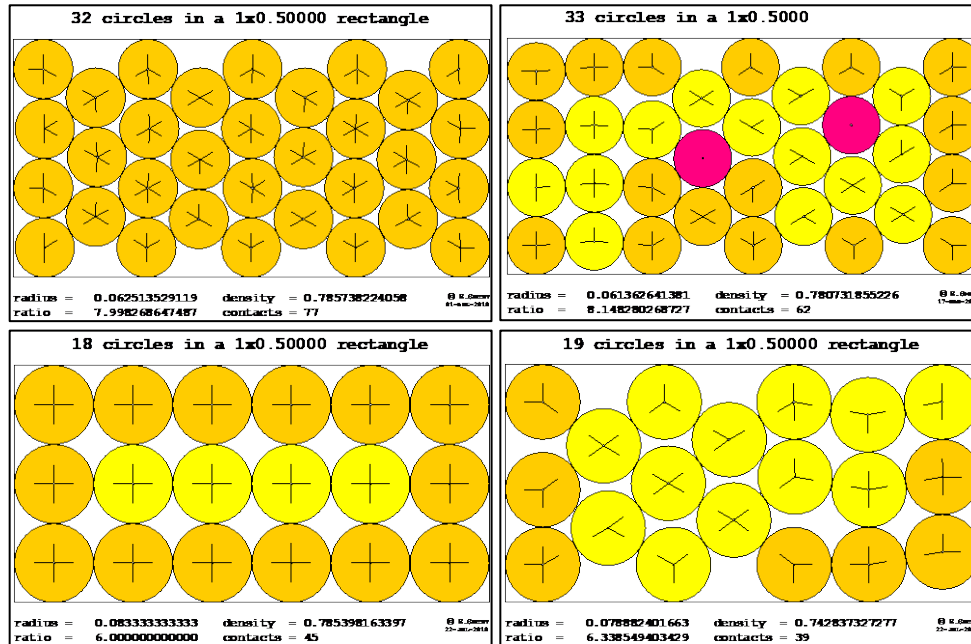


Figure 6.6: Example best-known packings of equal circles in a 1×0.5 rectangle. (top left) $N=32$ gives a near-perfect hexagonal lattice (top right) $N=33$ exploits a mix of rectangular and hexagonal-like lattices. (bottom left) $N=18$ is a rare case where a rectangular lattice achieves the largest diameter circles. (bottom right) $N=19$ is largely a hexagonal lattice, but the pattern is shifted to accommodate an asymmetric N . Source: [148] used with permission from E. Specht.

Nevertheless, the goal of traditional circle packing optimization does not directly match the required end state of determining optimal rooftop measurement locations. Circle packing often starts with a required number of circles and a designated aspect ratio; the objective is to determine the largest diameter possible such that all circles remain on the plane with no overlap. Conversely, in a rooftop detection scheme, the circle diameter is a fixed quantity that is akin to a contour line for a given source activity, detector, background rate, and collection time. The aim is to determine the minimum number of measurement locations to cover the space adequately. Furthermore, a uniform packing arrangement is desirable since the location of the source, if present, is unknown and often could be anywhere in the building. Consequently, a hexagonal lattice becomes an excellent starting point for a rooftop scheme.

To determine the number of measurement locations, N , one needs to know the length and width of the building, L and W respectively, and pitch, r . The following equation can be employed to estimate the ideal number of measurement locations for a given grid pitch. Some adjustment may be necessary, but in general, the ratio of $n:k$ should roughly mirror the aspect ratio of the building.

$$N = nk \approx \frac{L \cdot W}{r^2} \frac{2}{3\sqrt{3}} \quad (6.1)$$

Assuming one chooses a hexagonal lattice as the blueprint for potential measurement locations, the task remains to select a pitch. Though it was stated previously that the circle diameter is “fixed” for a given MDA, it still must be determined. As with anything that is a function of more than one parameter, there are tradeoffs. The first thing to look at is uniformity of response.

Like aerial detection, there are maxima and minima due to overlap from adjacent measurements. In this case, the overlap is more complicated than two line segments found in aerial detection. Regardless, the distance between points should be set such that the difference in sensitivity to a source located at the maximum versus one at the minimum meets an acceptable threshold. For example, a potential threshold might be to accept a sensitivity difference of no more than a 20–30% to a source located anywhere in the building.

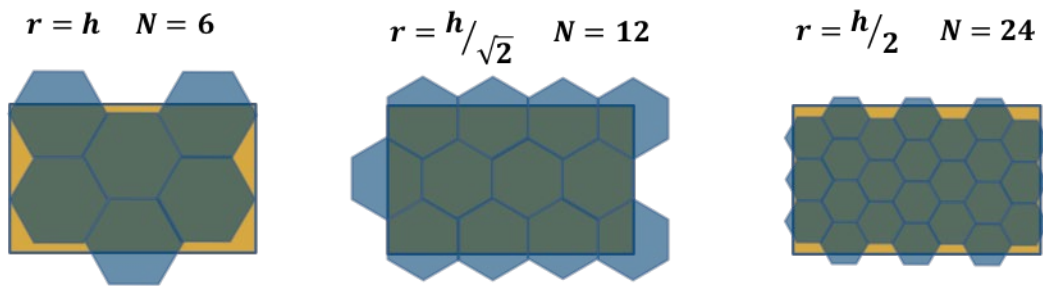


Figure 6.7: Example hexagonal lattice tiling on a rectangle with an aspect ratio of 1:0.6 for different pitch values as a function of building height.

Table 6.1: Comparison of measurement lattices for a 15×25 m building (~4000 sq. ft.) as a function of pitch. The figure of merit is the ratio of the worst case when a source is located furthest from a set of lattice point versus the ideal case when it is located directly under a point. Parameters are presented for a single independent measurement and aggregated for the seven closest measurement locations.

Pitch	Number of locations	n	k	Independent points		Up to closest seven points aggregated		Figure of Merit	Incremental Improvement Per Additional Location [%]
				Maximum Distance [h]	Sensitivity Ratio	Maximum Distance [h]	Sensitivity Ratio		
$2h$	1	1	1	1.41	0.50	1.53	0.43	0.11	–
$\sqrt{3}h$	2	1	2	1.32	0.57	1.41	0.50	0.19	60
$\sqrt{2}h$	3	1	3	1.22	0.67	1.29	0.60	0.23	40
h	6	2	3	1.12	0.80	1.15	0.75	0.76	30
$h/\sqrt{2}$	12	3	4	1.06	0.89	1.08	0.86	0.76	5
$h/\sqrt{3}$	18	3	6	1.04	0.92	1.05	0.90	0.79	2
$h/2$	24	4	6	1.03	0.94	1.04	0.92	0.82	1
$h/3$	52	6	9	1.01	0.97	1.02	0.96	0.89	1
$h/4$	92	8	12	1.01	0.98	1.01	0.98	0.93	0

Note that a pitch of $h/\sqrt{2}$ has the same figure of merit, in this instance, the ratio of the worst case to best case location, as a pitch of h . However, this does not reveal the 30% improvement in sensitivity achieved by doubling the number of measurement locations and thereby reducing the maximum distance to a potential source.

The use of the building height as a guide for measurement location separation results in a maximum source-to-detector distance no more than 1.155 times the building height in a hexagonal pitch arrangement. This limits the maximum reduction in signal to 33.4% when comparing a source directly below a detector versus one located at the outer circle of a cone of sensitivity. In a sufficient-sized lattice, the improvement is even more significant because the signals from adjacent measurement locations can be aggregated. The location of least sensitivity moves from the outer radius of a single cone to the intersection of three cones.

The take away from this investigation is that it is wise to choose a lattice pitch equal to or smaller than the building height. The prevailing factor to adjust from there is the required MDA to detect the anticipated activity of the target source with a projected background. Care should also be exercised to ensure adequate coverage of the entire building by conical projections of the measurement locations.

The concern with setting the sensitivity threshold too high is that it drives up the number of measurement locations, which then drives down the available measurement time at each location. Halving the distance to the source is more than twice as effective in increasing the signal-to-noise ratio as compared to doubling the time spent counting. However, the reality is that it takes power to move from location to location. Thus, a constrained optimization that seeks to maximize the probability of detection (or perhaps minimize the chance of a false negative) within a fixed time, power budget, and geometry starts to form.

In developing the optimization, however, the approach is not as straightforward as might be assumed. A naïve approach might be to determine the optimal lattice arrangement and then apply a traveling-salesman-problem methodology to determine the best path. However, this assumes that all measurement locations are of equal importance. While this assumption simplifies things considerably, it fails to maximize the objective quantity by squandering measurement time at locations that may have already been cleared by the superposition of adjacent measurements, and by neglecting the geometric advantages and disadvantages of particular locations.

For a medium-sized building, on the order of 300 m² (3230 sq. ft.), a conservative pitch of $h/2$ was used to determine the number of measurement locations—18 in this case. From these points, we examined two approaches—the shortest path and the longest path. For a building this size with a realistic number of measurement locations, the extended path was ~200% longer than the shorter path. The pathlength becomes almost a factor of six longer when the points are chosen on a rectangular lattice for a slightly bigger building, as seen in the bottom grids of Figure 6.8.

Table 6.2: Properties of example traveling-salesman-problem path selection for gridded search

<i>Grid Points and Lattice</i>	<i>Path type and length</i>	<i>Minimum length</i> [m]	<i>Maximum length</i> [m]	<i>Ratio of max/min</i>	<i>Center-weighted raster length</i> [m]	<i>Ratio of center-weighted/min</i>
18 points hexagonal		82	273	3.35	95	1.16
35 point rectangular		94	548	5.83	111	1.18

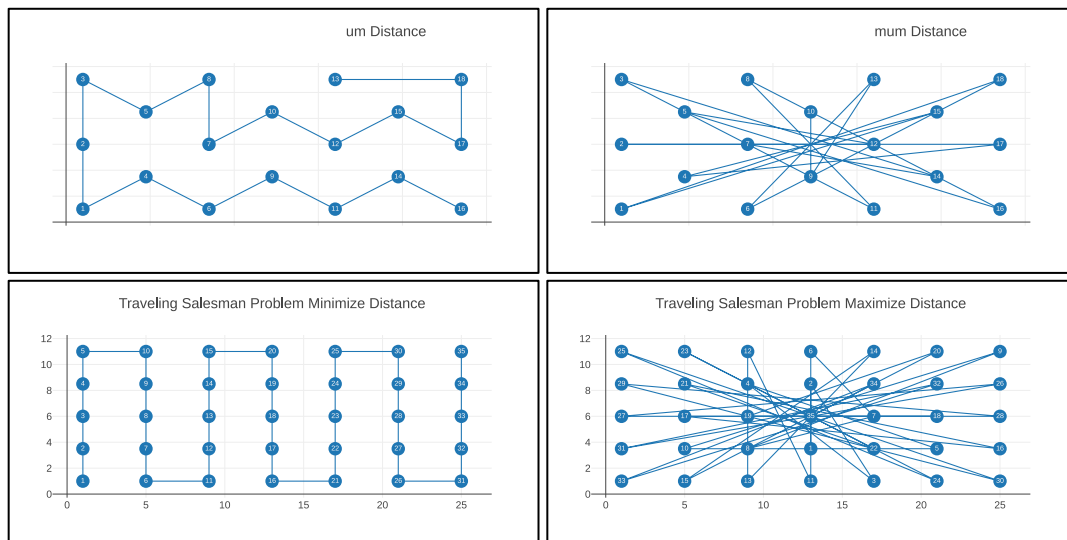


Figure 6.8: Modified Traveling Salesman Problem path optimizations for a 12×25 m building with (top) 18 measurement locations on a triangular pitch and (bottom) 35 measurement locations on a rectangular pitch.

It is somewhat intuitive that, for a given building, measurements taken in the center or along the centerline of the major axis provide the most coverage for an unknown source location. However, there are often geometries where an absolute center measurement is not optimal due to the superposition of adjacent measurement locations. Regardless, those on the edges and corners provide less value because there are locations within the detectors field of view where we assume that the probability of the source being there is zero, i.e., outside the building. Therefore, the goal should be to maximize the information potential of each measurement instead of maximizing the coverage area. That is, measurement locations and times are prioritized such that they provide the most significant increase in overall information supporting or refuting a hypothesized source at all possible locations.

A simple approach to balance path length while prioritizing a better field-of-view is to raster within the middle of the roof and then loop around to catch the outer measurement locations, as demonstrated in Figure 6.9. The length for both lattice arrangements is less than 20% longer than the shortest path.

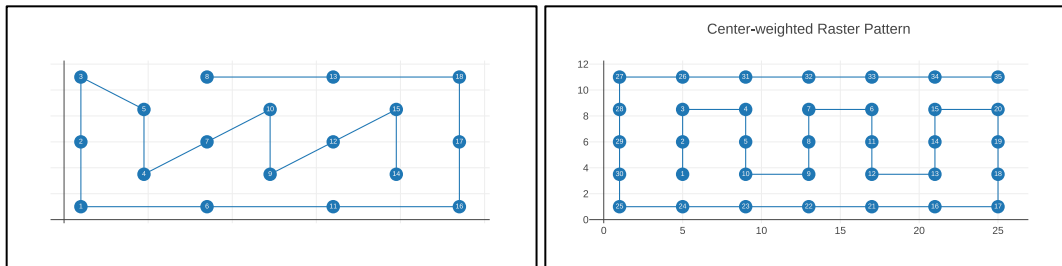


Figure 6.9: Example search patterns which prioritize locations with the better fields-of-view while still attempting to minimize the total path length. (left) Hexagonal lattice with 18 points (right) Rectangular lattice with 35 points.

While this approach heuristically improves the search by prioritizing locations with better fields-of-view, this only takes advantage of the spatial aspect of the problem. The amount of time spent at each location is another parameter that can be manipulated to improve the overall outcome of a search. The next section will discuss the temporal component of the measurement scheme in terms of information gathering.

6.2 Collection Time Allocation

Assuming a grid of possible measurement locations has been chosen for a building, there are two types of search plans envisioned for any given scenario. The first is a prescriptive approach, dubbed the playbook method, for which the search pattern must be developed before the deployment of the sensor and deviations from the plan are not possible. The approach is to travel to location $[A,1]$, collect for X minutes, go to location $[B,2]$, collect for Y minutes, and continue until all locations have been visited, then return to base to download data for analysis. This technique lends itself to scenarios where system size, weight, power, and computing resources are narrowly constrained. It lends itself best to the scenario in which clearing a target building is a primary goal, i.e., a source is not expected to be there, but a confirmation measurement is required to remove it from the list of possibilities.

The second is an adaptive control approach [150], nicknamed the Sastry method, where the search pattern can be adjusted in near real-time as the measurements are being taken, i.e., a measurement of a given length has ruled out the presence of a source of a given strength or higher within some distance of the detector. Example next steps are to move to location $[B,3]$, which is the nearest measurement location outside of this detection band, move to *location* $[E,4]$, which is the location that has the potential of provide the next biggest detection band, or remain in place for some number of minutes to rule out additional shielding of a given thickness for the photons emitted in the germane energy range.

As one can see, the adaptive approach presents many branches and sequels that will complicate an optimization routine. It is likely beyond what can be solved in polynomial time. However, certain assumptions and heuristics can be used to push towards near-optimal or at least provide an acceptable practical solution.

The primary currency for both approaches is information. That is, when a measurement is made, it provides information that supports the hypothesis that a source is present or is not present. Maximizing the information gained from each measurement lends itself well to either approach. In prescriptive mode, it drives a search pattern solution which takes measurements at locations which provide the most information to confirm or deny the presence of a threat source. In adaptive mode, a measurement provides an update to a prior hypothesis. Areas are targeted where the most information can be gained, much like in prescriptive mode, but decisions to move are based on measured data vice predetermined expectations.

Information Maximization

The inputs to maximize information potential are as follows:

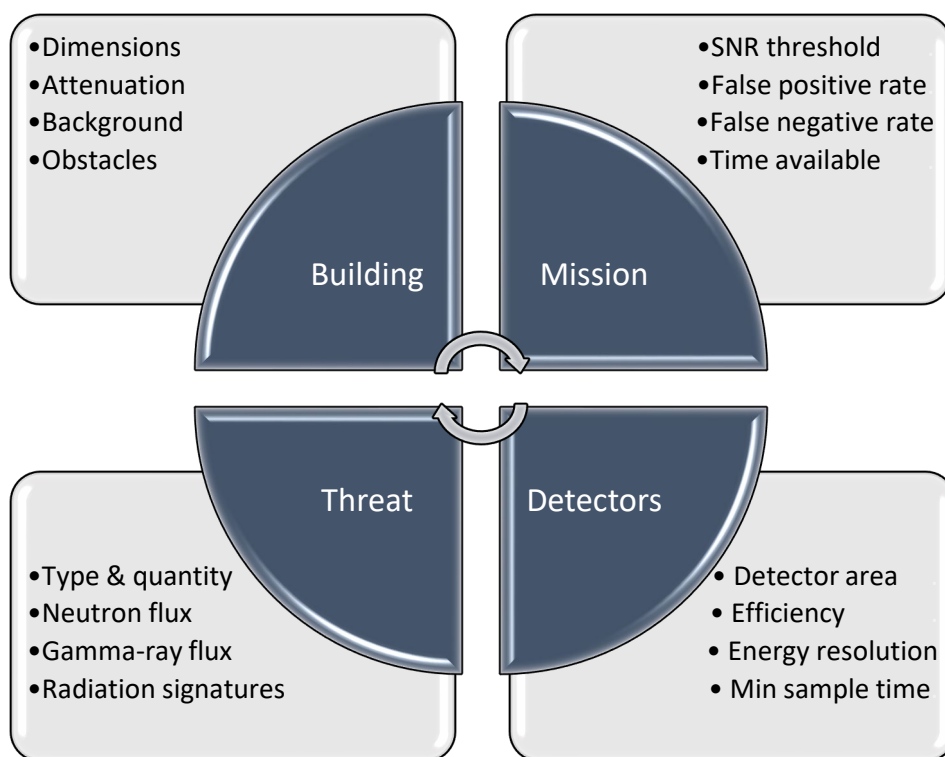


Figure 6.10: Cluster diagram of inputs to the information maximization model used to develop an ab initio collection scheme.

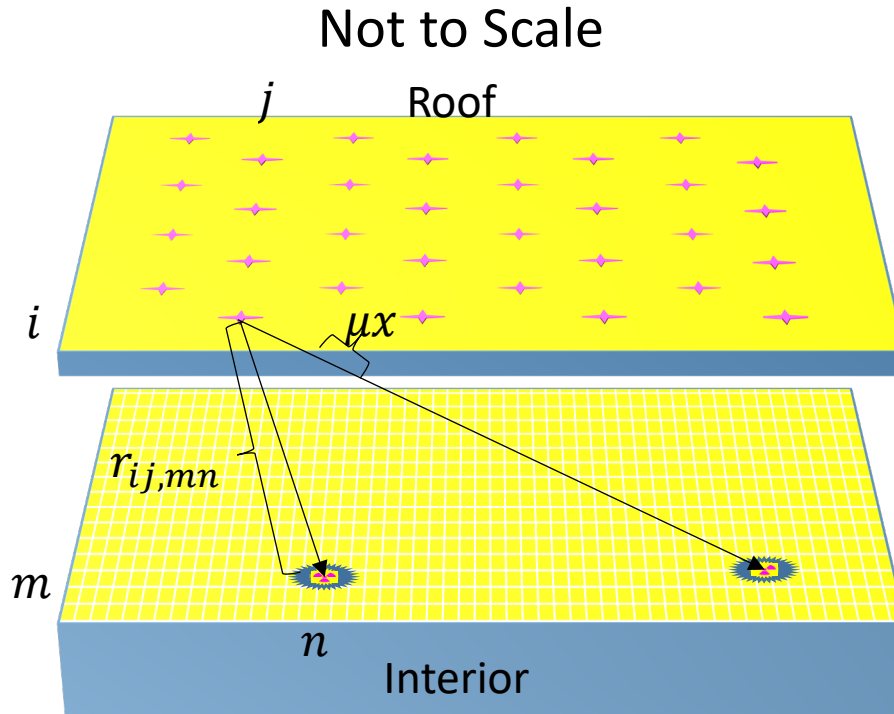


Figure 6.11: Schematic of variables required for information maximization routine used to develop an ab initio collection scheme.

The routine to maximize information potential is:

- Create a square grid m, n of possible source locations at a reasonable pitch (e.g., 25 cm)
- Develop a hexagonal lattice i, j that oversamples the space (i.e., gives more measurement locations than is possible to complete with given time and power)
- Calculate the source-to-detector distance for all possible locations, $r_{ij,mn}$
- Estimate the fraction of full-energy photons transmitted through the roof, $e^{-\mu x}$
- Calculate the expected source signal per second for every possible source location, m, n at each measurement location, i, j .
- Calculate the per second signal-to-noise ratio at each location with a background estimate
- Allow the specified time spent at each measurement location to float in order to optimize one of the following:
 - Minimize the mean MDA from any location
 - Minimize the mean MDA times the variance from any location
 - Minimize the ratio of the variance to the mean of the MDA from any location

The optimization is a smooth, nonlinear, and strictly concave maximization which can be solved using standard nonlinear programming solvers such as the generalized reduced gradient method. Some example optimizations are shown in Figure 6.12.

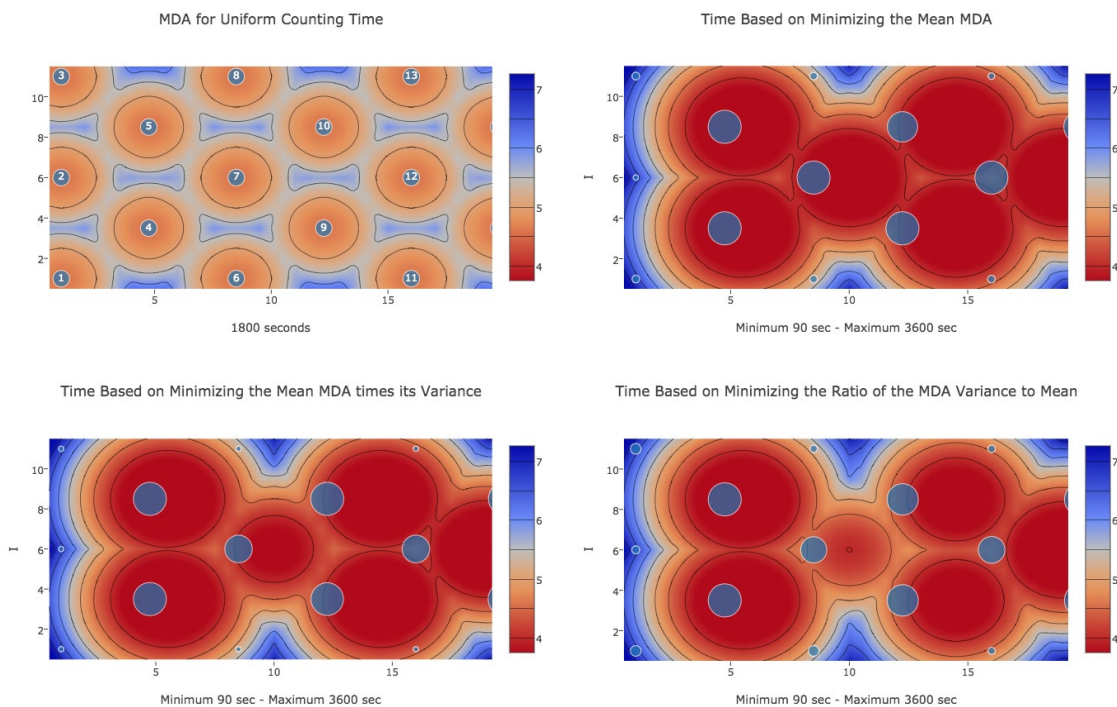


Figure 6.12: Sample optimization based on various functions of the minimum detectable activity (MDA). (top left) Uniform counting time for reference. (top right) Minimize the overall mean MDA. (bottom left) Minimize the product of the variance and mean of the MDA. (bottom right) Minimize the ratio of the variance to the mean of the MDA.

One can see that for a uniform approach, time is wasted in the corners that would be better spent in the center portion of the roof. Three approaches were taken in an attempt to improve the overall MDA and reduce the variation across all possible source locations. These approaches attempted to minimize functions using descriptive statistics of the MDA. Minimizing the mean performed the best, whereas including the variance in an attempt to smooth out the response had little effect at the edges and diluted performance in the middle.

From these results, we set about developing a different metric to optimize. We targeted the probability of detection and its complement as functions to optimize. However, to get these values in a reasonable amount of time, we had to give the optimization a boost by using a threshold value for each matrix value of the SNR. That is, if a measurement from location $[A, I]$ was not going to provide any useful information about a source located at $[k, 2]$, then we did not bother to calculate its contribution to the overall signal and background. For each source location, a cluster of nearby measurement locations provided the relevant signal and background contribution on a per-second basis. Using these values, we could calculate an SNR and then, using the Gauss error function, calculate a probability of detection based on the aggregated signal and background. The optimization can be tailored depending on the expectation of the target. That is, if the source is not expected at a particular target because of some other indicator, the objective might be to clear it. In that case, maximizing the minimum confidence that the source is not present is the objective.

- Apply a threshold cutoff value based on the confidence of no signal (e.g., 95%)
- Calculate and sum the expected total signal and background counts for a specified time at each measurement location that exceeds the threshold for every possible source location
- Using the established false-positive tolerance, calculate the probability of the source being at location m, n and detecting it given the measurements at each location
- Using the established false-negative tolerance, calculate the probability of a source being at location m, n and NOT detecting it given the measurements at each location
- Allow the specified time spent at each measurement location to float in order to optimize one of the following:
 - Maximize the average probability of detection of a source at any location
 - Maximize the minimum probability of detection of a source at any location
 - Maximize the minimum confidence that a source is not present at any location
 - Maximize a weighted sum of the true-positive and true-negative values

Time Based on Maximizing the Average Probability of Detection

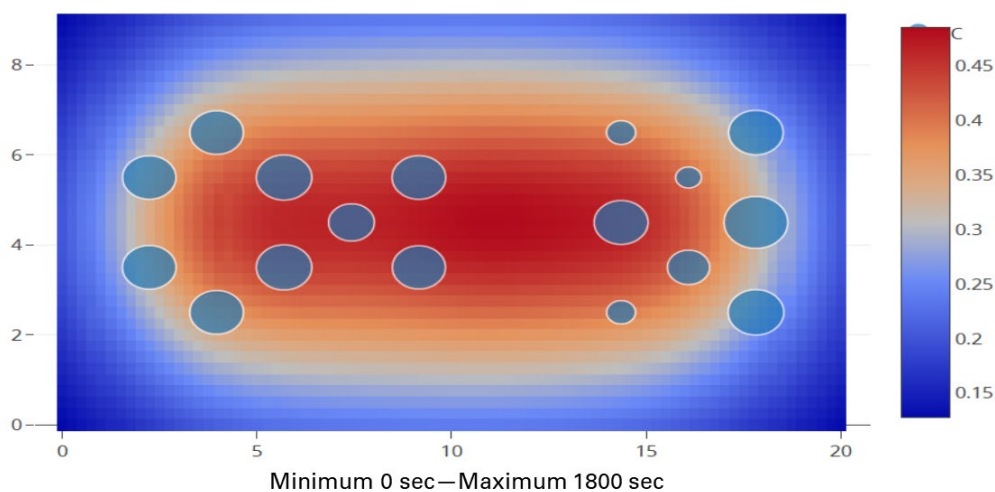


Figure 6.13: Sample optimization based on maximizing the average probability of detection across all possible source locations. The size of the circle is proportional to the counting time.

Given an optimal starting grid of measurement locations and collection times, the scheme is still not complete. The optimization is just an initial plan, and no plan survives first contact. The starting grid is based on an a priori probability of a source being located anywhere in the building. This could be a uniform probability density where the source is equally probably to be at any location in the building. Alternatively, an informed prior could be developed that is based on knowledge of the building interior. Locations that are more or less likely to contain a source might be identified by things like room size, proximity to power, privacy, or

securability. Regardless, the results of the first measurement will change the probabilities for source locations that are near the measurement location, thus updating the prior. Therefore, the optimization should be repeated following each update to the prior and could be updated while a current measurement is ongoing.

Depending on available processing power, this could be accomplished on-board a detection platform but might have to be determined before the mission if that is not feasible. Furthermore, there are competing requirements that influence the decision to move to another measurement location. For example, assuming the first measurement location was centered on the building.

- How long does the system wait to move to another location?
- Should the sensor collect data until the aggregated measurement supports the hypothesis at some confidence level (e.g., 68%, 95%, 99%) that a source of interest is not directly below the location?
- Ought the system remain at the location until it can support the same hypothesis for a source located some distance off-axis?
- If so, at what lateral distance does it become more advantageous, even when taking power consumption into account, to move closer to that location?

It is evident that the decision tree quickly becomes complicated. Ideally, an onboard processor could handle a near real-time optimization. If that is not possible, however, it is feasible to develop a simple playbook based on likely outcomes from each measurement. That is, create a decision tree with limited options, as seen in Figure 6.14. The three courses of action are: remain at the current location, move to the next measurement location from the original optimal grid, and cue the assault force. When there are no new measurement locations, the system can go back and finish uncleared locations if time remains.

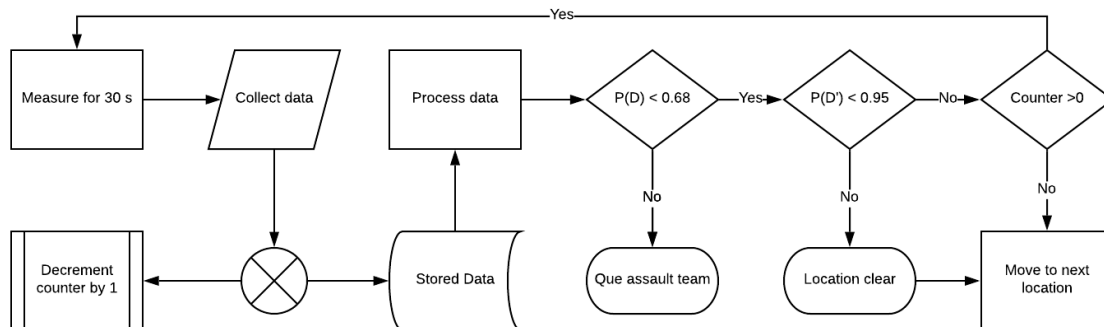


Figure 6.14: Flowchart for the simple playbook method.

A pseudocode algorithm is:

Counter = 20	{set counter to max iterations at location}
Do (measure for 30 seconds)	{collect spectra for 30 seconds}
Counter = Counter – 1	{decrement counter}
If $P(D) > 0.68$ indicate source detected	{analyze spectra for presence}
If $P(D') > 0.95$ Counter = Counter*0	{analyze spectra for absence and move}
While (Counter>0)	{continue counting for up to 600 s}
Move to Location [x,#]	{next location in playbook}

The playbook technique improves upon the initial optimal grid shortest path technique by spending time in locations where the actual measurement supports further investigation rather than the geometry of the building. It is like simple game theory strategies for a game of *Battleship* in that there are possible measurement locations (i.e., the grid of possible locations to attack) and possible source locations (i.e., locations of the opponent's ships). An initial plan is developed to attack areas with the highest probability of a hit, often the middle of the board because of arranging limitations placed on the larger ships. This strategy is akin to the development of a prior based on the building geometry and knowledge of the interior layout. Once a ship is hit, analogous to a measurement indicating signal above background, shots are fired nearby to determine the orientation of the ship and eventually sink it, thus identifying the type of ship.

The knowledge of the type of ship drives future decisions on where to fire, based on the size of the ships remaining; in the case of radiological and nuclear search, this is the MDA of the threat source. Imagine a variant of the game for which a particular ship, suppose the submarine, was the only one of value and sinking it ended the game. Hits on other ships would result in further shots fired in the immediate area surrounding until it could be determined that it was not a submarine. In the same manner, measured signal above background at a location would drive further collection there and at nearby locations to either confirm or rule out a threat source. Just as more shots are fired in the game, and the possible locations for a submarine to be hiding dwindle, the systematic approach to measuring at optimal positions limits a source of a given strength and configuration to fewer and fewer possible locations.

The constraints of the playbook technique are both limiting and beneficial. A decision is made to do something until a condition is met. That is, measure at location $[A, I]$ for at least 30 seconds and but no more than 600 seconds, until either the probability that a source is not present exceeds 95% or the probability that a source is present exceeds 68%, or the time limit is reached. These constraints ensure that at least some threshold amount of information is gained from a measurement. The limiting nature of this approach, however, is the incremental information gained while making that measurement could drastically change the optimization, such that measurements locations not identified in the initial analysis could have considerably more information potential.

Near real-time optimization, taking place even while measurements are ongoing, aims to maximize the information potential for the entire collection period. The collection scheme must incorporate the cost to move, both in time and power, with the information potential of each location. That is, there may be a distant measurement location that has the highest information potential; however, significant time and power (~120 seconds and 0.5 w-hr) would be expended moving there. The difficult task is to equate the information potential, time, and power in terms of a cost function.

The decision to remain at a location to gather more information can be viewed as an opportunity cost. To increase the certainty of a given hypothesis (e.g., to go from 68% to 95% probability that a source is not located within 10 m of the system) requires a trade-off of measurement time that could be spent somewhere else. If power were not an issue, moving from location to location and building confidence in the null hypothesis would be a viable approach. Likewise, building confidence in the hypothesis that a source is present is time well spent. As in the lawn mowing analogy, if one sees a tiny bit of something, it is undoubtedly worth the time spent to cut the grass down low enough to see if it is indeed the object one was searching for or the just a ball from the kid next door.

6.3 Future Considerations

Assuming near real-time optimization taking place, how soon into the measurement until a measurement taken at some other location offers higher information potential than the current location? Furthermore, should the system move in a raster scan, bound back and forth across the roof, spiral around outward from the center, or clear sub-areas sequentially? These questions remain to be answered, as does the question: is real-time optimization worth the extra effort? While near real-time optimization is superior to a playbook or optimal grid shortest path method in terms of total information gained, how much better is it when compared to the other techniques? Are there threat sources that would not be detected with a simple method that would have been had real-time optimization taken place?

The use of multiple platforms and multiple target buildings complicates the matter further. Ascribing to the “two is one, one is none” philosophy, multiple platforms are likely to be deployed to the same building. Allocating search space and communicating data between systems is a topic with broad interest across multiple research communities and sectors, such as the military. Additional platforms will likely change the number of collection points and the paths taken in order to cover the threat space efficiently and avoid collisions between systems. One can also envision a tiered approach whereby a system with enhanced capabilities conducts secondary screening at anomalous locations. The requirements for communications and data sharing increase with a multiplatform approach and may force trade-offs that were not required in a single platform approach.

7 Synopsis and Future Work

While this work may seem like the detector equivalent of an infamous Rickoveresque “paper reactor,” [151] there are already projects being funded and more than a few prototype systems in development geared towards several of the mission areas discussed here. Some examples include scene data fusion for point and distributed sources using LAMP, sUAS swarms for post-detonation forensics, and launched scout-sUAS for contamination avoidance.

7.1 Summary of Contributions to the Field

The primary focus of the research we conducted was exploring the feasibility of using unmanned systems to remotely and semi-autonomously detect radiological and nuclear threats in a directed search scenario by conducting rooftop measurements during a period of darkness. The two chief concerns were the optimization of the sensor package and the development of the search method. The choice of detector materials, the quantity and arrangement of detector elements, and the choice of auxiliary sensors are paramount in developing a system that can detect a sufficient number of threat materials under a given set of conditions. Beyond that, the most effective employment of a group of systems requires detailed analysis of individual search patterns, collective coverage schemes, and cooperative detection algorithms.

This work provides five distinct contributions to the field of remote radiation detection:

- 1) This study is the first to characterize the levels and variation of background radiation near light industrial buildings as measured from the rooftop. This work confirmed the relatively high background rates and variance of potassium contributions encountered in the industrial areas published by the RadMAP group.
- 2) The development of system requirements and the exploration of the trade space form the basis for a detailed project proposal and provide a roadmap for future system design.
- 3) The exploration of search patterns offers a preliminary method to develop a near-optimal solution for a prescribed or playbook search method. The techniques used to boost the efficiency of the optimization routine should enable further development of algorithms for adaptive control and multi-system collaboration.
- 4) The concepts presented in the appendix, *DoD Radiological and Nuclear Remote Detection Mission Areas*, provide additional areas for exploration and contribution from the broader community of researchers.
- 5) This work gained the attention of DoD leadership, including division chiefs and program managers at DTRA, the Joint Project Manager for Radiological and Nuclear Defense, and scientific advisors to the DoD Combatant Commands. Before engaging with them, the level of funding for sUAS-based detection was next to nothing. It has since blossomed into a significant part of their portfolio.

7.2 Future Work

We divide future work for this mission area into three primary areas: threat space mapping, cooperative algorithm development and improvement, and testbed iterations. As discussed in 5.3.2, the placement of neutron detectors on an unmanned platform could help or hinder the performance of the detector. The response of thermal neutron detectors placed near various UAV components, including lithium polymer batteries, is an ideal project for a group of undergraduates to investigate using both simulation and experimental testing.

7.2.1 Threat Space Mapping

Considerable effort has gone into developing a spanning set of threats by the Nuclear Detection Systems and Algorithms group at Lawrence Livermore National Laboratory [152]. We suggest coordinating a modest effort to assess the performance of the recommended sensor suite against the spanning set. The goals of the study would be threefold: (1) ensure that a reasonable percentage of threats would be detected under realistic but idealized conditions, (2) inform the trade space as to how one might improve most for the next version (e.g., improved energy resolution, larger detector sizes, increased number of systems), and (3) compare the playbook algorithm performance to an adaptive algorithm in order to gauge the benefit and evaluate whether the additional computational burden and system complexity is worthwhile.

With regards to a reasonable percentage of threats detected, one should pay particular attention to those material combinations that exhibit similarities to proliferated weapon designs to ensure that the most likely threats are addressed. One should also set the benchmark using the most likely threats, not the performance of the current capability. For example, if the current capability can detect 25% of the threats and the unmanned system is able to detect 50% of the threats (a two-fold increase in threats detected), but neither is able to detect the most likely threats, both systems fail to provide real operational value to the commander. In that case, one needs to rework the system design until it provides value. However, should the most likely threats be detected by both systems, then a threshold value for the threats detected might be 70% while an objective value for the system would be on the order of 95%.

Performance that is on par with current capability or only provides a modest increase in capability could be attractive if it came at a significantly lower cost, provided a lower risk to personnel and equipment, or afforded equivalent coverage of more target buildings in the same time. Otherwise, a system that only performs just slightly better than current capability is generally not worth pursuing.

7.2.2 Cooperative Algorithm Development

Though the recommended number of systems per target is six with a total basis of issue of eighteen, there is a likelihood that in a resource-constrained environment, a smaller number of systems, maybe four, are developed to provide an initial operational capability. This

potential limitation suggests focusing efforts on improving real-time algorithms to maximize the information gained at each measurement location to avoid having to resample locations. Determining when a location has sufficiently been sampled and time is better spent measuring elsewhere is harder to do when resources are constrained. A system must be able to adapt to the scenario where perhaps only half of the UAVs make it to the target for one reason or another. This issue lends itself well to cooperative algorithms developed for the division of labor that swarms of UAVs use to cover a given area.

The goal of this research would be to adapt and further develop algorithms for 1 to n systems to divide up the search space to maximize the probability of detection or reach an acceptable level of confidence that a threat is not present. The confounding scenarios that need exploration include when one or more systems fail while on the target, when systems become available after the initial deployment, and when an anomaly is detected and needs to be confirmed. Also, topics such as the minimum time spent at a location, the minimum distance between measurement locations, the shared data requirements and update cycle between systems, and general routing guidelines should be explored further.

7.2.3 Testbed Experimentation

The eventual goal is to develop and transition a capability to the DoD for the directed search mission area. In parallel, we are sowing the seeds for the exploration of the other mission areas initially discussed in Chapter 1 and further explored in the appendix. Several testbeds exist within the USG that could be used to explore the efficacy of the system and test different concepts of operations and employment. These range from a collection of high-fidelity threat objects at the Device Assembly Facility to relevant operational environments located at the DTRA Technical Evaluation Assessment Monitor Site.

Sub-components of the system need to be tested at increasing technology readiness levels before a complete system is built. Though modeling suggests that the recommended suite of radiation detectors can detect relevant threats, the burden of proof is operational testing. It does not make sense to push forward with a platform design and auxiliary sensor selection until the foundational radiation sensors are solidified. In the same regard, expending considerable resources on adapting the form, fit, and function of sensors to a particular platform does not make sense until the platform has demonstrated that it can meet the constraints and limitations outline for the system. That is, if the platform cannot make it to the target or is too conspicuous, then designing a sensor package to mate to it is a waste of time, effort, and money.

Bibliography

- [1] Office of the Chairman of the Joint Chiefs of Staff, Joint Publication 1-02 Department of Defense Dictionary of Military and Associated Terms, Washington, D.C.: The Joint Staff, May 2019.
- [2] Office of the Under Secretary of Defense for Acquisition and Sustainment, Assistant Secretary of Defense for Nuclear, Chemical, and Biological Defense Programs, Nuclear Weapon Accident Response Procedures, Washington, D.C.: United States. Department of Defense, 2018.
- [3] United States. Department of Defense, "Narrative summaries of accidents involving U.S. nuclear weapons 1950–1980," United States. Department of Defense, Washington, D.C. , 1981.
- [4] H. M. Kristensen and M. Korda, "Federation of American Scientists—Status of World Nuclear Forces," May 2019. [Online]. Available: <https://fas.org/issues/nuclear-weapons/status-world-nuclear-forces/>. [Accessed 23 July 2019].
- [5] United States Army Chemical School, Multiservice Tactics, Techniques, and Procedures for Chemical, Biological, Radiological, and Nuclear Contamination Avoidance, Washington D.C.: United States. Department of Defense, 2006.
- [6] United States Army Chemical School, Multiservice Tactics, Techniques, And Procedures For Nuclear, Biological, And Chemical Reconnaissance, Washington, D.C.: United States. Department of Defense, 2004.
- [7] E. C. Morse, *Analytical Methods for Nonproliferation*, 1st Edition ed., Springer International Publishing, 2016.
- [8] International Atomic Energy Agency, "Nuclear Forensics," 2019. [Online]. Available: <https://www.iaea.org/topics/nuclear-forensics>. [Accessed 26 July 2019].
- [9] Mechtronic Solutions Inc., "Aerostructures," 2019. [Online]. Available: <https://www.msiabq.com/payload-pods/>. [Accessed 26 July 2019].
- [10] A. Kopeikin, S. Heider, D. Larkin, C. Korpela, R. Morales and J. E. Bluman, "Unmanned Aircraft System Swarm for Radiological and Imagery Data Collection," in *American Institute of Aeronautics and Astronautics Science and Technology Forum and Exposition*, San Diego, 2019.
- [11] Headquarters, Department of the Army, Chemical, Biological, Radiological, Nuclear, and Explosives Command, Washington, D.C.: Headquarters, Department of the Army, 2018.
- [12] J. Medalia, "Detection of Nuclear Weapons and Materials: Science, Technologies, Observations," U.S. Congressional Research Service, Washington, 2010.
- [13] J. F. Burns, "A Region Inflamed: Nuclear Weapons; Theft of Cobalt in Iraq Prompts Security Inquiry," *The New York Times*, p. A00001, 25 November 2003.
- [14] L. J. Blais, Interviewee, Comments on source recovery mission circa 2003, Iraq. [Interview]. Jan 2011.
- [15] C. Williams, Interviewee, Comments on source recovery mission circa 2003, Iraq. [Interview]. January 2011.

- [16] International Atomic Energy Agency, IAEA Safeguards Glossary, 2001 Edition ed., Vienna: International Atomic Energy Agency, 2002.
- [17] Albright, David; Berkhout, Frans; Walker, William; Stockholm International Peace Research Institute, Plutonium and Highly Enriched Uranium 1996 World Inventories, Capabilities and Policies, Oxford: Oxford University Press, 1997, p. 345.
- [18] K. E. Nelson, S. E. Labov and B. Seilhan, Interviewees, *Discussions with Nuclear Detection Systems and Algorithms group*. [Interview]. December 2015.
- [19] J. Curtis, "Benchmarking the Gamma-Ray Response of the Radiological Multi-sensor Analysis Platform," *Masters Thesis, Nuclear Engineering, University of California, Berkeley*, 2014.
- [20] P. Wasiolek and I. Halevy, "Aerial Measuring System (AMS) / Israel Atomic Energy Commission (IAEC) Joint Comparison Study Report," National Security Technologies, LLC., Las Vegas, NV, 2013.
- [21] R. T. Pavlovsky, A. Haefner, T. H. Joshi, V. Negut, K. D. McManus, E. Suzuki, R. Barnowski and K. Vetter, "3-D Radiation Mapping in Real-Time with the Localization and Mapping Platform LAMP from Unmanned Aerial Systems and Man-Portable Configurations," *arXiv*, no. arXiv:1901.05038, 2018.
- [22] Lawrence Berkeley National Laboratory Applied Nuclear Physics Program, "Instrumentation and Data Integration," 2016. [Online]. Available: <https://anp.lbl.gov/workgroups/instrumentation-and-data-integration/>. [Accessed 24 March 2016].
- [23] A. L. Hutcheson, B. F. Philips, E. A. Wulf, L. J. Mitchell, W. N. Johnson and B. E. Lees, "Maritime Detection of Radiological/Nuclear Threats with Hybrid Imaging System," in *IEEE International Conference on Technologies for Homeland Security (HST)*, Waltham, MA, 2013.
- [24] T. J. Aucott, M. S. Bandstra, V. Negut, D. H. Chivers, R. J. Cooper and K. Vetter, "Routine Surveys for Gamma-Ray Background Characterization," *IEEE Transactions on Nuclear Science*, vol. 60, no. 2, p. 1147–1150, April 2013.
- [25] Department of Energy—Energy Information Administration, "A Look at Commercial Buildings in 1995: Characteristics, Energy Consumption, and Energy Expenditures," Department of Energy, Washington, D.C., 1998.
- [26] Mason Contractors Association of America, "Masonry Facts," [Online]. Available: <https://www.masoncontractors.org/facts/>. [Accessed 03 06 2019].
- [27] Tilt-Up Concrete Association, *The Construction Of Tilt-Up*, First Edition ed., C. C. Wendy Ward, Ed., Mount Vernon, Iowa: Tilt-Up Concrete Association, 2011.
- [28] Texas Masonry Council, "Masonry vs. Tilt-up in Texas School Construction," Texas Masonry Council, Houston, 2010.
- [29] T. Henriksen and J. Baarli, "The Effective Atomic Number," *Radiation Research*, vol. 6, no. 4, p. 415–423, 1957.
- [30] National Security Technologies, LLC—Remote Sensing Laboratory, "An Aerial Radiological Survey of the California Bay Area," U.S. Department of Homeland Security Domestic Nuclear Detection Office, Washington, D.C., 2012.

- [31] E. Raguso, "Low-flying helicopter to measure radiation in Berkely," *Berkeleyside [digital]*, 31 August 2015.
- [32] A. Haefner, Interviewee, *Comments on ARES test near Richmond, CA*. [Interview]. September 2015.
- [33] Bell Helicopter, Bell Model 412 Rotorcraft Flight Manual, Revision 9 ed., Fort Worth, Texas: Bell Helicopter Textron Inc., 2002.
- [34] G. F. Knoll, *Radiation Detection and Measurement*, 4th ed., Hoboken, New Jersey: John Wiley & Sons, Inc., 2010.
- [35] P. Goldhagen, "Use of cosmic-ray neutron data in nuclear threat detection and other applications," U.S. Department of Homeland Security—Science and Technology, Honolulu, 2015.
- [36] R. T. Kouzes, J. H. Ely, A. Seifert, E. R. Siciliano, D. R. Weier, L. K. Windsor and M. L. Woodring, "Cosmic-ray-induced ship-effect neutron measurements and implications for cargo scanning at borders," *Nuclear Instruments & Methods in Physics Research Section A*, vol. 587, no. 1, p. 89–100, 2008.
- [37] J. F. Ziegler, "Terrestrial cosmic rays," *IBM Journal of Research and Development*, vol. 40, no. 1, p. 19–38, January 1996.
- [38] J. A. Simpson and W. C. Fagot, "Properties of the low energy nucleonic component at large atmospheric depths," *Physical Review*, vol. 90, no. 6, p. 1068, 15 June 1953.
- [39] E. Regener and G. Pfozter, "Vertical intensity of cosmic rays by threefold coincidences in the stratosphere," *Nature*, vol. 136, no. 3444, p. 718–719, November 1935.
- [40] K. Abe et al., "Measurements of cosmic-ray proton and helium spectra from the BESS-Polar long-duration balloon flights over Antarctica," *The Astrophysical Journal*, vol. 822, no. 2, p. 1–16, 5 May 2016.
- [41] Particle Data Group, Tanabashi, M. et al., "2018 Review of Particle Physics - 29. Cosmic rays," *Physical Review D*, vol. 98, no. 030001, p. 424–432, 17 August 2018.
- [42] J. S. Duval, J. M. Carson, P. B. Holman and A. G. Darnley, "Terrestrial radioactivity and gamma-ray exposure in the United States and Canada," U.S. Geological Survey, Reston, VA, 2005.
- [43] M. W. Swinney, D. E. Peplow, A. D. Nicholson and B. W. Patton, "NORM Concentration Determination in Common Materials in an Urban Environment," in *Transactions of the American Nuclear Society*, New Orleans, 2016.
- [44] A. S. Murray, R. Marten, A. Johnston and J. Martin, "Analysis for naturally occurring radionuclides at environmental concentrations by gamma spectrometry," *Journal of Radioanalytical and Nuclear Chemistry, Articles*, vol. 115, no. 2, p. 263–288, 13 April 1987.
- [45] U.S. Environmental Protection Agency, "Radiation Sources and Doses," 14 June 2019. [Online]. Available: <https://www.epa.gov/radiation/radiation-sources-and-doses>. [Accessed 29 July 2019].
- [46] National Council on Radiation Protection and Measurements, "Ionizing Radiation Exposure of the Population of the United States," National Council on Radiation Protection and Measurements, Bethesda, 2009.

- [47] U.S. Environmental Protection Agency, "RadTown—About background radiation," [Online]. Available: <https://www.epa.gov/radtown/background-radiation>. [Accessed 6 JUNE 2019].
- [48] United Nations Environment Programme, Radiation Effects and Sources, Nairobi: United Nations Environment Programme, 2016.
- [49] United Nations Scientific Committee on the Effects of Atomic Radiation, "Radio-active Contamination of the Environment by Nuclear Tests," United Nations, New York, 1964.
- [50] United Nations Scientific Committee on the Effects of Atomic Radiation, "UNSCEAR 2000 Report to the General Assembly, with Scientific Annexes," United Nations, New York, 2000.
- [51] S. L. Simon, A. Bouville and H. L. Beck, "The geographic distribution of radionuclide deposition across the continental US from atmospheric nuclear testing," *Journal of Environmental Radioactivity*, vol. 74, no. 1-3, pp. 96-100, 2004.
- [52] T. J. Yasunari, A. Stohl, R. S. Hayano, J. F. Burkhardt, S. Eckhardt and T. Yasunari, "Cesium-137 deposition and contamination of Japanese soils due to the Fukushima nuclear accident," *Proceedings of the National Academy of Sciences of the United States of America*, vol. 108, no. 49, pp. 19530-19534, 6 December 2011.
- [53] M. Hvistendahl, "Coal Ash Is More Radioactive Than Nuclear Waste," *Scientific American*, 13 December 2007.
- [54] U.S. Department of Health & Human Services, "Radiation Emergency Medical Management (REMM)," U.S. Department of Health & Human Services, August 2016. [Online]. Available: <https://www.remm.nlm.gov/index.html>. [Accessed 27 June 2019].
- [55] World Nuclear Association, "Uranium Mining Overview," February 2019. [Online]. Available: <http://www.world-nuclear.org/information-library/nuclear-fuel-cycle/mining-of-uranium/uranium-mining-overview.aspx>. [Accessed 8 June 2019].
- [56] World Nuclear Association, "Uranium and depleted uranium," September 2016. [Online]. Available: <http://www.world-nuclear.org/information-library/nuclear-fuel-cycle/uranium-resources/uranium-and-depleted-uranium.aspx>. [Accessed 10 June 2019].
- [57] T. E. Sampson, "Precision Measurement of Gamma Ray Energies from U-238," *Nuclear Instruments and Methods*, vol. 98, no. 1, p. 37–40, 1972.
- [58] D. Reilly, N. Ensslin, H. J. Smith and S. Kreine, "Passive nondestructive assay of nuclear materials," U.S. Government Printing Office, Los Alamos, 1991.
- [59] R. Collé, L. Laureano-Pérez, S. Nour, J. J. La Rosa, B. E. Zimmerman, L. Pibida and D. E. Bergeron, "Natural Uranium Radioactivity Solution Standard: SRM 4321d," *Journal of Research of the National Institute of Standards and Technology*, vol. 122, no. 44, 2017.
- [60] I. I. Bashter, "Calculation of radiation attenuation coefficients for shielding concretes," *Annals of Nuclear Energy*, vol. 24, no. 17, p. 1389–1401, 1997.
- [61] J. H. Hubbell and S. M. Seltzer, "Tables of X-Ray Mass Attenuation Coefficients and Mass Energy-Absorption Coefficients (version 1.4). [Online]," National Institute of Standards and Technology, 12 July 2004. [Online]. Available: <http://physics.nist.gov/xaamdi>. [Accessed 24 June 2019].

- [62] B. Rooney, S. Garner, P. Felsher and P. Karpus, *PeakEasy 4.98 [Computer Program]*, Los Alamos National Laboratory, 2018.
- [63] M. E. Anderson and J. F. Lemming, "Selected Measurement Data for Plutonium and Uranium," Mound Laboratory, Miamisburg, 1982.
- [64] D. J. Mitchell, L. T. Harding, G. G. Thoreson and S. M. Horne, *Gamma Detector Response and Analysis Software Version 18.7.9.0 [computer program]*, Albuquerque, NM: Sandia National Laboratories, 2018.
- [65] R. B. Oberer, L. G. Chiang, M. J. Norris, C. A. Gunn and B. C. Adaline, "The use of Tl-208 gamma rays for safeguards, nondestructive-assay (NDA) measurements," Babcock & Wilcox Technical Services Y-12, LLC, 2009.
- [66] K. J. Moody, P. M. Grant, I. D. Hutcheon and Y. Varoufakis, *Nuclear Forensic Analysis*, 2nd Edition ed., Boca Raton, FL: CRC Press - Taylor & Francis Group, 2015, p. 383.
- [67] S. Fetter, V. A. Frolov, M. Miller, R. Mosley, O. F. Prilutsky, S. N. Rodionov and R. Z. Sagdeev, "Detecting nuclear warheads," *Science & Global Security*, vol. 1, no. 3–4, p. 225–253, 1990.
- [68] Dodd, B.; McKenna, T.; Wheatley, J.; Division of Radiation and Waste Safety, "Categorization of Radioactive Sources," International Atomic Energy Agency, Vienna, 2003.
- [69] Oak Ridge Institute for Science and Education, "Radiological and Chemical Properties of Uranium [ORISE slide presentation]," [Online]. Available: <https://www.nrc.gov/docs/ML1122/ML11227A233.pdf>. [Accessed 09 July 2019].
- [70] Nordion (Canada) Inc., "Medical-grade Cobalt-60," Excentric, 2019. [Online]. Available: <https://www.nordion.com/products/medical-grade-cobalt-60/>. [Accessed 29 July 2019].
- [71] J. Masefield, B. Morrissey, J. Chitra, N. Bennett, L. Mathias and R. Brinston, "Cobalt-60 Use and Disposal: An Established Pathway," in *International Meeting on Radiation Processing*, London, 2008.
- [72] World Nuclear News, "Power plant to boost cobalt isotope supplies," *World Nuclear News*, 21 January 2009.
- [73] T. Bielefeld, "Mexico's stolen radiation source: It could happen here," *Bulletin of the Atomic Scientists*, 23 January 2014.
- [74] R. Romo, N. Parker and M. Castillo, "Mexico: Stolen radioactive material found," *Cable News Network (CNN)*, 04 December 2013.
- [75] International Atomic Energy Agency, "The radiological accident in Samut Prakarn.," International Atomic Energy Agency, Vienna, 2002.
- [76] G. Nelson and D. Reilly, "Gamma-ray interactions with matter," in *Passive nondestructive assay of nuclear materials*, S. Kreiner, Ed., Washington, D.C., U.S. Government Printing Office, 1991.
- [77] R. D. Evans, *The Atomic Nucleus*, New York: Krieger, 1982.

- [78] M. Chen, "PHYS 352: Measurement, Instrumentation and Experiment Design - Photon Interactions Lecture," 2011. [Online]. Available: <https://www.physics.queensu.ca/~phys352/>. [Accessed 03 July 2019].
- [79] M. J. Berger, J. H. Hubbell, S. M. Seltzer, J. Chang, J. S. Coursey, R. Sukumar, D. S. Zucker and K. Olsen, "NIST Standard Reference Database 8 (XGAM)," National Institute of Standards and Technology, November 2010. [Online]. Available: <https://www.nist.gov/pml/xcom-photon-cross-sections-database>. [Accessed 03 July 2019].
- [80] Ureview@bell.net, "Quantum Field Theory, Compton Scattering," October 2002. [Online]. Available: <http://universe-review.ca/R15-12-QFT10.htm>. [Accessed 29 June 2019].
- [81] S. M. Blinder, "Klein-Nishina Formula for Compton Effect," 03 December 2009. [Online]. Available: <http://demonstrations.wolfram.com/KleinNishinaFormulaForComptonEffect/>. [Accessed 17 July 2019].
- [82] Qwerty123uiop, "Photomultiplier tube," 30 11 2013. [Online]. Available: https://en.wikipedia.org/wiki/Scintillation_counter#/media/File:PhotoMultiplierTubeAndScintillator.svg. [Accessed 19 June 2019].
- [83] Hamamatsu Solid State Division, Opto-semiconductor Handbook, Hamamatsu City: Hamamatsu Photonics K.K., 2019.
- [84] KETEK, "SiPM," KETEK GmbH, 2019. [Online]. Available: <https://www.ketek.net/sipm/>. [Accessed 10 July 2019].
- [85] ON Semiconductor, "A Brief Introduction to Silicon Photomultiplier (SiPM) Sensors," Semiconductor Components Industries, LLC, 2019. [Online]. Available: <https://www.onsemi.com/pub/Collateral/AND9795-D.PDF>. [Accessed 10 July 2019].
- [86] ON Semiconductor, "Linearity of the Silicon Photomultiplier," 2019. [Online]. Available: <https://www.onsemi.com/pub/Collateral/AND9776-D.PDF>. [Accessed 10 July 2019].
- [87] L. H. Heilbronn, "The Health Risks of Extraterrestrial Environments (THREE)—Basic Concepts of Space Radiation," 09 July 2015. [Online]. Available: https://three.jsc.nasa.gov/articles/Heilbronn_Neutron_Supplement.pdf. [Accessed 19 June 2019].
- [88] International Atomic Energy Agency, "Neutron generators for analytical purposes," International Atomic Energy Agency, Vienna, 2012.
- [89] J. L. Lacy, A. Athanasiades, C. S. Martin, L. Sun and G. L. Vazquez-Flores, "The Evolution of Neutron Straw Detector Applications in Homeland Security," *IEEE Transactions on Nuclear Science*, vol. 60, no. 2, p. 1140–1146, April 2013.
- [90] D. S. McGregor, W. J. McNeil, S. L. Bellinger, T. C. Unruh and J. K. Shultis, "Microstructured semiconductor neutron detectors," *Nuclear Instruments and Methods in Physics Research Section A: Accelerators, Spectrometers, Detectors and Associated Equipment*, vol. 608, no. 1, p. 125–131, 2009.
- [91] N. Blasi, S. Brambilla, F. Camera, S. Ceruti, A. Giaz, L. Gini, F. Groppi, S. Manenti, A. Mentana, B. Million and S. Riboldi, "Fast neutron detection efficiency of ^6Li and ^7Li

- enriched CLYC scintillators using an Am-Be source," *Journal of Instrumentation*, vol. 13, p. 11010, November 2018.
- [92] N. D'Olympia, P. Chowdhury, C. J. Guess, T. Harrington, E. G. Jackson, S. Lakshmi, C. J. Lister, J. Glodo, R. Hawrami, K. Shah and U. Shirwadkar, "Optimizing Cs₂LiYCl₆ for fast neutron spectroscopy," *Nuclear Instruments and Methods in Physics Research Section A: Accelerators, Spectrometers, Detectors and Associated Equipment*, vol. 694, p. 140–146, 01 December 2012.
- [93] National Research Council, *Existing and Potential Standoff Explosives Detection Techniques*, Washington, DC: The National Academies Press, 2004, p. 71–96.
- [94] R. L. e. b. Woodfin, *Trace chemical sensing of explosives*, Hoboken, New Jersey: John Wiley & Sons, Inc., 2007.
- [95] L. Mokalled, M. Al-Husseini, K. Y. Kabalan and A. El-Hajj, "Sensor Review for Trace Detection of Explosives," *International Journal of Scientific & Engineering Research*, vol. 5, no. 6, p. 337–350, June 2014.
- [96] R. Barnowski, A. Haefner, L. Mihailescu and K. Vetter, "Scene data fusion: Real-time standoff volumetric gamma-ray imaging," *Nuclear Instruments and Methods in Physics Research Section A: Accelerators, Spectrometers, Detectors and Associated Equipment*, vol. 800, p. 65–69, 11 November 2015.
- [97] J. S. Peterson, "File:Dice-5-b.svg," 30 November 2012. [Online]. Available: <https://commons.wikimedia.org/wiki/File:Dice-5-b.svg>. [Accessed 25 June 2019].
- [98] UC Regents, "Richmond Field Station Frequently Asked Questions (FAQ)," 2005. [Online]. Available: <http://rfs-env.berkeley.edu/faq.html>. [Accessed 16 July 2019].
- [99] S.-b. Liao, P. Dourmashkin and J. W. Belcher, "MIT Physics 8.02 Electricity and Magnetism Course Notes Chapter 4 Gauss' Law," 2004. [Online]. Available: <http://web.mit.edu/8.02t/www/802TEAL3D/visualizations/coursenotes/modules/guide04.pdf>. [Accessed 11 July 2019].
- [100] Woodproducts, "Plywood," 2019. [Online]. Available: <https://www.woodproducts.fi/content/plywood>. [Accessed 11 July 2019].
- [101] M. W. Marshdeh, I. F. Al-Hamarneh, E. M. Abdel Munem, A. A. Tajuddin, A. Ariffin and S. Al-Omari, "Determining the mass attenuation coefficient, effective atomic number, and electron density of raw wood and binderless particleboards of *Rhizophora* spp. by using Monte Carlo simulation," *Results in Physics*, vol. 5, p. 228–234, 2015.
- [102] K.-P. Ziock and K. E. Nelson, "Maximum detector sizes required for orphan source detection," *Nuclear Instruments and Methods in Physics Research A*, vol. 579, no. 1, p. 357–362, 2007.
- [103] J. S. Duval, "Aerial gamma-ray color contour maps of regional surface concentrations of potassium, uranium, thorium and composite-color maps of uranium, potassium, thorium, and their ratios in New Mexico," U.S. Geological Survey, Reston, VA, 1989.
- [104] Google Earth, "Map of Richmond, CA [37°54'53.81" N 122°20'04.81" W] with USGS radiometric potassium KZM overlay," Google Earth, 2018.
- [105] U.S. Department of Energy Office of Counterterrorism and Counterproliferation, "U.S. Department of Energy International Reachback Capabilities," Washington, D.C., 2019.

- [106] National Nuclear Security Administration Nevada Field Office, "National Security Technologies, LLC Fiscal Year 2015 Performance Evaluation Report," National Nuclear Security Administration, North Las Vegas, NV, 2016.
- [107] U.S. Nuclear Regulatory Commission, "Safeguard categories of SNM," 14 August 2017. [Online]. Available: <https://www.nrc.gov/security/domestic/mca/snm.html>. [Accessed 04 August 2019].
- [108] Defense Acquisition University, "DAU Acquisition Encyclopedia," 2019. [Online]. Available: <https://www.dau.mil/acquipedia/Pages/acquipedia.aspx>. [Accessed 22 July 2019].
- [109] K. D. McManus, "Concept of Operations and Employment for Radiological / Nuclear Search and Reconnaissance Using Small Unmanned Aircraft Systems (sUAS)," Fort Belvoir, 2016.
- [110] Office of the Chairman of the Joint Chiefs of Staff, Joint Publication 5-0 Joint Planning, Washington, D.C.: The Joint Staff, June 2017.
- [111] Department of the Army, Field Manual 5-0 The Operations Process, Washington, D.C.: Headquarters, Department of the Army, 2010.
- [112] C. Morey, M. F. Bauman and P. Works, "Constraints, Limitations, and Assumptions Code of Best Practice," U.S. Army TRADOC Analysis Center, Fort Leavenworth, KS, 2012.
- [113] J. Hines, L. Bennett, C. Ligetti, J. Banks and S. Nestler, "Cost-Benefit Analysis Trade-Space Tool as a Design-Aid for the U.S. Army Vehicle Health Management System (VHMS) Program," in *Annual Conference of the Prognostics and Health Management Society*, San Diego, CA, 2009.
- [114] C. A. Bond, L. A. Mayer, M. E. McMahon, J. G. Kallimani and R. Sanchez, Developing a Methodology for Risk-Informed Trade-Space Analysis in Acquisition, Santa Monica, CA: RAND Corporation, 2015.
- [115] A. M. Ross, H. L. McManus, D. H. Rhodes and D. E. Hastings, "Revisiting the Tradespace Exploration Paradigm: Structuring the Exploration Process," in *American Institute of Aeronautics and Astronautics Space 2010 Conference & Exposition*, Anaheim, CA, 2010.
- [116] DJI, "Enterprise Products Drones," SZ DJI Technology Co., Ltd., 2019. [Online]. Available: <https://enterprise.dji.com/products/drones>. [Accessed 05 July 2019].
- [117] Frazier, Alan; Deputy Sheriff Grand Forks County Sheriff's Department, "Law Enforcement use of Unmanned Aircraft Systems," in *National Sheriffs' Association Annual Conference*, Minneapolis, MN, 2016.
- [118] productz.com, "AeroVironment Shrike VTOL Specifications," Productz MiB GmbH, [Online]. Available: <https://productz.com/en/aerovironment-shrike-vtol-drone>. [Accessed 08 July 2019].
- [119] AeroVironment, Inc., "VAPOR Helicopter UAS," AeroVironment, 19 July 2019. [Online]. Available: https://www.avinc.com/images/uploads/product_docs/Vapor_datasheet_07192019.pdf. [Accessed 30 July 2019].

- [120] U.S. Department of the Interior, "Office of Aviation Services—Unmanned Aircraft Systems—DOI UAS Fleet," 2019. [Online]. Available: <https://www.doi.gov/sites/doi.gov/files/uploads/Pulse%20Vapor%2055TM%20Helicopter%20Data%20Sheet.pdf>. [Accessed 09 July 2019].
- [121] R. Whittle, "Robot Aircraft For Robot Tanks: GD & AeroVironment Team Up," *Breaking Defense [digital magazine]*, 09 October 2018.
- [122] Vertical Technologies, "The DeltaQuad," 2019. [Online]. Available: <https://www.deltaquad.com>. [Accessed 09 July 2019].
- [123] A. Lacaze, "Pegasus transforming UAV/UGV hybrid vehicle," in NDIA Ground Vehicle Systems Engineering And Technology Symposium—Autonomous Ground Systems (AGS) Technical Session, Novi, MI, 2017.
- [124] Robotic Research, LLC, "Pegasus Transformable Air-Ground Robotic System," Robotic Research, LLC, Gaithersburg, 2018.
- [125] Raytheon, "Pike Munition—Miniaturize, Laser-Guided Weapon," Raytheon Company, 2019. [Online]. Available: <https://www.raytheon.com/capabilities/products/pike>. [Accessed 08 July 2019].
- [126] G. W. Cooke, "40mm Low-Velocity Grenades," 25 February 2010. [Online]. Available: https://www.inetres.com/gp/military/infantry/grenade/40mm_amm0.html. [Accessed 08 July 2019].
- [127] DefendTex, "D40-81 Brief International," Melbourne, 2019.
- [128] AeroVironment, "Switchblade," AeroVironment, Inc., 2019. [Online]. Available: <https://www.avinc.com/uas/view/switchblade>. [Accessed 08 July 2019].
- [129] J. Trevithick, "Army Buys Small Suicide Drones To Break Up Hostile Swarms And Potentially More," *The War Zone [digital news outlet]*, 17 July 2018.
- [130] B. Quam, B. Vogel and S. Ono, "Alternative radiation detectors," Special Technology Laboratories (STL), Santa Barbara, CA, 2013.
- [131] Kromek Group, "SIGMA scintillator detectors," 2018. [Online]. Available: <https://www.kromek.com/product/sigma-scintillator-detectors/>. [Accessed 08 July 2019].
- [132] Proportional Technologies, Inc., "Products," Out of the Sandbox, 2019. [Online]. Available: <https://proportionaltech.myshopify.com/pages/products>. [Accessed 05 July 2019].
- [133] Radiation Detection Technologies, Inc., "Domino neutron detector," 01 November 2017. [Online]. Available: http://radectech.com/content/Domino_V5.40_general_spec_sheet_30percent-rev1.pdf. [Accessed 05 July 2019].
- [134] LND, Inc., "Cylindrical He-3 neutron detector general specifications," Maxburst Web Design, [Online]. Available: <https://www.lndinc.com/products/neutron-detectors/25193/>. [Accessed 08 July 2019].
- [135] FLIR Systems, Inc., "sUAS Cameras & Kits," 2019. [Online]. Available: <https://www.flir.com/browse/home--outdoor/drone-cameras/>. [Accessed 08 July 2019].

- [136] F. Corrigan, "10 Thermal Vision Cameras For Drones And How Thermal Imaging Works," 17 February 2019. [Online]. Available: <https://www.dronezon.com/learn-about-drones-quadcopters/9-heat-vision-cameras-for-drones-and-how-thermal-imaging-works/>. [Accessed 08 July 2019].
- [137] LeddarTech, "Leddar Vu8," 2018. [Online]. Available: <https://d2euypccftd53r.cloudfront.net/prod/app/uploads/2018/04/21135401/Spec-Sheet-Leddar-Vu8-20190618-EN.pdf>. [Accessed 8 July 2019].
- [138] Velodyne LiDAR, Inc., "Puck LITE," 2016. [Online]. Available: <https://www.velodynelidar.com/vlp-16-lite.html>. [Accessed 08 July 2019].
- [139] R. T. Pavlovsky, "Digital Photo of DJI Matrice 600 Pro with LAMP-D3S payload," Richmond, 2016.
- [140] Military Factory, "Unmanned Helicopters," 2019. [Online]. Available: <https://www.militaryfactory.com/aircraft/uav-helicopters-and-related.asp>. [Accessed 09 July 2019].
- [141] Unmanned Systems Technology, "Hybrid VTOL Fixed-Wing UAV Manufacturers," EchoBlue Ltd., 2019. [Online]. Available: <https://www.unmannedsystemstechnology.com/category/supplier-directory/platforms/hybrid-vtol-uav-manufacturers>. [Accessed 09 July 2019].
- [142] AeroVironment, Inc, "Quantix™," 2018. [Online]. Available: [https://www.avdroneanalytics.com/source/files/AV%20Quantix_2019_4pg_05_no_crop\(2\).pdf](https://www.avdroneanalytics.com/source/files/AV%20Quantix_2019_4pg_05_no_crop(2).pdf). [Accessed 30 July 2019].
- [143] National Urban Security Technology Laboratory, "Neutron-detecting personal radiation detectors (PRDs) and spectroscopic PRDs market survey report," U.S. Department of Homeland Security Science and Technology, Washington, D.C., 2015.
- [144] Kromek Group, "D3S ID gamma neutron detector," 2016. [Online]. Available: <https://www.kromek.com/images/products/D3S-NETA4ERev1.pdf>. [Accessed 04 August 2019].
- [145] National Coordination Office for Space-Based Positioning, Navigation, and Timing, "GPS Accuracy," 05 December 2017. [Online]. Available: <https://www.gps.gov/systems/gps/performance/accuracy/>. [Accessed 5 July 2019].
- [146] C. Lyons, "Aerial Measuring System (AMS) Baseline Surveys for Emergency Planning," Nevada Test Site/National Security Technologies, LLC (United States), Washington D.C., 2012.
- [147] Seilhan, Brandon S., Lawrence Livermore National Laboratory, "Spectral Accumulator," unpublished, Livermore, 2016.
- [148] E. Specht, "Packomania," 29 June 2018. [Online]. Available: <http://www.packomania.com/>. [Accessed 01 July 2019].
- [149] Wikipedia contributors, "Circle packing," 2019. [Online]. Available: https://en.wikipedia.org/wiki/Circle_packing. [Accessed 29 June 2019].
- [150] S. Sastry and M. Bodson, Adaptive Control, Englewood Cliffs, NJ: Prentice-Hall, Inc., 1989.

- [151] United States, AEC authorizing legislation, fiscal year 1971. Hearings, Ninety-first Congress, second session..., Washington, DC: U.S. Government Printing Office, 1970, p. 1702.
- [152] K. Nelson and P. Sökkappa, "A Statistical Model for Generating a Population of Unclassified Objects and Radiation Signatures Spanning Nuclear Threats," Lawrence Livermore National Laboratory, Livermore, 2008.
- [153] S. Farrell and D. Williams, "Israel admits bombing suspected Syrian nuclear reactor in 2007, warns Iran," *Reuters World News [digital]*, 20 March 2018.
- [154] World Nuclear Association, "Fukushima Daiichi Accident," October 2018. [Online]. Available: <http://www.world-nuclear.org/information-library/safety-and-security/safety-of-plants/fukushima-accident.aspx>. [Accessed 10 July 2019].
- [155] Office of the Assistant Secretary of Defense for Nuclear and Chemical and Biological Defense Programs, "Nuclear Weapon Accident Response Procedures," United States. Department of Defense, Washington, D.C., 2005.

Appendix—Department of Defense Radiological and Nuclear Detection Missions

DIRECTED SEARCH

- **UJTL TASK:** SN 9.2.6 Conduct operations to locate and identify radiological material
- **CONDITIONS:** given a known source that is likely within an area <10 km², a number of suspect locations that exceeds manned search capabilities, and a time sensitive target available over a period of darkness
- **STANDARDS:** conduct a search of 1 – 3 targets in a 24 hour period to confirm at >70% confidence or deny at >95% confidence, or return data for manual analysis

I. Google earth v7.1.5.1557. (2015 October 30). El Cerrito, CA, USA. <http://www.earth.google.com> [2016 August 15]

II. Property Wala. www.propertywala.com [2015 October 14]

III. Various - listed below graphic counter-clockwise from top left [2015 October 14]

IV. GADRAS v18.6.5. (2016 May 19). Analysis of inject spectrum based on user-built model with background. [2016 August 10]

Source: [109]

Directed Search

Radiological and nuclear search is the main effort when it comes to nuclear detection research and development efforts for the DoD, and arguably across other government agencies as well. Nevertheless, what “search” means and what that term implies to different user groups is exceedingly diverse. Therefore, the term “directed search” is defined and used here.

Directed search assumes that law enforcement, security forces, or intelligence functions have confirmed the loss, theft, or possession of radiological or nuclear material of concern by a state or non-state actor (e.g., individuals, extremist organizations, and non-governmental entities). The type, quantity, total mass, chemical form, and geometric configuration of the material are likely known or can be approximated. The suspected location of the material has been narrowed to a reasonable-sized search area through intelligence collection and assessment. For directed search, a reasonable-sized search area is defined here as less than ten square kilometers (e.g., a small town, a large neighborhood or section of a city, several small villages). Furthermore, intelligence assets may have identified light industrial or commercial structures within the search area as possible device fabrication, assembly, or material storage sites.

Efforts to neutralize attempts to smuggle nuclear weapons or radioactive materials into the country have been ongoing since the advent of the Atomic Age. Fortunately, there have not

been any publicly confirmed attempts to locate an improvised nuclear device (IND) or radioactive dispersal device (RDD). That is not to say that search teams have not been employed to find lost or stolen material. In 2003, DoD radiological search assets were used to locate two radioactive capsules stolen by looters from a nuclear testing site located at Saddam Hussein's main battlefield testing center in the desert west of Baghdad [13].

The site, built in the early-1980s, was used to test equipment, and possibly human subjects, in a simulated battlefield radiation environment by raising large-activity radioactive sources on towers arranged in an arc around a test pad. Small metal capsules, each initially containing approximately 370 giga-becquerels (GBq)—10 curies (Ci)—of the isotope ^{60}Co , had been stored in concrete containers at the bases of each of the eight 23 m (75 ft.) testing poles. By 2003, the sources had decayed to approximately 10% of their original activity but remained a significant health hazard and possible RDD threat at ~ 37 GBq (1 Ci) each.

Finding sources of that strength is “the slow pitch softball” [14] of search operations. It was quickly accomplished by mounting a large detector system containing thallium-doped sodium iodide (NaI[Tl]) scintillation gamma-ray detectors and ^3He -filled proportional tube neutron detectors into a military helicopter and scanning the nearby area at low altitude and airspeed. The two sources were found along with remnants of the tower poles, which were the target of the looting, in two adjacent villages approximately 16 kilometers (10 mi.) north of the testing site.

Though this search and recovery operation was swift and successful, changes in the conditions could have made the mission far more difficult. For example, the source strength and primary gamma-ray energies associated with the decay of the ^{60}Co isotope allowed search forces to locate the material from an altitude of more than 100 meters. Suppose instead it was special nuclear material (SNM), secretly hidden from inspectors, that went missing from the Baghdad Nuclear Research Facility. Depending on the material properties—including fissile isotope(s), enrichment levels, impurities, and other factors—the gamma and neutron flux produced by the material could range several orders of magnitude and be much more difficult or nearly impossible to detect from the air.

For this exemplification, assume that the material consisted of 25 kg of weapons-grade (WG) highly enriched uranium (HEU). That amount is classified as a significant quantity (SQ) by the International Atomic Energy Agency (IAEA), which denotes the approximate amount of nuclear material for which the possibility of manufacturing a nuclear explosive device cannot be excluded [16]. Prior to its removal by the IAEA after the 1991 Gulf War, Iraq possessed more than 12 kg of slightly irradiated 93%-enriched uranium fuel purchased from France as part of the Tammuz-2 reactor. They also possessed more than an SQ of both fresh and irradiated 80%-enriched uranium fuel from the Russian-supplied IRT-5000 research reactor [17].

Unlike the ^{60}Co sources, which were found lying in the yard of a house and partially buried in a field near another, assume that the value and hazards associated with the stolen SNM were known to the thieves and kept in a secure location, such as a non-descript building in Fallujah. The concept of operations calling for a helicopter to fly low and slow to locate the material fails quickly. First, the expected radioactive signature from the material would be

undetectable above background, even at the lowest operating altitude and speed of a helicopter, except for perhaps hovering directly above or landing on the roof. Second, the geographic area that the cobalt sources were recovered from was semi-permissive during the operation; that is, the villagers, while not completely forthcoming with details regarding the missing material, were not actively hostile towards U.S. forces at the time. Had operations taken place later in the conflict, those villages at the southern end of the so-called Sunni triangle may have been much more hostile, thereby precluding the low and slow flight of a manned helicopter or necessitating a much larger security presence. Third, the presence of a helicopter flying a search pattern over buildings would certainly trigger apprehension in the minds of those possessing the material, prompting them to flee the area or to shield the material if they were working with it at the time.

Given these realities, the conditions for high-consequence directed search operations involving SNM require pushing detectors as close to the source location as possible while not tipping off the adversary to one's actions and reducing the risk to personnel and equipment where possible. To that end, a remote sensing platform that can be flown, dropped, or launched to a location is an attractive solution. As such, a modest collection of small unmanned aerial systems (sUAS) outfitted with radiation detectors coupled to contextual sensors could meet those requirements for under \$2 million.

sUAS can fly much closer to buildings and could perhaps land on them undetected. Furthermore, reducing the distance between potential sources and the sensors allows one to use smaller and more sophisticated detectors to achieve equal or better sensitivity but with much higher specificity. Moreover, the reduction in risk across-the-board is unparalleled. Not only are several warfighters and tens of millions of dollars of equipment removed from a potentially high-risk situation, but the risk to mission compromise via adversary tip-off is also significantly reduced.


Of course, there are engineering challenges that we must overcome and trade-offs that we need to weigh when designing such a system of systems for this application. Considerations for this mission area are the primary focus of the research conducted and presented in this work. The two chief concerns are the optimization of the sensor package and the development of the search method. The choice of detector materials, the quantity and arrangement of detector elements, and the choice of auxiliary sensors are paramount in developing a system that can detect a sufficient number of threat materials under a given set of conditions. Beyond that, the effective employment of a group of systems requires detailed analysis of individual search patterns, collective coverage schemes, and cooperative detection algorithms.

The other mission areas illustrate various conditions that might dictate a different approach than that of directed search. However, there are likely to be overlaps and synergies that exist between several missions that would permit adaptable or modular multipurpose design approaches that employ the same or similar unmanned platforms, sensors, search schemes, or algorithms.


BATTLE DAMAGE ASSESSMENT

- **UJTL TASKS:** SN 9 Countering Weapons of Mass Destruction (CWMD) and OP 2.8.4.1 Conduct Battle Damage Assessment (BDA)
- **CONDITIONS:** given a single attack on a single weapons of mass destruction (WMD) target with an expected and measurable post-blast signature
- **STANDARDS:** assist with battle damage assessment (BDA) results to confirm presence of and/or locate radiological or nuclear material in < 24 hours


I.



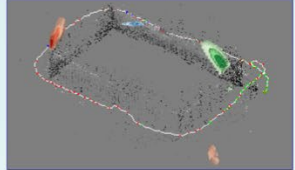
II.



III.



IV.



I. <http://www.4law.co.uk/cnr24a.jpg> [2016 August 15]

II. <http://static.jbcgroup.com/news/pictures/38a92850676ff4da3d9955d8ccb2dba.jpg> [2016 August 15]

III. <http://www.4law.co.uk/cnr24h.jpg> [2016 August 15]

IV. 3-D rendering graphic courtesy of Andrew Haefner, Lawrence Berkeley National Laboratory

Source: [109]

Battle Damage Assessment

Battle damage assessment (BDA) encompasses the estimate of the damage resulting from the application of lethal or nonlethal military force. Traditionally, it is associated with assessing the damage inflicted on a target from a stand-off weapon, such as a bomb or guided missile. Assessment of the physical damage, functional damage, and effect on the targeted systems are made to inform further actions [1]. As an example, physical damage to an underground hangar complex or airfield that prevents an enemy from launching fighter jets for some number of hours might be the commander's desired effect of a given strike. Verification of craters of a certain depth and placement informs the commander of a functional kill; the strike has not destroyed any of the fighter jets yet has delayed their employment long enough to make their threat moot. Alternatively, if the strike did not achieve the desired effect on-target, it may drive a commander to authorize another sortie or to adjust plans to account for the possible employment of the enemy fighter jets.

While BDA to some extent is unique to military operations, there are corollaries with civil applications that involve the spread of radiological or nuclear sources, especially in an urban area. This spread might be from a "dirty bomb" scenario or an improvised nuclear device that fails to achieve a significant nuclear yield, known as a fizzle. The radiation detection requirements for the offensive military BDA scenario are likely to be quite similar to that of a civil response to an incident where radiological or nuclear material is explosively spread over an urban or industrial area.

The bombings of the Al-Kibar reactor site in the Deir ez-Zor region of Syria in 2007, as well as the bombings of the Osirak reactor at the Al Tuwaitha Research Nuclear Center in

Iraq in 1981, both conducted by the Israeli Defense Forces (IDF), are prime examples of where BDA enhanced with radiation detection capabilities could have proved useful.

Though Syria signed and ratified the Treaty on the Non-proliferation of Nuclear Weapons (NPT), they failed to declare Al-Kibar to the IAEA. Intelligence collected by Israeli-operatives over some time determined that they were building a clandestine reactor at Al-Kibar in the remote desert of eastern Syria, near the Euphrates river. The facility was built in cooperation with North Korea and modeled after the Yongbyon facility [153]. Shortly after conclusive intelligence was gathered that proved the existence and purpose of the facility, a decision was made to execute a strike on the suspected plutonium production reactor. As such, they anticipated that the Syrians had not yet fueled the reactor, but that construction was complete, and the facility was nearing operational capability. Recently released cockpit footage and photographs suggest that standard BDA means were sufficient for the circumstances encountered. However, had the Syrian's fueled the reactor or stored fissile material onsite, a method to confirm or deny such a condition would be highly desirable.


The bombing of Osirak was conducted under similar auspices, though it is interesting to note that Iran attacked and initially damaged the site first in 1980, shortly after the outbreak of the Iran-Iraq war. However, due to concerns about spreading radioactive material, they did not attack the actual reactor building dome. Instead, they targeted the control room, research facilities, and adjacent centrifuge buildings. While both sides disputed the efficacy of the attack, Iran dropped nearly a dozen 500-pound bombs on the site resulting in severe damage to several buildings along with the plant cooling mechanisms. However, based on the reactor building remaining intact, suspected rebuilding efforts of the ancillary infrastructure, and the desire to send a message to Arab nations regarding the pursuit of nuclear weapons, the IDF completed the mission and destroyed the reactor complex with an overwhelming strike in June of 1981.

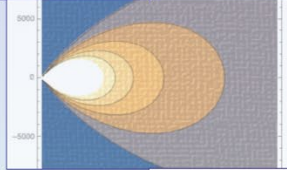
While other remote sensing modalities may have informed targeteers that the bombing achieved the desired effect, it is unlikely that they were able to sense whether nuclear material was present at the site or if such material had been dispersed or otherwise released in conjunction with the bombing. The advantages of a remote sensing radiation detection platform that conducts BDA following a strike on a suspected nuclear or radiological target are numerous. First, the ability of a team of people to rapidly access the target area is likely to be far more limited. Second, the synchronization required to deploy remote platforms on target is far more flexible than that required to put BDA teams on the ground. Third, several remote platforms could easily be deployed to achieve redundant coverage, corroborate findings between systems, or investigate multiple targets.


The employment of remote sensing radiation detection platforms allows the commander to preserve limited critical resources, such as a force designated to recover weapons-usable material, until measurement confirms the presence of the material at a specific target. Furthermore, timely and accurate information gathered by a remote platform may have strategic messaging implications concerning the spread of radioactive contamination or the presence of materials which violate international treaties or agreements.


CONSEQUENCE MANAGEMENT

- **UJTL TASK:** ST 9.9 Conduct Chemical, Biological, Radiological, and Nuclear Consequence Management (CBRN CM)
- **CONDITIONS:** given a radiological or nuclear incident which may or may not be attributed to a WMD attack (such as a beyond design basis loss of coolant accident at a nuclear power plant)
- **STANDARDS:** conduct actions to prepare for, respond to, and recover from the effects of the incident e.g. mapping the radioactive plume and fallout from the incident hazard area in order to recommend appropriate protective measures

I. 

II. 

III. 

IV. 

I. http://apj1.org/data/reactor_explosion.png

II. Concentration plot created using Wolfram Mathematica Student Edition

III. Photograph courtesy of John Kau, Lawrence Berkeley National Laboratory

IV. <http://www.slideshare.net/energy/radiation-monitoring-data-from-fukushima-area-05062011>

Source: [109]

Consequence Management

The term consequence management comprises those measures taken to protect public health and safety, restore essential government services, and provide emergency relief to governments, businesses, and individuals affected by the consequences of a chemical, biological, nuclear, or high-yield explosive situation [1]. From a DoD perspective, there are several reasons to maintain the capability to conduct nuclear consequence management operations. First and foremost, the DoD possesses, operates, and maintains nuclear reactors and weapons that could be the source of the situation. Second, DoD forces could be part of those affected by the consequences of a nuclear situation. Third, the DoD could be called to assist civil authorities with executing the measures taken to protect the public, restore services, and provide emergency relief.

One only needs to look to the relatively recent past to find an example where autonomous, remote radiation detection could have proved invaluable to a consequence management situation; specifically, the significant release of radioactive cesium and iodine triggered by the massive earthquake and follow-on tsunami that occurred in Japan on March 11, 2011. While the reactors automatically shut down as designed immediately after the earthquake, the six external power sources to operate the cooling systems were lost and the tsunami that followed within an hour wiped out the emergency backup generators. Insufficient cooling to three of the reactors caused partial melting of the fuel and led to hydrogen gas buildup from high-temperature reactions with the zirconium cladding, which eventually triggered explosions in the containment buildings and an above-grade fuel cooling storage pond.

The release of an estimated 570 petabecquerel's (15.4 MCi) resulted in the government-

directed evacuations of the area within 30 kilometers of the Fukushima Daiichi Nuclear Power Plants. In support of the Japanese government, the U.S. Department of Energy aided in producing a survey of the initial contamination. Members of the combined team completed the survey with a combination of fixed and rotary-wing aircraft as well as various ground stations to provide calibration reference data. The first measurements flown near the Fukushima Daiichi Nuclear Power Plant took place six days after the earthquake and tsunami. The delay was caused by the time it took to deploy assets and obtain the clearance to begin work. While this was undoubtedly beneficial and the efforts of those who conducted the surveys should be commended, a small fleet of instrumented fixed-winged UAVs could have provided a more rapid response along with higher fidelity knowledge of the extent and deposition of contamination.


There are several aspects of the response that would have benefited from the technology discussed herein, the main uses would have been (plume/fallout) drove evacuation recommendations, status of the reactor site (flew manned and unmanned helicopters on site - could have been deployed much faster, flown closer to the source, and limited exposure of flight crews. “A significant problem in tracking radioactive release was that 23 out of the 24 radiation monitoring stations on the plant site were disabled by the tsunami” [154]. With regards to ground stations, a handful of multi-rotor detection platforms would have provided a better representation of the average contamination for a given monitoring site rather than relying on measurements from a single position, owing to the inhomogeneous spatial distribution of the deposited radioactive material.

Remediation and recovery efforts represent an even broader application space. The government is allowing people to move back into areas that they have “cleared,” often through hand-collected and recorded monitoring data. The alternative drone-based detection system could cover the same area in a much short amount of time with sub-meter position resolution, and provide a detailed radiation “heat map” survey to residents to assure them that the area is safe as well as providing a baseline measurement record to monitor for change over time.


ACCIDENT RESPONSE

- **UJTL TASK:** SN 3.4.11 Coordinate Nuclear Security in response to a nuclear weapons accident / incident.
- **CONDITIONS:** given a nuclear weapons accident response scenario where aerial radiological and photographic survey is required
- **STANDARDS:** conduct a deliberate and systematic search over a possibly large and complex scene to facilitate the recovery of nuclear weapons and components in a safe and timely manner

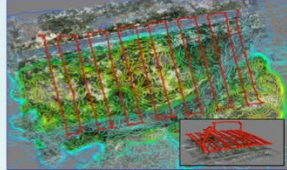
I.




II.



III.



IV.



I. Photograph by Eric Bowen <https://theaviationist.com/wp-content/uploads/2015/12/F-15E-nuke-take-off.jpg> [2016 August 15]
 II. Photograph by Bernard White. http://chef.bbci.co.uk/news/660/media/images/78095000/jpg/_78095892_tcrash2.jpg [2016 August 15]
 III. <http://articles.sae.org/13195/> [2016 August 15]
 IV. 3-D rendering graphic courtesy of Andrew Haefner, Lawrence Berkeley National Laboratory

Source: [109]

Accident Response

The priorities for the DoD response to U.S. nuclear weapon accidents are the location, security, and recovery of the weapon; the protection of lives and property; and remediation of the site [2]. Even though accidents involving nuclear weapons are particularly low occurrence events—just thirty-two documented U.S. “broken arrow” events since 1950—they remain a low-probability high-consequence event, even when taking modern safety design features into account [3]. While the high-alert nature of Cold War-era strategies, particularly Operation Chrome Dome, increased the probability of such events, the estimated 1,750 U.S. weapons that remain operationally deployed is a sober fact that must be taken into consideration for when planning a response to mishaps involving special nuclear materials [4]. Some of the tasks where an unmanned capability could prove are assessing the extent of the accident site, confirming or denying the release of radioactive material, mapping the radioactive contamination, locating aircraft or missile parts, locating nuclear material or weapons components, and verifying site remediation.

Two events that exemplify the need for a robust capability to remotely detect, locate, identify, characterize, and map radiological and nuclear material and contamination involve U.S. Air Force bombers that crashed with nuclear weapons onboard during Operation Chrome Dome. The first was the crash of a B-52 during airborne refueling operations taking place near Palomares, a small fishing village on the Mediterranean coast of Spain. The second involved the abandonment of a B-52 due to a fire in the cockpit. The crew was attempting to make an emergency landing at Thule Airbase in Greenland but became overwhelmed by the smoke.


Each accident required significant recovery efforts and involved personnel looking for bomb material in austere environments. In the Thule accident, four thermonuclear weapons were on-board, and radioactive material was released from the bombs upon impact and detonation of the high explosives, though a nuclear detonation did not occur. The recovery effort took months; sub-zero conditions and lack of daylight made the effort that much more difficult. The blacken snow from the burning of the aircraft fuel delineated the general search area. Officials estimated recovery of 94% of the plutonium and 85% of the uranium, as well as 2,100 m³ of contaminated liquid which was shipped to Savannah River, SC for storage and processing.

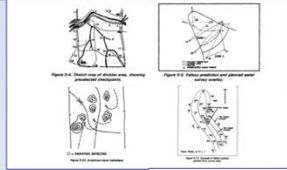
Nevertheless, if at the time they could remotely map the spread of the contamination as well as indicate potential hot spots, the recovery of the special nuclear material and contaminated snow and ice could have been more efficient and thorough. Large-scale human involvement would still have been integral to the recovery and cleanup effort. However, a remotely acquired map of the contaminated area with hot spots identified would have given those planning and supervising the operation valuable situational awareness and allow them to focus initial efforts in key locations. It would also give them better fidelity on the effectiveness of their removal efforts. Alas, these two events occurred before the advent and widespread use of global navigation satellite systems, though drones and remote sensing capabilities were on the rise at the time.


Current response procedures entail the use of fixed-wing aircraft for aerial photography and imagery collection (e.g., multispectral, hyperspectral, thermal) and previously discussed rotary-wing assets for aerial search and radiological mapping. There is also mention of a four-wheel-drive vehicle with detectors capable of high-spatial-resolution mapping of contamination [155]. While we should not discount these capabilities and agree they still have relevance to the mission, they all require putting human operators into the debris field and do not provide the speed, fidelity, specificity, and coverage that a swarm of sUAS-based detectors flying close to the ground could. The essential take away is that the risk of accidents involving nuclear weapons still exists, yet the organizations responsible for the assessment, consolidation, recovery, disposition, and site remediation phases currently possess little or no capability to locate nuclear material and assess the spread of contamination by remote means.


NUCLEAR CONTAMINATION AVOIDANCE

- **UJTL TASK:** ST 9.5 Provide Countering Weapons of Mass Destruction (CWMD) Defense
- **CONDITIONS:** given a yield-producing nuclear blast or significant radioactive dispersal in the area of operations
- **STANDARDS:** deploy a system of sUAS reconnaissance platforms to map the radioactive plume and associated fallout contamination in order to recommend appropriate measures to protect forces conducting follow-on missions in the area of operations

I. 

II. 

III. 

IV. 

I. Photographs courtesy of National Nuclear Security Administration / Nevada Site Office and PA photos via janes.com

II. Figures taken from inactive Field Manual 3-1-1 *Nuclear Contamination Avoidance* (1994 September 9) accessed at <http://www.militarymanuals.com> [2016 August 15]

III. <http://newatlas.com/switchblade-uas-kamikaze-drone/20611/> [2016 August 15]

IV. Plume by Colorado State Department of Public Health. - <http://www.cdph.state.co.us/rf/charta.htm> [dead link], PD-US, <https://en.wikipedia.org/w/index.php?curid=33248063> and vehicle from Dr Dan Saranga via <https://www.the-blueprints.com>

Source: [109]

Nuclear Contamination Avoidance

Limited nuclear warfare requires forces, on both sides of the conflict, to be prepared to operate in and cross through a nuclear-contaminated area. A required supporting task is to conduct a terrain-oriented zone or route reconnaissance to plan a route that minimizes the radiation exposure to forces, subject to the constraints of other competing military factors [5]. Current doctrine employs either Chemical, Biological, Nuclear, and Radiological (CBRN) reconnaissance platoons or rotary-wing aircraft outfitted with dosimeters and survey meters. Current generation M1135 Stryker Nuclear, Chemical, Biological Reconnaissance Vehicles (NBCRV) are medium armored vehicles which use readings from a vehicle-mounted beta and gamma probe—the Army-Navy Vehicle or Dismounted Radiac-meter (AN/VDR-2)—that measures dose rate and records accumulated dose [6]. There are efforts to integrate the data from the AN/VDR-2 with automated collection and mapping software, known as nuclear, biological, and chemical sensor processing group (NBCSPG), however, it is not currently fielded to CBRN units.

Although the threat of limited nuclear warfare may not be at the top of the list of the most likely conflict scenarios, it remains possible and is a driver of validated materiel requirements within the DoD. The potential benefits of developing an unmanned reconnaissance system for contamination avoidance are numerous: (1) reduce dose to personnel, (2) increase coverage area, (3) avoid terrain limitations, (4) allow CBRN personnel to conduct other missions, (5) lower cost, and others. A UAV could even be launched from an M1135 Stryker NBCRV.

While accurate meteorological data and dose rate level of specificity may be enough to plan a route, the requirement to use manned armored vehicles or aircraft to probe the contours of a high radiation area is nonsensical. One could easily outfit NBCRV with one or more small, tube-launched, fixed-wing unmanned aerial systems with onboard sensors optimized for aerial monitoring of radioactive plumes and fallout. Moreover, the sensor for chemical, biological, and meteorological information requirements could potentially be integrated into the same platform, thereby streamlining and modernizing the reconnaissance and collection capabilities of CBRN units.

The potential benefits of such a system are numerous. First, the idea of sending a \$5M-vehicle with a crew of four highly trained, low-density personnel to gather dose rate information to help protect the rest of the force is archaic. The DoD can, and certainly should have a capability beyond this 1930's chemical warfare-based approach. In fact, during the nuclear weapons testing conducted as part of Operation Crossroads in 1946, drone aircraft and boats were used to assess the radiation intensities before anyone was permitted to enter the area following a detonation.

Second, aerial collection, while not immune to becoming contaminated, offers a far better option in terms of reducing contamination to the vehicle and sensing instruments and is much easier to decontaminate. That is, the 21-ton vehicle kicking up dust and debris while traveling through the contaminated area is far more likely to become inundated with contamination and therefore systematically over-estimate dose rates because of the near field effects of radioactive particles stuck to the vehicle. It is also much easier to decontaminate or abandon equipment costing ~\$100k with a surface area $< 0.5 \text{ m}^2$ than it is to do the same with a \$5M vehicle with a surface area greater than 75 m^2 .

Third, a small, unmanned aerial system is a much lower priority target for enemy engagement than an armored reconnaissance vehicle. While an unmanned aerial system is still susceptible to enemy fire and countermeasures, a peculiar-looking group of armored vehicles traveling in and around the vicinity where a nuclear weapon was employed is much more likely to attract a lethal enemy response. The loss of one M1135 Stryker NBCRV, not including the personnel, specialized equipment, armament, and ammunition, represents at least fifty sUAS.


Even so, this integration effort is not quite as simple as mounting a dosimeter on a UAV and calling it a capability. Some excellent work along in pursuing an initial capability, including autonomous search, was carried out by investigators at the Johns Hopkins Applied Physics Laboratory (APL). Unfortunately, the work was not pursued further by the sponsor and a true capability never made it through the research and development "valley of death" into the hands of a user.

Some of the further tasks in designing such a system would include (1) developing the radiation detection element so that it provided an adequate response across the entire range of possible radiation environments while optimizing it for the most likely, (2) engineering the system from radiation hardened electronic components, and (3) ensuring the range, duration, and recovery of the system meets or exceeds threshold user requirements, and (4) integrate the data from the multiple radiation sensors into a situational awareness tool.


NUCLEAR FORENSICS

- **UJTL TASKS:** TA 1.2.6 Collect Forensic Material in support of ST 9.8 & 9.9 Conduct Chemical, Biological, Radiological, and Nuclear (CBRN) Passive Defense and Consequence Management (CBRN CM)
- **CONDITIONS:** given the detonation or deployment of a radiological or nuclear device resulting in contamination or fallout
- **STANDARDS:** map the radiation field with suitable spectral fidelity in order to identify primary locations to collect samples; if feasible, use the same or other remote platform to collect ground samples for laboratory analysis


I.



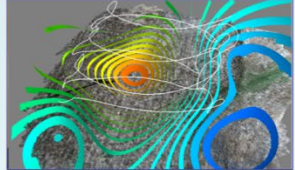
II.



III.



IV.



I. Screen shot from Nuclear Sunrise 2010 After Effects Composite, www.bmf-studios.com hosted on YouTube [2016 August 15] III. <http://www.avinc.com/uas/sdc/shrike> [2016 September 8]

II. <https://sfr.llnl.gov/AprMay12/knight.html> [2016 August 15] IV. 3-D rendering graphic courtesy of Andrew Haefner, Lawrence Berkeley National Laboratory

Source: [109]

Nuclear Forensics

Nuclear forensics is the examination of nuclear and other radioactive materials, either pre- or post-detonation, using various collection methods and analytical techniques to determine the composition, origin, age, and history of a material [8] [7]. Arguably the most advanced capabilities in remote sensing of radiation reside within the field of nuclear forensics. Endeavors sponsored by government agencies to develop pre-detonation capabilities focus primarily on nonproliferation and monitoring efforts. In monitoring for nuclear testing, the source term is generally located deep underground and very little of the fission products make it out into the atmosphere unless there is a major malfunction during the test; or a nation could decide that it is necessary and prudent to conduct atmospheric testing of their nuclear weapons, which makes forensic collection easier. Such a capability has been demonstrated as a bolt-on pod with the collection and measuring systems integrated onto a UAV [9].

However, we do not possess an advanced capability to collect materials for post-detonation nuclear forensics. Should a nation-state or violent extremist organization detonate a nuclear device in the U.S. or one of our partner-nations, our response policies dictate the collection and measurement of forensic materials from the nearby fallout area to attribute the device or fissile material to a source, especially when it is not readily evident or needs to be confirmed. An unmanned system has many benefits but would likely have the most stringent constraints of all the mission areas. Not only would it need to operate in a complex and high radiation setting, like that of a contamination avoidance mission, it would also need to be capable of excellent specificity and localization in a highly inhomogeneous environment. Current efforts are focused on using swarms of UAVs to characterize a debris field to direct

follow-on forces to auspicious collection areas with lower dose rates [10].

These requirements point to a very sophisticated radiation sensor package, likely using cutting edge detection materials such as GaGG, which has excellent timing characteristics for high count rate environments, medium energy resolution for isotope identification and characterization, and it can be finely pixelated for imaging applications. Other potential detection materials include LaBr₃. Current semiconductor materials would likely incur significant dead time as well as crippling radiation damage.

NUCLEAR DISABLEMENT

- **UJTL TASK:** ST 9.7 Conduct Weapons of Mass Destruction (WMD) Disablement Operations
- **CONDITIONS:** given access to a major component of a WMD program such as an nuclear enrichment or weapons fabrication, assembly, and storage area
- **STANDARDS:** conduct a deliberate and detailed exterior and interior reconnaissance of the area / facility to precisely locate, identify, and classify threats in order to take actions to exploit, degrade, or destroy critical and at-risk components



I. <http://brainfire9.ddns.net/wp-content/uploads/2016/05/aprilairia1photo.png> [2016 August 15]

II. <http://theiranproject.com/wp-content/uploads/2014/11/centrifuges-in-natanz.jpg> [2016 August 15]

III. Photograph courtesy of Andrew Haefner, Lawrence Berkeley National Laboratory

IV. 3-D rendering graphic courtesy of Andrew Haefner, Lawrence Berkeley National Laboratory

Source: [109]

Nuclear Disablement

This mission area is a bit nebulous but is somewhat aligns with consequence management and environmental monitoring. Nuclear disablement includes those operations associated with the assessment and handling of supporting nuclear infrastructure that might be encountered or targeted as part of military actions in a given area of operations. Most likely this involves the safe shutdown of enrichment or reactor facilities, securing materials not yet assembled as a weapon, and any other tasks that fall into the category of nuclear-related, excluding weaponized or deployed systems [11].

Current capabilities reside in small teams of military personnel (~15 personnel) with specialized training in the operation of such facilities, and a limited amount of hand-operated or vehicle-mounted detection equipment. Due to the uncertain nature of the mission, location, and conditions, most tasks are completed by hand. However, teams usually conduct an initial survey of a facility using either a small, all-terrain vehicle, a vehicle-towed trailer system, or a helicopter, outfitted with a set of large directional gamma and thermal neutron detectors.

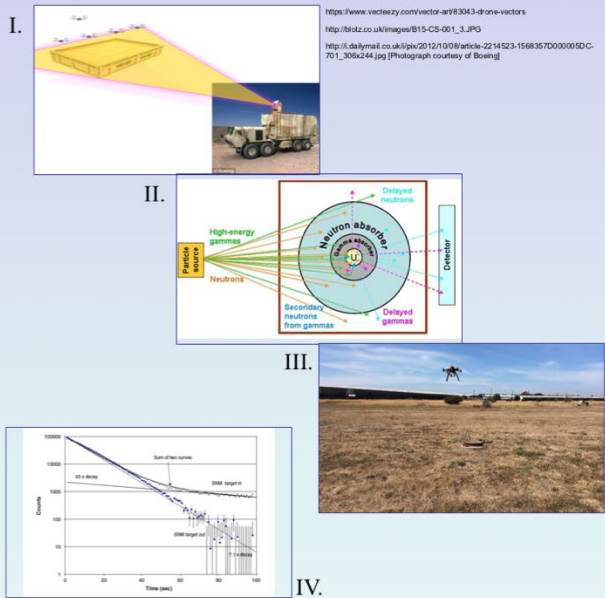
The scale of facilities like a centrifuge plant is on the order of a square kilometer or more. This vast area presents a challenge to small nuclear disablement teams that are quickly triaging a vast site to identify and classify threats in order to take actions to exploit, degrade, or destroy critical and at-risk components. While these operations are likely to take place in a semi-permissive environment (e.g., the area is protected by a sizable security force, or the enemy threat is negligible in that area), nuclear disablement forces could also be high-value targets for snipers or insurgents in the area.

A small number of autonomous radiation sensors could prove invaluable for deliberately

conducting exterior and interior reconnaissance of the facility. These would relieve a good portion of the NDT members from swinging a meter and free them to use their human sensors—primarily their eyes and ears coupled with their intellect and training. Anyone who has operated a radiation detector in the field recognizes the tunnel vision that goes along with it and how difficult it is to conduct other tasks simultaneously. Moreover, an autonomous capability does not rule out the need to maintain a certain level of human-operated equipment or other specialized detectors. It merely acts as a combat multiplier by alleviating a monotonous task that drained personnel resources for a good portion of the initial phase of an operation.

ACTIVE INTERROGATION

- **UJTL TASK:** SN 9 Countering Weapons of Mass Destruction (CWMD)
- **CONDITIONS:** given a mature, deployable active interrogation source (bremsstrahlung, neutron generator, etc.), use small UASs to transport bistatic sensors to the target, thereby significantly improving signal detection efficiency
- **STANDARDS:** exceed the efficiency of largest reasonable monostatic detector scheme and successfully detect significant quantity (SQ) levels of SNM



I. Various - listed right of graphic counter-clockwise from top left [2016 September 8]

II. MIT News, <http://web.mit.edu/nse/news/2013/shielded-nuclear-materials.html> [2016 August 15]

III. Photograph courtesy of Andrew Haefer, Lawrence Berkeley National Laboratory

IV. D.R. Slaughter et al. / Nud. Instr. and Meth. in Phys. Res. B 241 (2005) 780 (Figure 3)

Source: [109]

Active Interrogation

Active interrogation involves directing neutrons or high-energy photons toward a target and measuring the secondary radiation to gather information about the target. Government agencies have expended tens of millions of dollars or more on active interrogation projects since 2001. Whether the method includes a sizeable bremsstrahlung source, a pulsed neutron source, or some other novel source, such as cosmic muons or a photon beam driven by laser-wake field electron acceleration, they all suffer from one common limitation: the signal they induce, while unique and identifiable, obeys the same inverse square law as the passive signal and is therefore difficult to detect at any operationally significant range [7].

While several schemes also have issues with delivering potentially harmful dose to humans, both to the operator as well as persons within the screening area, the biggest hurdle is the need for large detectors often located away from the interrogation source (known as a bi-static or bicentric arrangement). So, not only is a trailer-sized source required, but one or more trailer-sized detectors must be arranged around the target but away from the source as to not be washed out by the source signal. This sine qua non is insupportable for most military applications, aside from using the source as a directed energy weapon.

However, there is continuing research that could provide more compact sources that deliver an acceptably-low dose to operators and potential bystanders within the target area. Couple that to a detection platform that is small, autonomous, remote, and has a sensor with high energy resolution and imaging capabilities, and a tractable concept of operations begins to emerge. That is, a suite of remote detectors could be flown, dropped, or launched to locations on or around the target of interest, thereby significantly decreasing the detector size

required to achieve the same sensitivity. With this reduction in detector size, employment of high-resolution detection materials becomes feasible, thereby improving specificity and reducing the minimum detectable amount of material. Moreover, the use of a position-sensitive arrangement of detectors, from simple occlusion up to a pixelated Compton imaging array, is conceivable and could provide additional information regarding the quantity, location, and arrangement of material being interrogated.